PhD degree in Systems Medicine (curriculum in Molecular Oncology)

European School of Molecular Medicine (SEMM),

University of Milan and University of Naples “Federico II”

Settore disciplinare: BIO/11

ASTRAL MICROTUBULE REGULATION IN MITOSIS

Federico Zucca

IEO, Milan

Tutor: Dr. Visintin Rosella

IEO, Milan

PhD Coordinator: Prof. Giuseppe Viale

Anno accademico 2019-2020

TABLE OF CONTENTS

LIST OF ABBREVIATIONS

AID	Auxin inducible degron
aMT	Astral microtubule
APC	Adenomatous Polyposis Coli
APC/C	Anaphase promoting complex / cyclosome
ATP	Adenosine triphosphate
CDK	Cyclin dependent kinase
CPC	Chromosomal passenger complex
DDR	DNA damage response
EM	Electron microscopy
ER	Endoplasmic eeticulum
FEAR	cdc-Fourteen Early Anaphase Release
GAP	GTPase Activating protein
GDP	Guanosine diphosphate
GEF	Guanine nucleotide exchange factors
GTP	Guanosine triphosphate
IF	Immunofluorescence
IL1	Intermediate layer 1
IL2	Intermediate layer 2
iMT	Interpolar microtubule
kMT	Kinetochore microtubule
MAP	Microtubule associated protein
MCC	Mitotic checkpoint complex
MEN	Mitotic exit network
MTOC	Microtubule organizing center
PLK1	Polo-like kinase 1
PP2A	Protein phosphatase 2A
SAC	Spindle assembly checkpoint
SC	Synthetic minimal medium
SCD	SC supplemented with glucose
SPB	Spindle pole body

SPIN	SPB inheritance network
SPoC	Spindle positioning checkpoint
SUMO	Small ubiquitin-related modifiers
TMT	Tandem mass tag
YEP	Yeast extract peptone (Yeast rich medium)
YEPD	YEP supplemented with glucose
YEPR	YEP supplemented with raffinose
YEPRG	YEP supplemented with raffinose and galactose
γ-TuRC	γ-Tubulin ring complex
γ-TuSC	γ-Tubulin small complex

TABLE OF FIGURES

INTRODUCTION

RESULTS

DISCUSSION

TABLE OF TABLES

MATERIAL AND METHODS

RESULTS

ABSTRACT

The faithful generation of two daughter cells genetically identical to each other relies on a complex cellular machinery called the mitotic spindle, which binds to each sister chromatid pair in a bipolar fashion and drives their segregation to the two newly generated daughters. The mitotic spindle is mainly composed of microtubules, microtubule-associated proteins and motor proteins. Spindle microtubules are conventionally divided into three different categories: (i) kinetochore microtubules (kMTs), which connect the spindle poles to chromosomes, (ii) interpolar microtubules (iMTs), which form a bundle that connects the two poles together, and (iii) astral microtubules (aMTs), which connect the poles to the cellular cortex. Proper spindle functions require drastic changes in microtubule dynamics. kMTs are unstable while searching for chromosomes, stabilized upon reaching a correct bipolar attachment and destabilized again soon after sister chromatids separation. iMTs remain unstable up to anaphase, when they become stable to drive spindle elongation. Finally, aMTs are stabilized and destabilized upon binding to different zones of the cellular cortex, to correctly direct the spindle. If differences in microtubules dynamics have been reported, the molecular mechanisms underneath them remain elusive. To gather insights into the machinery controlling spindle microtubules, we took advantage of *cdc14 cdc5* double mutant cells. These cells already proved to be precious as they revealed an essential requirement for spindle microtubule regulation – that is the activity of the phosphatase Cdc14 and the polo-like kinase Cdc5 for iMT stabilization in anaphase. We now show that central to the regulation of each type of spindle microtubule is the activity of the Anaphase Promoting Complex or Cyclosome in combination with its activator subunit Cdc20 (APC/C^{Cdc20}), that via removal of a yet to be identified substrate triggers aMT stabilization. We propose that the signalling cascade initiated by the APC/C^{Cdc20} – namely the metaphase to anaphase transition – sets the order

of events that finely control the chromosome segregation process through the regulation of specific types of spindle microtubule.

1. INTRODUCTION

At the end of the nineteenth century, concomitantly with the development of microscopy technologies, different laboratories began to study one of the most characterized processes in biology, namely mitosis. Already in 1882, Flemming described two peculiar structures that were visible in dividing epithelial cells: the "thick" fibers, now defined as mitotic chromosomes, and some connected "thin" fibers, alias the mitotic spindle[1]. Soon after that, Weissman, Boveri and Sutton found that chromosomes contain the genetic information, which was first described by Mendel fifty years before, and that their correct segregation during cell division is fundamental for the functionality of the newly generated cells. A first understating of the role and composition of the mitotic spindle came with the development of the Electron Microscopy (EM) in the mid-twentieth century, which allowed the visualization of the spindle as a structure made of filaments called "microtubules" that attach to chromosomes and guide them during the whole cell division process. The correct functionality of this machinery is fundamental to prevent missegregation of chromosomes, which in turn can generate cells with an incorrect chromosomal content, a condition known as aneuploidy. Aneuploidy is common in several tumor types, and it has been reported to play a crucial role in cancer development as it can both promote or inhibit tumorigenesis[2]. As such, understanding the complex network that regulates the mitotic spindle dynamics is of crucial importance and has been extensively studied by researchers over the years.

An important layer of information comes from studies performed using budding yeast cells. This organism proved to share many biological properties with mammals and has been essential for the characterization of different biological processes, such as cell cycle control[3], autophagy[4], exocitosis[5], splicing[6], and chromosome segregation[7]. The budding yeast spindle was one of the first structures to be visualized by EM[8] and has been almost completely reconstructed during the different steps of chromosome segregation[9], thus

driving the characterization of spindle dynamics, as well as the classification of the different types of microtubules that compose the spindle. For instance, budding yeast has been a crucial tool in the investigation of the molecular mechanisms that regulate the spindle elongation process[10], the mechanism that distances the two sets of chromosomes from each other at the end of mitosis. However, the complexity of this machinery is so high that much remains to be investigated.

One important structure whose regulation still needs to be fully characterized is the subset of spindle microtubules called astral microtubules (aMTs), which anchor the spindle to the cellular cortex and guide spindle positioning along the polarity axis[11]. The spindle positioning process is fundamental to achieve a proper chromosome segregation, and it is also implicated in the generation of cellular diversity during development[12,13]. Although aMTs are often considered just "passive players", they are now emerging as active players in the positioning process, together with many other proteins that control aMT dynamics[14]. As such, the main goal of my PhD project was to take advantage of budding yeast to characterize the regulation of aMTs in mitosis.

In this chapter, I will briefly introduce the cell cycle machinery, focusing in particular on mitosis, describe spindle architecture and dynamics, and finally present the current models of spatio-temporal regulation of aMTs in budding yeast mitosis.

1.1. The eukaryotic cell cycle

The cell cycle is the process that drives the generation of two cells, starting from a single cell, that are genetically identical to the mother cell. To ensure a correct transmission of the genome, cells duplicate their chromosomal content during the so-called "Synthesis" phase (S), and subsequently segregate it in an equal manner to the two daughter cells during the "Mitotic" phase (M). Three phases called Gap phases (G0, G1 and G2) compose the mitotic cell cycle. While the G0 phase is often defined as a "resting phase", since it is characterized by the lack of cellular growth, cells in G1 and G2 are normally typified by a huge amount of protein synthesis and consequent increase in the cellular size. However, it is important to notice that not all cell types, when residing in a G0 state, become less active and remain quiescent after their full differentiation, for example neurons, which are among the most active cells in the human body.

G1 and G2 start at the end of M and S phase, respectively (the combination of G1, S and G2 is normally defined as "interphase", since it stands between two cycles of mitosis), while G0 normally arises in a G1 cell deprived of nutrients and proliferative factors or following a genetically encoded developmental path. A commonality of the three G phases is that they make cells very sensitive to intra and extra-cellular signals, such as that their time span can last for the required time. For instance, some G0 cells can eventually return in the proliferative G1 phase when nutrients become available. Similarly, a group of internal and external signals determine when a G1 cell can enter the "restriction point", a commitment point that allows cells to proceed from G1 to S phase[15]. When cells reach the "restriction point", they become insensitive to nutrient availability and proceed in the cell cycle independently of proliferative factors. Furthermore, several surveillance mechanisms exist, which are activated for example after incomplete DNA replication or DNA damage, arresting thus cells in G2 until the problem is resolved.

At the heart of these complex mechanisms are the Cyclin-Dependent Kinases (CDKs), a family of proteins that governs cell cycle progression through the phosphorylation of multiple targets[16]. CDK activity varies during different cell cycle phases thanks to the association with different cyclin subunits[17]. Depending on the cell cycle phase, distinct cyclin-CDK complexes are formed and initiate a series of events that determine the progression through that particular cycle stage. CDK association with cyclin A promotes DNA replication, thus coordinating G1-S phase transition. Each chromosome is associated with its own copy (together called sister chromatids) during replication through a protein ring complex called cohesin. Although some DNA linkages between the two sister chromatids exist and cooperate with the cohesin complex to maintain the two sister chromatids together, these protein-mediated linkages are considered to be the main factors that generate cohesion. Again, at the G2-M transition, CDK association with the cyclin B subunit promotes entry into M-phase[17]. Together, cyclin A-CDK and cyclin B-CDK orchestrate M-phase progression.

M-phase can be divided into two different phases: mitosis, the process that guides the segregation of the two identical sets of chromosomes to the two newly generated cells; and cytokinesis, the process that physically separates the two daughter cells. Furthermore, mitosis can be divided into five different sub-phases based on cellular cytology: prophase, prometaphase, metaphase, anaphase, and telophase. In prophase, the genetic material condenses into discrete pairs of duplicated chromosomes. During prometaphase, the nuclear envelope breaks down and two fundamental structures are assembled: the mitotic spindle and the kinetochores. The mitotic spindle is a complex filamentous structure composed of microtubules, Microtubule Associated proteins (MAPs) and motor proteins. Spindle microtubules originate from two distinct Microtubule Organizing Centers (MCOCs), called centrosomes in mammalian cells and Spindle Pole Bodies (SPBs) in yeast cells, and assemble a bipolar structure that controls the whole segregation process.

Kinetochores are protein-based structures that associate with the centromeric region of each chromosome and have the fundamental function of connecting microtubules with chromosomes. In metaphase, each chromosome pair binds to the spindle through kinetochore-microtubule interactions in a bipolar manner (in every chromosome pair, each sister chromatid binds to a different centrosome) and is guided toward the equatorial zone of the spindle (a process named "chromosome congression"), forming the so-called metaphase plate. Importantly, a surveillance mechanism called Spindle Assembly Checkpoint (SAC) exists, which maintains cells in metaphase until all pairs of sister chromatids are correctly bi-oriented. Once this complex series of events is completed, cells progress into anaphase, during which the cohesin complex is cleaved, the spindles are elongated and chromosomes are equally segregated to the opposite poles. While M-phase CDKs orchestrate mitotic events until metaphase is reached, their inactivation is required for cells to progress from anaphase to the end of mitosis[17]. In telophase, the spindle dissembles, two new nuclear envelopes are formed in the proximity of the segregated chromosomes, and DNA decondensation begins. For a complete division of the two newly generated cells, a contractile ring is formed around the division site, which finalizes the separation of the two cytoplasms during cytokinesis.

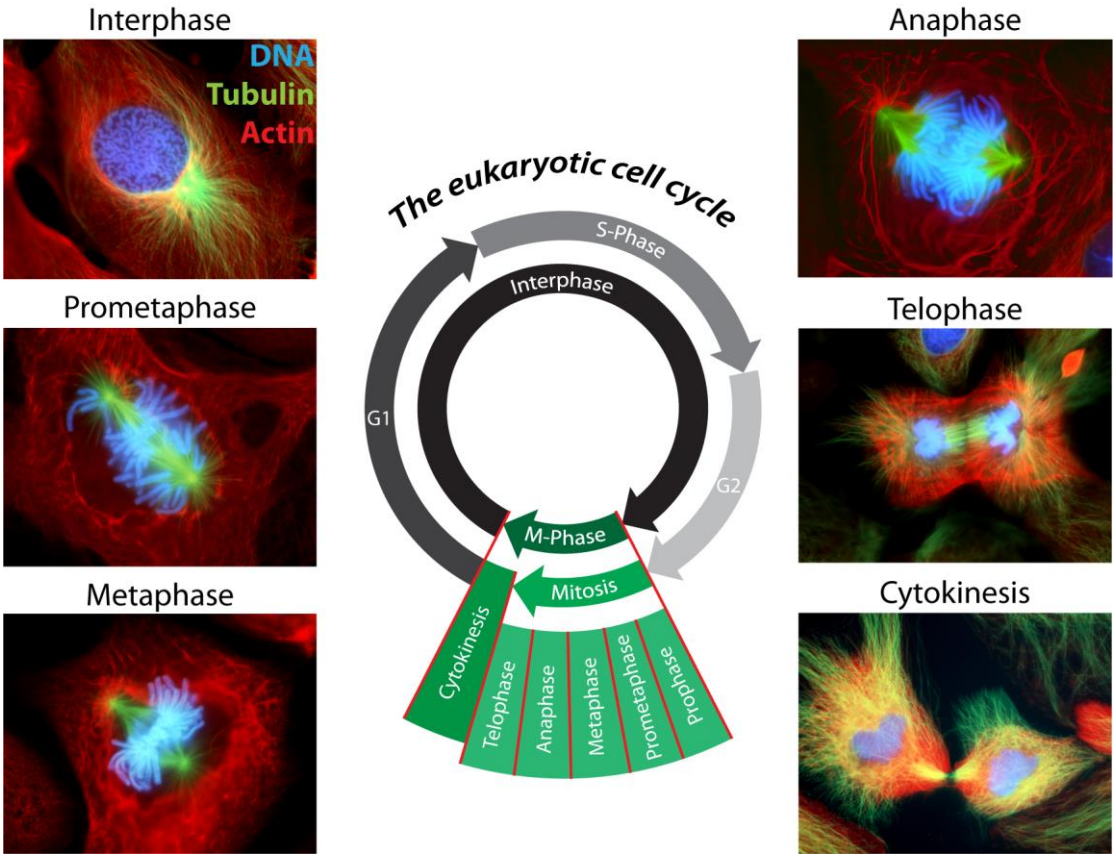

Figure 1.1. The eukaryotic cell cycle.

(Images are courtesy of Conly Rieder)

1.2. The yeast cell cycle

The budding yeast *Saccharomyces cerevisiae* is a simple and unicellular eukaryote that can exist in both a haploid and a diploid state, and it is characterized by a fast proliferation: its entire cell cycle lasts about 90 minutes in a *wild-type* strain supplemented with glucose, while in a typical proliferating human cell, one cell cycle lasts about 24 hours. Furthermore, in contrast to higher eukaryotes, the nuclear envelope in budding yeast does not break down during M phase (a peculiarity known as "closed mitosis") and the metaphase plate is not formed since a proper chromosome congression does not take place. Despite these differences, the cell cycle machinery in general, and in particular the mitotic spindle, is highly conserved from yeast to human and budding yeast has been highly used to study this complex process.

Budding yeast undergoes asymmetric cell division and generates two cells, called mother and bud cells, which retain different sizes and fates[18]. The mother cell is normally big in size and has a limited proliferative potential, depending on the number of cell divisions that it has already gone through. In contrast, the bud cell is normally smaller than the mother cell, but it acquires a full proliferative potential. The bud emerges from the mother cell in S phase, following the accumulation of several polarizing proteins on the pre-division site that is also called bud-neck. The polarizing proteins septins (called Cdc3, Cdc10, Cdc11, Cdc12 and Shs1 in yeast) and formins (Bnr1 and Bni1 in yeast) cooperate to polarize the mother and the bud compartments. Septins generate a barrier that controls the diffusion of plasma membrane- and ER-associated proteins[19]. Around the bud-neck, formins assemble filamentous structures called actin cables[20] that are used as platforms by different actin motor proteins to segregate proteins and organelles into the bud.

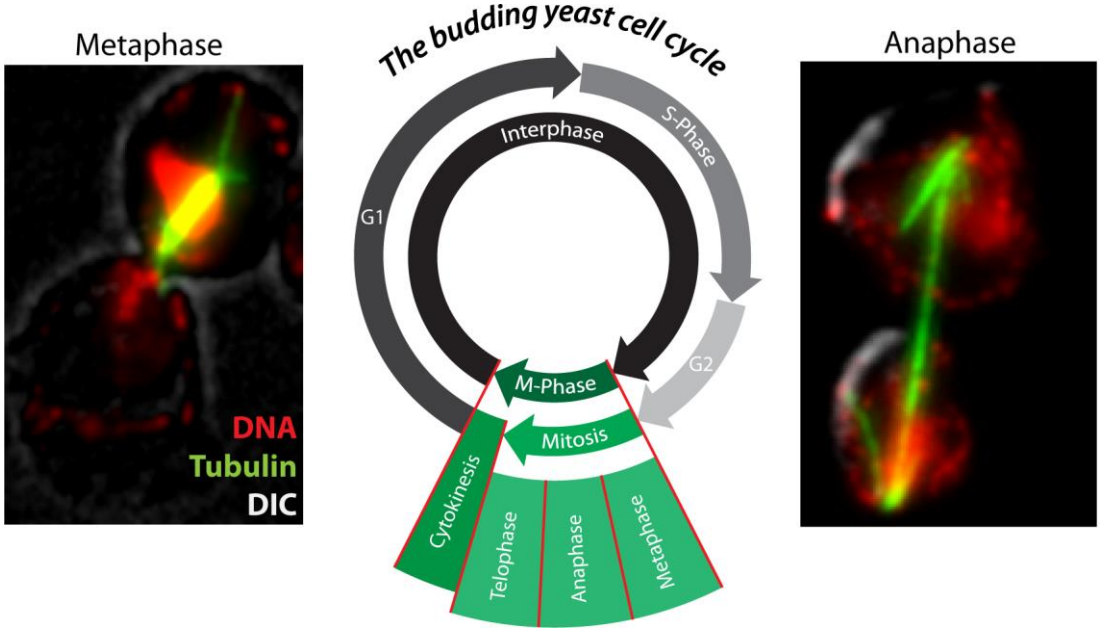

Figure 1.2. The budding yeast cell cycle

1.2.1. CDK, Cdc14 and mitotic kinases: three to tango

While eukaryotes usually possess several CDKs, budding yeast expresses a single CDK, namely Cdc28, to orchestrate the whole cell cycle process. Cdc28 regulates the different cell cycle phases by associating with the different cyclin subunits that are express at the specific stages. In yeast, nine phase-specific cyclins exist: Cln1, Cln2 and Cln3, which associate with Cdc28 in G1 and are required in the selection of the pre-division site; Clb5 and Clb6, which are expressed in S phase and drive DNA replication; and Clb1, Clb2, Clb3 and Clb4, which are involved in M phase and finely guide mitosis progression up to metaphase. Similar to other eukaryotes, cell cycle progression from metaphase to G1 requires both inactivation of the CDK and activation of a CDK-counteracting phosphatase[17,21], which in yeast is Cdc14[22]. These events occur in a two-step manner: first, during "the metaphase to anaphase transition", CDK activity is lowered and Cdc14 is partially activated by the protein network called "Cdc-Fourteen Early Anaphase Release" (FEAR)[23,24]; secondly, at the end of mitosis, CDK is inactivated and Cdc14 is fully activated by the protein network called "Mitotic Exit Network" (MEN)[3]. These two protein networks control Cdc14 activity and localization, modulating the phosphorylation

level of both the phosphatase and its associated inhibitor Cfi1, which sequesters the phosphatase in the nucleolus[25]. From G1 to metaphase, Cdc14 and Cfi1 are un-phosphorylated, a condition that promotes their association and, in turn, sequesters Cdc14 in the nucleolus. FEAR and MEN networks induce Cdc14 and Cfi1 phosphorylation, thus promoting their dissociation and the release of the phosphatase in different cellular compartments. The FEAR network induces a partial and temporally limited release of Cdc14 from the nucleolus to the nucleoplasm, while the MEN promotes its full release in the cytoplasm[3]. A "two-hit model" has been proposed, which properly explains the dynamics of Cdc14 release[26]. Since the polo-like kinase Cdc5 is the only component that is shared between the two networks, this model suggests that Cdc14 release is induced by Cdc5-mediated phosphorylation of Cdc14 together with the phosphorylation of Cfi1 by a "partner kinase" that changes depending on the network. Cdc14 is released from the nucleolus only when both phosphorylation events take place. Interestingly, the role of mitotic kinases is not limited to the release of Cdc14 phosphatase. Indeed, concomitantly with the dephosphorylation of many CDK targets by Cdc14, different mitotic kinases, such as Cdc5, the Aurora kinase Ipl1, and the Hippo pathway kinases Cdc15 and Dbf2, phosphorylate many proteins to such a degree that the same number of amino acid residues are both phosphorylated and dephosphorylated in late mitosis[27]. These kinases cooperate with Cdc14 to drive late mitotic events and to reset the conditions for cells to progress into G1.

1.2.2. Metaphase to anaphase transition

The metaphase to anaphase transition starts when each pair of chromosomes is bipolarly attached to the mitotic spindle and culminates with cohesin cleavage, the final event that defines anaphase entry. The first step of the transition is the activation of the E3 ubiquitin ligase called Anaphase Promoting Complex/Cyclosome (APC/C) that associates with its regulatory subunit Cdc20[28] and targets for degradation a variety of substrates that act as

anaphase inhibitors. The APC/C^{Cdc20} induces the degradation of the S phase cyclins Clb5 and Clb6, and the partial degradation of the M phase cyclin Clb2, with the overall effect of lowering CDK activity. Importantly, the APC/C^{Cdc20} also promotes the inactivation of securin/Pds1, which keeps the caspase-related protein separase/Esp1 in an inactive state up to metaphase. Once activated, Esp1 cleaves the cohesin subunit Scc1[29,30], releasing the cohesion between the two sister chromatids and triggering anaphase entry. In addition, Esp1 is a member of the FEAR network[31]. Additional members of the this network are the kinetochore protein Slk19, which forms a complex together with Esp1, the polo-like kinase Cdc5, the Clb2-CDK complex, the Protein Phosphatase Type 2A (PP2A) associated with Cdc55, the replication fork protein Fob1, and the nucleolar protein Spo12 (and its paralog Bns1)[31]. The Esp1/Slk19 complex acts in two branches of the network, in parallel with Cdc5 and upstream of the other components. On the one hand, Esp1/Slk19 lowers the activity of PP2A, allowing thus the Clb2-CDK-mediated phosphorylation of Cfi1 that fosters Cdc14 release. On the other hand, Esp1/Slk19 indirectly induces the Clb2-CDK-mediated phosphorylation of Spo12, which antagonizes Fob1. Fob1 promotes Cfi1 association with Cdc14, thus, its inhibition further increases Cdc14 activation. Finally, Cdc5 cooperates with the other members of the network by phosphorylating Cdc14. The already mentioned[26] "two-hit model" proposes that CDK, in combination with Clb2, is the Cdc5 "partner kinase" of the FEAR network that phosphorylates Cfi1 and is thus required to release Cdc14. Given that APC/C^{Cdc20} is known to degrade both cyclin subunits, this model may explain the transient nature of the FEAR-induced Cdc14 release.

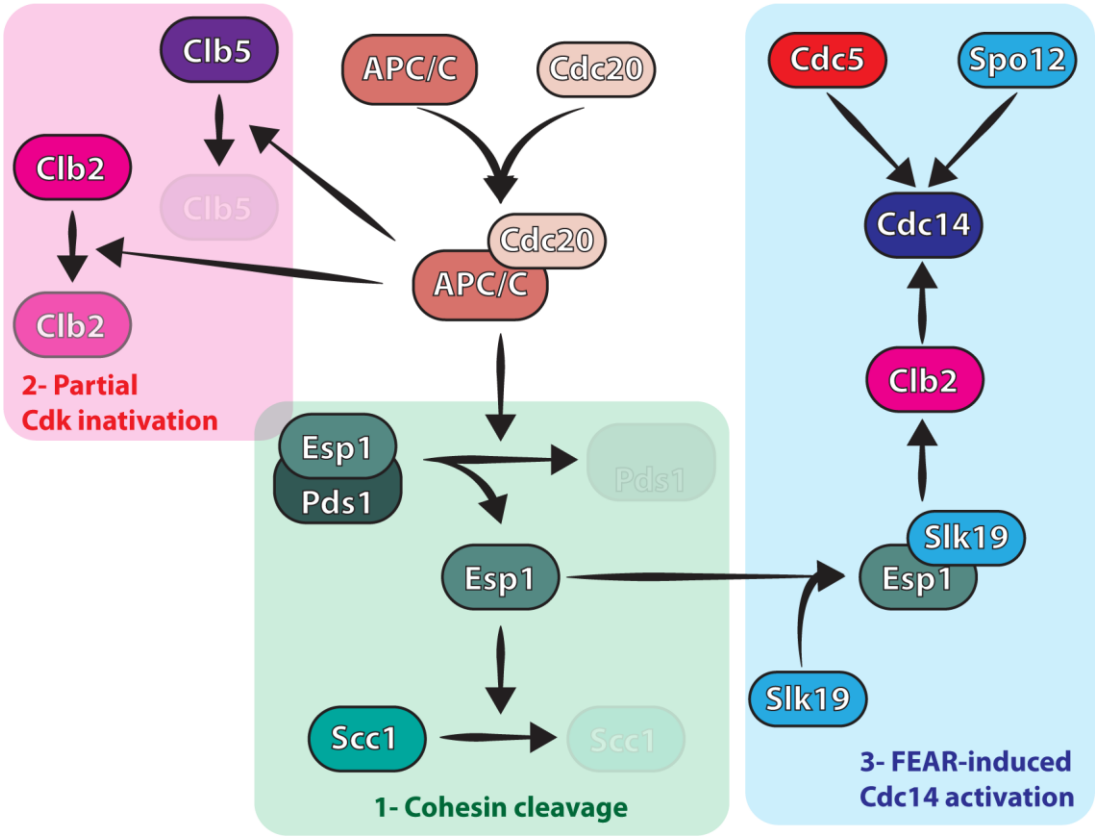

Figure 1.3. The metaphase to anaphase transition

1.2.3. Exit from mitosis

Mitotic exit is an irreversible process that starts at the end of metaphase to anaphase transition and terminates with cytokinesis. Mitotic exit is characterized by the disassembly of the mitotic spindle, the decondensation of mitotic chromosomes and the separation of the two daughter cells mediated by the contraction of the actomyosin ring located at the bud-neck. Exit from mitosis requires complete Cdc14 activation and CDK inactivation, two events that are strongly connected to each other[17]. Indeed, Cdc14 activity promotes CDK inactivation both by activating the APC/C^{Cdh1} complex[28], which in turn targets M phase cyclins for degradation, and by promoting the accumulation of the CDK inhibitor Sic1[22]. On the other hand, the partial CDK inactivation driven by APC/C^{Cdc20} is essential for MEN activation, the signaling cascade that mediates Cdc14 activation in late anaphase, as Clb2-CDK has been reported to phosphorylate and inhibit the protein kinases Cdc15 and Dbf2[32], two downstream components of the MEN. Given

that APC/C^{Cdc20} activation occurs only when cells progress from metaphase to anaphase, this limitation provides a temporal signal to the MEN machinery and ensures unscheduled mitotic exit prior to chromosome segregation. In addition, MEN activity is limited upon the entry of the SPB into the bud through the regulation of the GTPase Tem1. Tem1 localizes to the bud-directed SPB, is kept inactive by the GTPase-Activating Protein (GAP) complex Bub2-Bfa1, and is activated by the GTP-GDP Exchange Factor (GEF) Lte1 that is localized in the bud cell[33]. The GTPase acts upstream of Cdc15 and Dbf2, which in association with Mob1 acts as the Cdc5 "partner kinase" and phosphorylates Cfi1[26]. Besides directly phosphorylating Cdc14, Cdc5 phosphorylate Bfa1, promoting the dissociation of the Bub2-Bfa1 complex[34], hence facilitating the inactivation of the complex and therefore also Tem1 activity. Interestingly, Cdc14 released by the MEN acts in a negative feedback loop to promote its inactivation, a required condition to re-start the next cell cycle. On the one hand, Cdc14 dephosphorylates Bfa1, promoting its activation[35]; on the other hand, APC/C^{Cdh1}, whose activity is promoted by MEN-activated Cdc14, targets Cdc5 for degradation, inducing thus Cdc14 re-sequestration in the nuclelous[36].

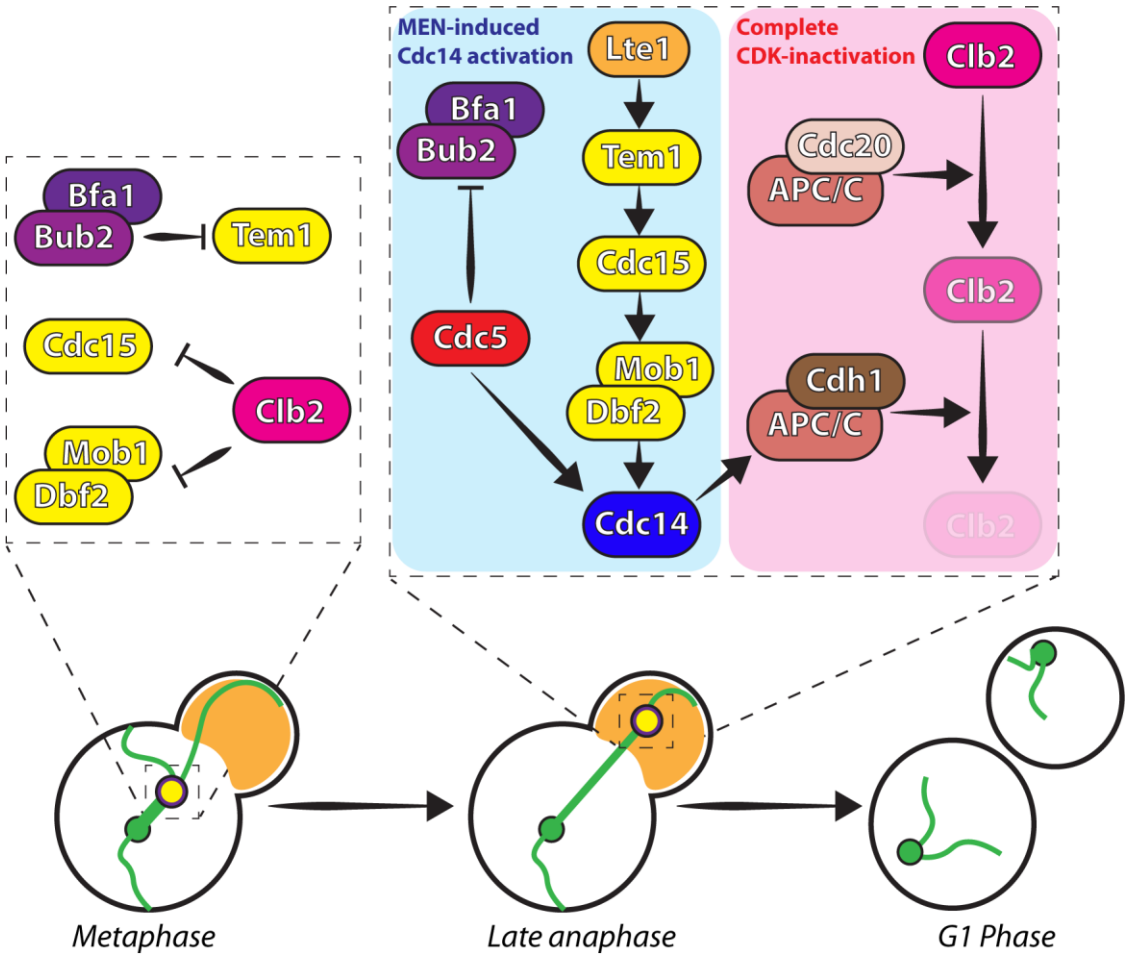

Figure 1.4. Mitotic exit

1.2.4. Mitotic checkpoints

In order to preserve genome integrity, multiple proteins monitor cell cycle progression by acting as "checkpoints", delaying the beginning of a particular cell cycle phase until certain conditions have been satisfied. One of the most characterized checkpoints is the DNA Damage Response (DDR), which senses the status of the DNA and, when activated, delays cell cycle progression and arrest cells in metaphase. The upstream sensor of the pathway is the essential phosphoinositol-3-kinase-related Mec1, which hyper-phosphorylates the DNA-binding protein Rad9. This phosphorylation triggers Rad9 interaction with two effectors of the pathway, namely Chk1 and Rad53. On the one hand, Chk1 antagonizes anaphase progression through the phosphorylation of securin Pds1, which prevents its APC/C-mediated degradation and consequently inhibits cohesin

cleavage. On the other hand, Rad53 antagonizes exit from mitosis by activating the Bfa1-Bub2 complex[34] and inhibiting Cdc5, with the overall effect of preventing MEN activation. Another important mitotic checkpoint is the Spindle Assembly Checkpoint (SAC), which senses kinetochores/microtubule binding and inhibits anaphase progression until every chromosome is bipolarly attached. Briefly, the "sensor" of the SAC is the Mitotic Checkpoint Complex (MCC), a complex composed of Mad2, Bub1R and Mad3 that is activated when kinetochores are unattached or incorrectly attached, consequently sequestering the APC/C cofactor Cdc20[37]. The MCC, in combination with Bub1, Mad1 and Mps1, inhibits Cdc20, thus preventing the key step that initiates the metaphase to anaphase transition[37]. Lastly, the Spindle Positioning Checkpoint (SPoC) senses whether the spindle is in the mother or in the bud cell and prevents mitotic exit until at least one SPB has entered the bud cell compartment[38]. This checkpoint acts through the activity of the kinase Kin4[39,40], which is specifically located in the mother cell and affects MEN activation by fostering the inhibitory effect of the Bfa1-Bub2 complex on the network. This complex binds to the bud-directed SPB, and is hence targeted by Kin4 only when the SPB is retained in the mother cell. When the SPB enters the bud, normally during anaphase, the Bfa1-Bub2 complex loses its Kin4-mediated phosphorylation, is targeted by the Cdc5-mediated inhibitory phosphorylation and thus licenses MEN activation.

1.3. The mitotic spindle

Cells take advance of a sophisticated machinery called the mitotic spindle, whose building blocks are polymers of αβ-tubulin called microtubules, to correctly segregate the chromosomes. Microtubules are characterized by cycles of growth and shrinkage, a property defined as dynamic instability[41], which allow quick and transitory changes in the spindle structure that are required to accomplish its role. Microtubules grow by the addition of αβ-tubulin heterodimers, bound to GTP, at the extremity of the microtubule. Once inside the lattice, GTP is hydrolyzed to GDP thanks to the GTPase activity of tubulin. The αβ-tubulin subunits in which GTP is not hydrolyzed compose the "cap" and favor microtubule growth. The absence of the "cap" generates a catastrophe event, in which several subunits detach from the microtubule lattice, inducing the shrinking of the microtubule. Microtubules can eventually reform the "cap" and restart the growth phase, an event defined as rescue. The two ends of a microtubule are structurally and functionally distinct: the plus-end, which terminates with β-tubulin subunits and gives rise to the majority of catastrophe and rescue events; and the minus-end, which terminates with α-tubulin subunits and is normally more stable than the plus-end. Microtubules can originate spontaneously, but this process requires many unfavorable steps, and cells avoid this problem by using templates to nucleate microtubules and MAPs to increase the nucleation efficiency. MAPs are not only involved in microtubule nucleation but, together with motor proteins, also regulate microtubule dynamics and functions. For example, MAPs can stabilize or destabilize microtubules, connect them with other cellular structures and guide them toward specific locations. The vast majority of spindle microtubules originate from two MTOCs[42], which are called SPBs in yeast cells. These structures are located at the minus-end, contain the γ-Tubulin Ring Complex (γTuRC) that acts as a template for microtubule nucleation, and allow the organization of microtubules in a bipolar structure called mitotic spindle.

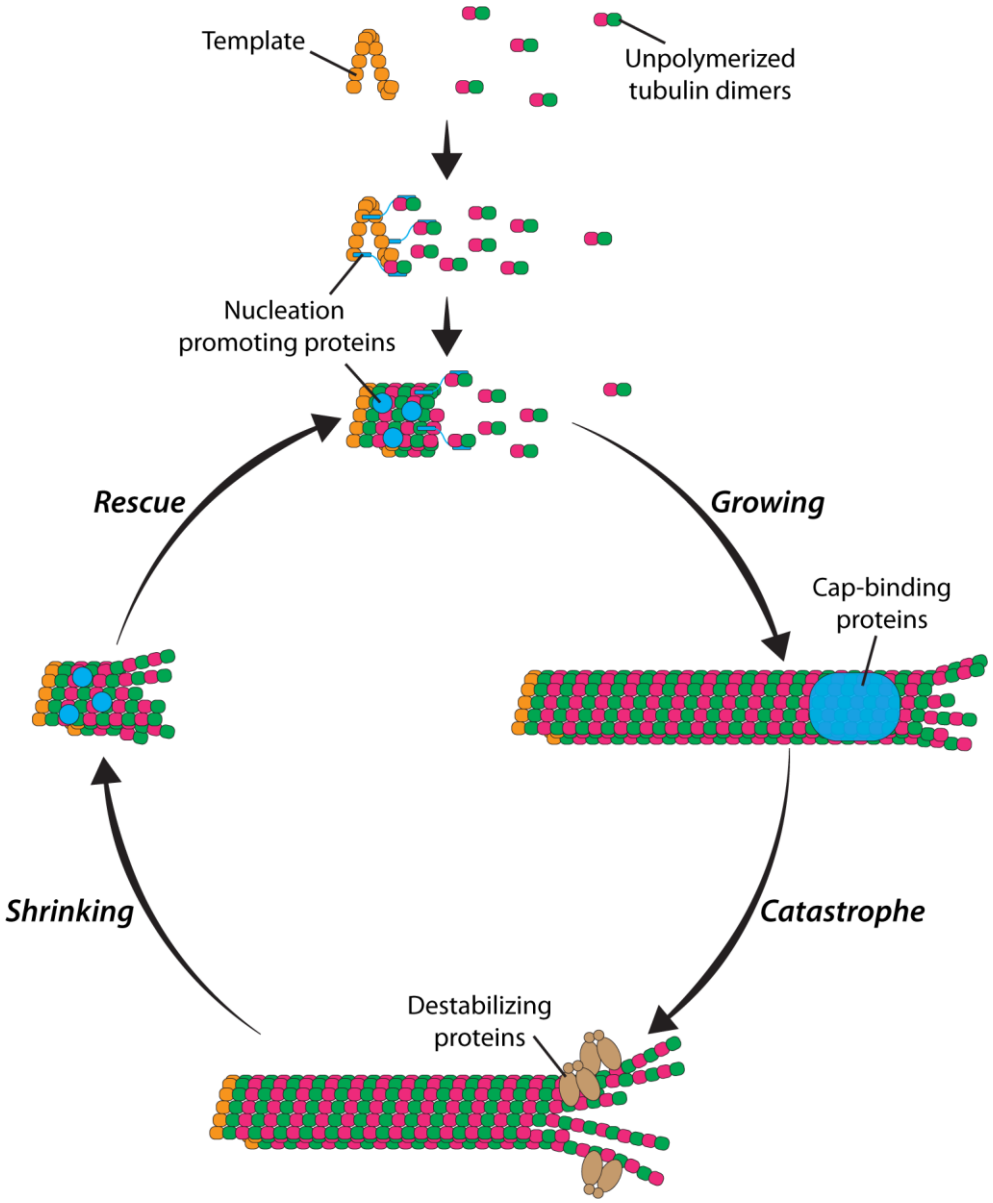

Figure 1.5. The microtubule cycle

The mitotic spindle is composed of microtubules, two SPBs, motor proteins, and MAPs. Cells contain a single SPB from G1 to late S phase, during duplication, in order to generate the bipolar conformation that is typical of the mitotic spindle. Based on their function, microtubules of the mitotic spindle can be divided into three different categories[43]: (i) interpolar microtubules (iMTs), which form a bundle that connects the two poles; (ii) kinetochore microtubules (kMTs), which connect the poles to chromosomes; and (iii) astral microtubules (aMTs), which connect the poles to the cellular cortex. In order to accomplish its function, the mitotic spindle drastically changes

during mitosis, mostly due to the modulation of several motor proteins and MAPs that affect microtubule dynamics.

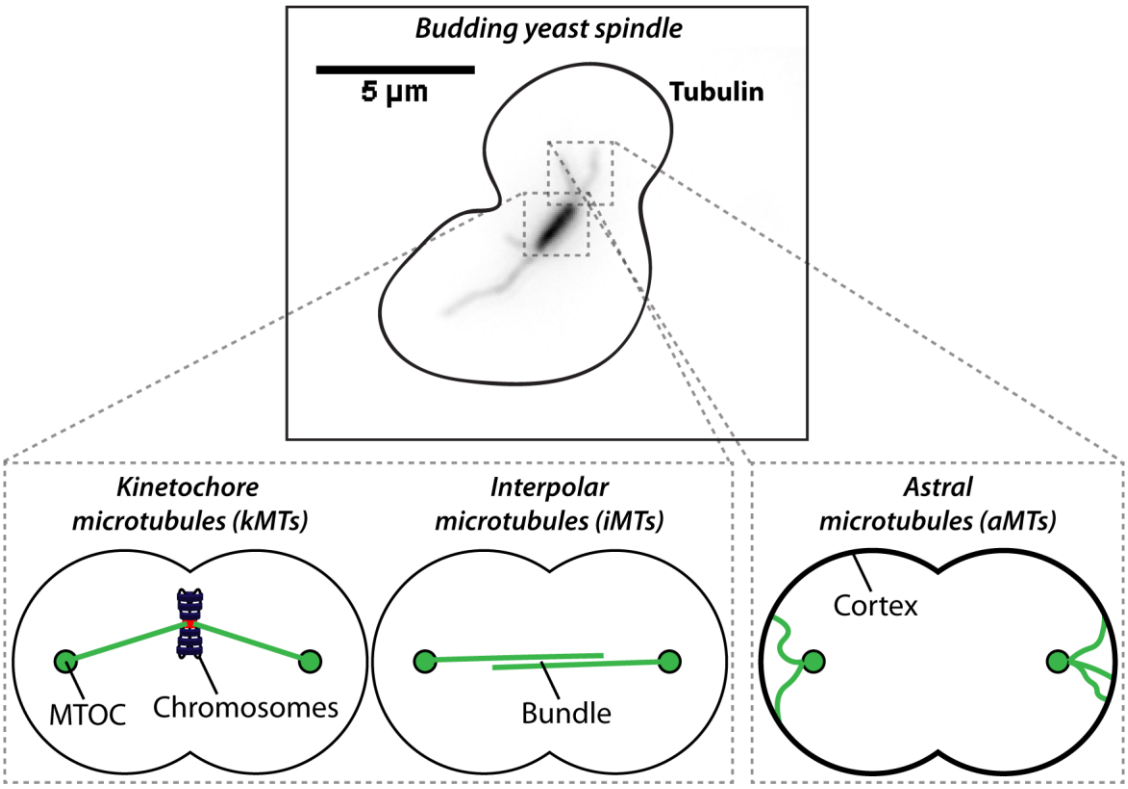

Figure 1.6. The three types of spindle microtubules

1.3.1. Microtubule associated proteins

MAPs are proteins that bind to microtubules and affect their dynamics and function. As such, it is not surprising that many MAPs are part of the core mitotic spindle machinery: the plus-end tracking proteins Bim1 and Bik1; Ase1, the Esp1/Slk19 complex and the chromosomal passenger complex (CPC), which are components of the "spindle midzone" structure; and the microtubule nucleating factor Stu2.

Bim1 and Bik1 are members of the EB1 and CLIP170 families, respectively, and have been shown to have antagonizing effects on microtubule stability. Indeed, both proteins associate at microtubule plus-ends, but while Bim1 promotes microtubule growth by lowering the frequency of catastrophe events, Bik1 destabilizes microtubules[44]. Bim1 and Bik1 can assemble together in complexes, but the significance of this trait is unclear at

the moment[44]. Additionally, Bim1 and Bik1 are involved in promoting the attachment of different proteins to aMT plus-ends: Bim1 favors the association of the spindle orientation protein Kar9, which links aMTs with the actin cytoskeleton, while Bik1 associates with the motor protein Dyn1[45].

Several MAPs are involved in the formation of the "spindle midzone", a specialized structure of the spindle that forms during spindle elongation. The microtubule bundling protein Ase1, which belongs to the family of human PRC1, covers a fundamental role in the formation of this structure. Ase1 is expressed during mitosis, is phosphorylated by CDK up to metaphase, is dephosphorylated by Cdc14 at anaphase onset and is ubiquitinated by APC/C^{Cdh1} at the end of mitosis[46]. Ase1 phosphorylation stabilizes the spindle, while its dephosphorylation is required for the formation of a proper spindle midzone and thus a correct spindle elongation[47]. Importantly, lack of Ase1 dephosphorylation results in the delocalization of the other midzone components and delays the switch between fast and slow elongation rate of the spindle[47]. One of these midzone components is the Esp1-Slk19 complex, which is formed upon Esp1 activation at the metaphase to anaphase transition and whose role is to center and limit the spindle midzone to the middle of the mitotic spindle[48]. Esp1-Slk19 recruitment to the spindle also requires the CPC[49]. This complex is associated with kinetochores up to metaphase since it is part of the tension-sensing mechanism that corrects erroneous kinetochore-microtubule connections. Once in anaphase, FEAR-released Cdc14 dephosphorylates the CPC component Sli15 and promotes its spindle localization and thus midzone assembly[50].

Although with a different function than the other MAPs already mentioned, the XMAP215 homologue Stu2 has an important role in the regulation of spindle dynamics. Stu2 binds to the SPB component Spc72 and drastically increases the nucleation efficiency of the Spc72/γTuSC complex[51]. Importantly, Spc72/Stu2 complexes have been shown to nucleate microtubules both *in vitro* and *in vivo*, even in the absence of γ-

Tubulin[51]. Moreover, Stu2 nuclear export is regulated differently during the cell cycle: it presents a high export rate in G1 that, however, decrease during mitosis in order to favor kMT- and iMT nucleation over that of aMTs[52].

1.3.2. Microtubule motor proteins

Microtubule motor proteins use the energy derived from ATP hydrolysis to generate the mechanical energy required to move and segregate chromosomes. The budding yeast genome encodes for six kinesin-related motor proteins (Cin8, Kip1, Kar3, Kip2, Kip3 and Smy1) and a single Dynein heavy chain (Dyn1)[53]. Among the kinesin motor proteins, only Smy1 is not implicated in mitosis. The big overlap in functions of these proteins underlines the fact that none of them is individually essential for cell viability despite their involvement in essential events of cell division[53].

Cin8 and Kip1 are part of the kinesin-5 (BimC) subfamily of motor proteins and are known regulators of spindle assembly and elongation. Although BimC family members are generally plus-end-directed motor proteins, it has been shown that Cin8 can switch its directionality and move in both directions on spindle microtubules even if the significance of this peculiarity is not yet fully understood[54]. Cin8 and Kip1 share a high sequence similarity in the motor domain and act by promoting the sliding of anti-parallel iMTs to generate an outwardly-directed force that is important to fulfil their functions in spindle dynamics. Before anaphase onset, Cin8 and Kip1 are required for SPB separation and bipolar spindle formation[55]. During anaphase, the two motor proteins stabilize the spindle midzone[56] and regulate the switch from the fast- to the slow phase of anaphase B spindle elongation[57]. Furthermore, it has been shown that Cin8 levels affect aMT number and length[58,59], although the underlying mechanism is still unknown. Kinesin-5 motor expression is cell cycle-regulated and their expression pattern resembles the one of mitotic cyclins. These motor proteins peak in mitosis and their stability relies on the APC/C ubiquitin-mediated pathway. In particular, Kip1 is degraded at the metaphase to

anaphase transition after being targeted by the APC/C^{Cdc20} [60], while Cin8 is degraded late in anaphase through the activation of APC/C^{Cdh1} [61]. Additionally, Kip1 and Cin8 are regulated by phosphorylation events. On the one hand, CDK directly phosphorylates Cin8 and Kip1, promoting their activity in SPBs separation and bipolar spindle formation[62]. At the metaphase to anaphase transition, instead, Cin8 seems to be directly activated by FEAR-released Cdc14, thus promoting spindle elongation[63]. Additionally, Cin8 localization at the spindle midzone requires Ase1 dephosphorylation by Cdc14.

Kar3 is a kinesin-14 family member characterized by a minus-end-directed motility [53] and is involved in the regulation of both nuclear and cytoplasmic microtubule dynamics. Kar3 produces inwardly-directed forces, antagonistic to the outwardly-directed forces generated by the kinesin-5 motors[64]. Kar3 activity depends on the heterodimerization with either of the two non-motor proteins Cik1 and Vik1, two accessory subunits associated with different cellular functions[53]. Kar3/Vik1 localizes to SPBs, while Kar3/Cik1 mainly concentrates on astral MTs[65]. According to their specific localization pattern, Kar3/Vik1 cross-links and stabilizes parallel MTs at the SPBs, while Kar3/Cik1 slides, stabilizes, and depolymerizes aMTs[66,67].

Kip3 belongs to the kinesin-8 family, controls spindle position, and the timing of spindle disassembly[68,69]. Kip3 possesses a plus-end specific MTs depolymerase activity that correlates with its catastrophe-promoting effect in cells[69]. This motor localizes predominantly on aMTs and SPBs and it has been shown to regulate aMTs length and function[20,70,71], thus influencing spindle- and nuclear positioning. In particular, Kip3 is involved in Bud6-mediated spindle movements in early mitosis[72]. Kip3 randomly binds to the microtubule lattice and moves to aMT plus-ends where it promotes a catastrophe event[69,73], a mechanism of action that intrinsically favors the depolymerization of long rather than short aMTs. Finally, the distal tail region of Kip3 controls its recruitment on the spindle midzone at the end of mitosis, where it promotes spindle disassembly.

Kip2 is a kinesin-related protein whose main function is the regulation of aMT dynamics and function. It has been recently shown that Kip2 association with aMTs starts at their minus-ends, followed by moving to aMT plus-ends where it promotes the stabilization of the microtubule-cap[73]. Additionally, Kip2 serves to target cargo-proteins involved in nuclear- and spindle positioning, such as Bik1 and Dyn1, to aMT plus-ends[53].

Finally, the only microtubule motor protein that does not belong to the kinesin family is the dynein heavy chain Dyn1, a minus-end-directed motor protein that guides the segregation of the bud-directed SPB in late mitosis. Dyn1 forms a complex together with the dynein intermediate chain Pac11, dynein light chain Dyn2 and the dynactin complex which is composed of Nip100, Jnm1 and Arp1. Although in higher eukaryotes dynein is involved in the transport of different cargos on microtubules, in budding yeast it mainly acts associated with the plasma membrane and generates a pulling force on the spindle machinery by moving toward aMT minus-ends. Dyn1 is transported from aMT minus-ends to the cellular cortex in an inactive state by Kip2[74], and its activity is normally kept low until anaphase onset via She1-mediated inhibition[75].

1.3.3. Spindle pole bodies structure, duplication and separation

The SPB is a cylindrical structure embedded in the nuclear envelope, which acts as the MTOC of yeast cells. Listed here are the 5 different layers that can be recognized in the SPB, starting from the nuclear interface: the inner plaque, the central plaque, the intermediate layers 1 and 2 (IL1 and IL2), and the outer plaque[7]. The inner plaque generates iMTs and kMTs, the central plaque anchors the SPB to the nuclear envelope, IL1 and IL2 connect the central plaque to the outer plaque, which in turn nucleates aMTs. The core of the central plaque is primarily composed of Spc42, whose N-terminal associates with the inner plaque component Spc110, while the C-terminal binds Cnm67. Spc110 is directly connected to the nuclear microtubule-nucleating γ-Tubulin Small Complex (γTuSC), composed of Spc97, Spc98 and the yeast γ-Tubulin Tub4, while

Cnm67 links the SPB core to the outer plaque-component Nud1, which in turn is connected to the γTuSC via Spc72.

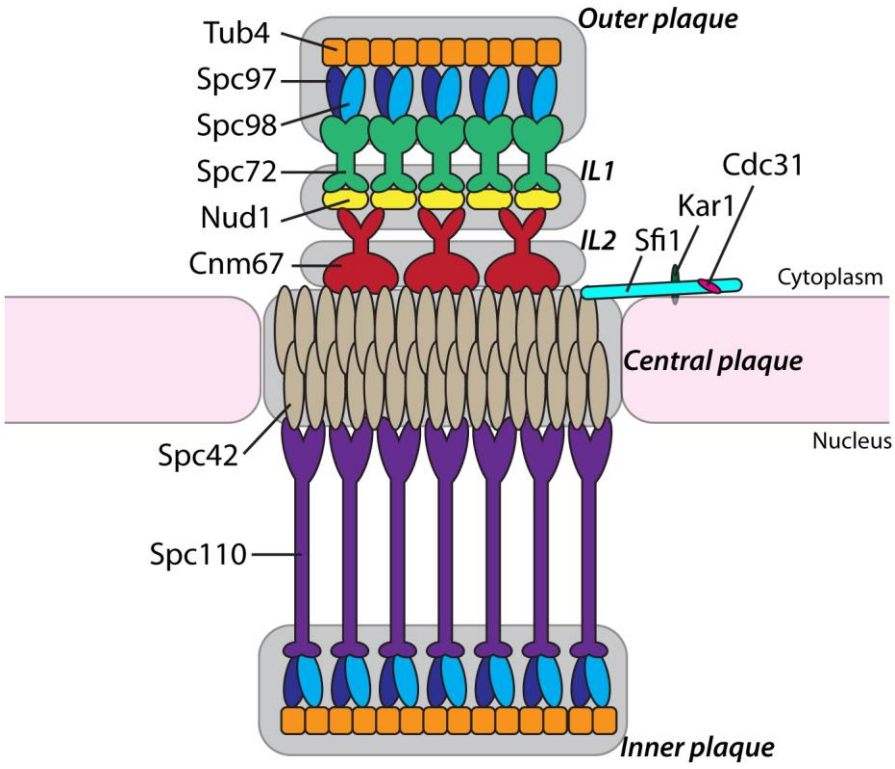

Figure 1.7. The spindle pole body

SPB duplication starts at the end of mitosis, when CDK downregulation and the activation of CDK-counteracting phosphatase Cdc14 set the conditions to elongate the Sfi1 bridge, a filamentous structure bound to the SPB core that faces the cytosol and acts as a platform for its duplication. Other components of the bridge are Kar1, Cdc31 and Mps3[7]. Later on, Mps1-mediated phosphorylation of Sfi1 allows the deposition of the "satellite", an intermediate status of the newly formed SPB containing only SPB core proteins[76]. Outer plaque components were thought to be added to the new SPB in G1/S, prior to both satellite insertion in the nuclear envelope and inner plaque formation[7]. This idea came from the analysis of mutants impaired in satellite insertion, which carried the new SPB with a fully formed outer plaque but lacked the inner plaque components[77]. However, a recent study[78] argued against this view, finding that in *wild-type* cells satellite insertion

and inner plaque formation precede the complete formation of the outer plaque. In addition, this ordered maturation partially depends on Clb5-CDK-mediated phosphorylation of Nud1, since its impairment anticipates outer plaque assembly on the maturating SPB[78]. After SPB insertion in the nuclear envelope, the newly formed SPB have to be separated from each other, a process that involves breakage of the Sfi1 bridge and that usually occurs in late S phase. A clear picture of this process is still lacking, but it probably requires the generation of microtubule-generated forces that physically disrupt the linkage between the two SPBs, probably coming from the forming microtubule bundle that is typical of early spindle assembly. Indeed, several evidences suggest that proteins involved in the formation of the microtubule bundle, in particular the two kinesin-5 motor proteins Kip1 and Cin8 and the MAP Ase1, are fundamental in triggering SPB separation. First, cells lacking Kip1 and Cin8 functions arrest with unseparated SPBs[56]. Secondly, a similar phenotype occurs in cells with an impaired CDK activity due to the aberrant activation of the APC/C^{Cdh1}, which in turn targets Kip1, Cin8 and Ase1 for degradation[79]. Lastly, the expression of a mutated form of Cin8 impaired in its motor activity rescues the phenotype of cells lacking CDK activity, but fails to do so when its microtubule bundling activity is impaired[79]. Once the two SPBs have been separated, CDK- and Cdc5-mediated phosphorylation of Sfi1 prevents the initiation of another round of SPB duplication[80–82]. Importantly, the two SPBs segregate non-randomly: the pre-existing SPB (namely old-SPB) is directed toward the bud cell, while the SPB generated during this particular cell cycle (new-SPB) remains in the mother cells. Non-random segregation of the two MTOCs is a highly conserved process and it has often been connected to the transmission of renewal potential in stem cells[83]. The complex mechanisms that drive this controlled segregation will be addressed in the next chapters.

1.3.4. Kinetochore microtubules

Following SPB separation, kMTs take advantage of the increased microtubule dynamic instability due to the rise in CDK activity[84,85] in order to search for cellular spaces undergoing cycles of growth and shrinkage, until the connection with a kinetochore is established. Upon binding to the kinetochore, two possible scenarios can occur: if the connection produces enough tension, which normally happens in an amphitelic attachment, a kMT plus-end is stabilized, its dynamic instability is suppressed and the connection is enforced; if the connection does not produce enough tension, as in syntelic or monotelic attachments, a tension-sensing mechanism inhibits the connection and promotes kMT shrinkage. This tension-sensing mechanism relies on the Aurora kinase Ipl1, which phosphorylates different kinetochore proteins in order to inhibit kinetochore binding to microtubules[86].

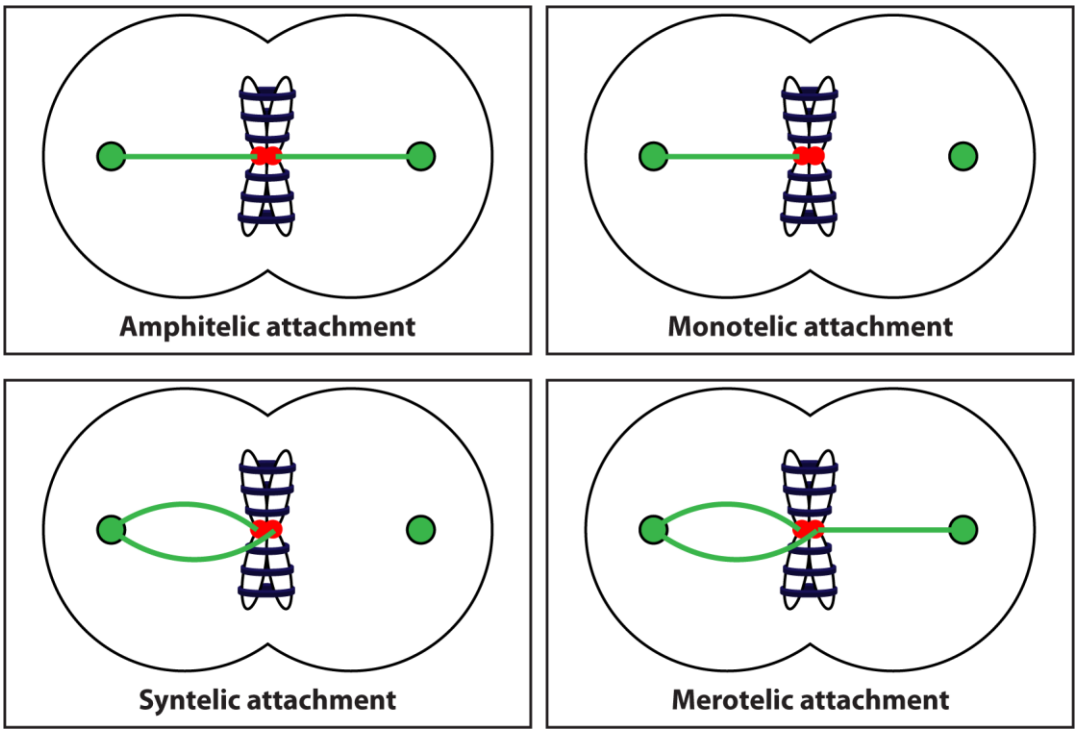

Figure 1.8. Possible types of kinetochore/kMT attachments

The old "search and capture" model proposed that this process is repeated until every sister chromatid pair is bipolarly bound to the spindle, the required condition for SAC

inactivation and hence progression into anaphase. However, mathematical modelling of the process argues that, during the limited time of mitosis, chromosomes cannot reach a bipolar attachment only by relying on the stochastic movements of kMTs, and as such these movements require a bias toward kinetochores[87]. Indeed, a new version of the model takes into account signals coming from the kinetochore, chromatin or centrosome-induced microtubule nucleation and microtubule-mediated microtubule nucleation, which in turn generate the required bias[42]. A RAN-GTP gradient has been shown to form around the chromatin of mammalian cells, which activates different microtubule nucleating factors and hence promoting kinetochore capture[42]. However, the main bias that promotes kinetochore capture in the small budding yeast seems to be mediated by kinetochore attachments to the lateral surface of microtubules, which can be further facilitated by microtubules nucleated from kinetochores[88]. At anaphase onset, kMTs shorten in order to bring each set of chromosomes in close proximity to the connected spindle pole, a process called Anaphase A. In higher eukaryotes, this process is the main driver of chromosome segregation, while budding yeast relies mostly on iMT-mediated spindle elongation[10]. The reason for this discrepancy is probably the different lengths of the mitotic spindle in metaphase, which is only around 2μm in budding yeast, while it is much longer in mammalian cells. kMTs have been shown to depolymerize from both minus-ends and plus-ends depending on the cellular type. In budding yeast, kMT shortening mostly comes from plus-end depolymerization; however, the molecular mechanism coupling the kinetochore with a depolymerizing microtubules is still unclear. In mammalian cells, minus-end-directed motor proteins like dynein may accomplish this task, moving onto microtubules and triggering their depolymerization while binding to the kinetochore. However, in budding yeast, the minus-end-directed motors do not seem to be required[89]. Although other microtubule binding proteins may be involved, an interesting alterative explanation takes into account the fact that in budding yeast, each

kinetochore is bound to a single microtubule, and suggests that the curvature of the depolymerizing microtubule itself may pull the kinetochore toward kMT minus-ends[89].

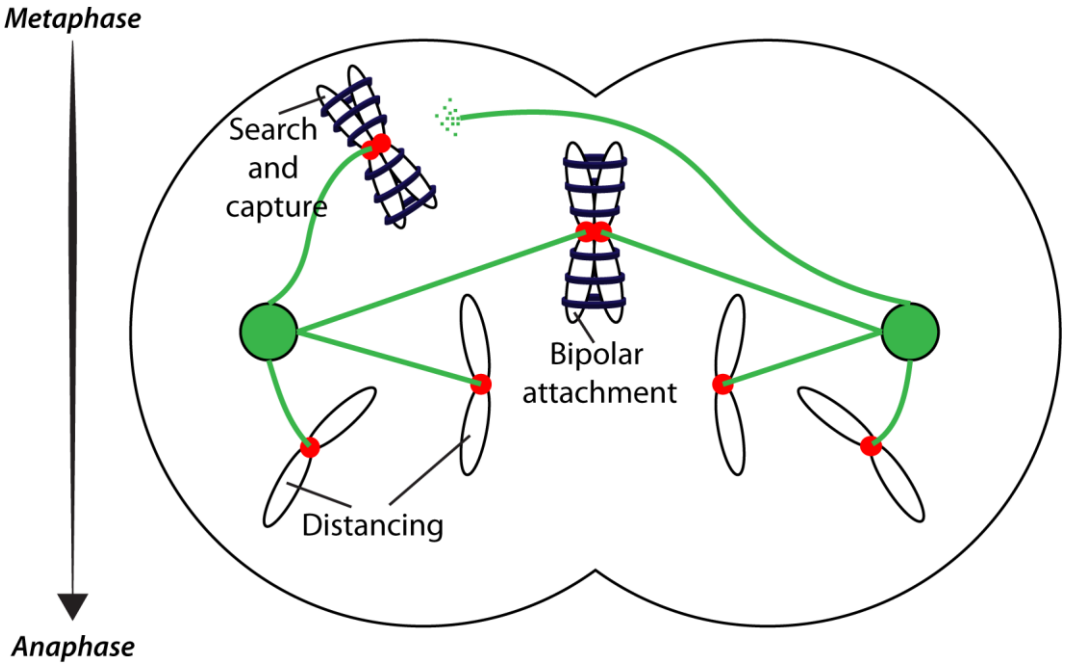

Figure 1.9. Kinetochore microtubules in mitosis

1.3.5. Interpolar microtubules

Although anaphase A occurs even in budding yeast[90], in this model organism, chromosome segregation relies mainly on anaphase B, the process that increases the distance between the two spindle poles. iMTs and aMTs drive anaphase B, generating the pushing force coming from the central part of the spindle and the pulling force generated by cortically bound proteins, respectively. However, at least in budding yeast, aMT-generated pulling forces are not essential for anaphase B completion, as parting of the two SPB can occur even without aMTs[91], and the iMT-generated pushing forces are particular important[10]. Spindle elongation comes in two steps, first a fast elongation phase (around 0.54 μm/min), followed by a slow elongation phase (around 0.21 μm/min)[92]. The first phase is thought to be mainly mediated by the sliding of the two antiparallel sets of iMTs and, as such, is not limited by microtubule growth. In support of this hypothesis,

the first phase lasts until the elongating spindle has reached the double of its metaphase length (from 2/3 to 4/6 μm in metaphase μm). The second phase requires the polymerization of iMTs and their subsequent sliding onto each other, taking the spindle at a maximum length of around 10 μm. The basis of spindle elongation is the stabilization of iMT dynamics at the transition from metaphase to anaphase[47,93], which relies on the correct assembly of the "spindle midzone". This structure is composed of iMTs, MAPs and motor proteins, and is located in the central part of the spindle. The formation of the structure relies on Cdc14 activation, which in turn dephosphorylates several midzone components[46,47]. Indeed, Cdc14 inactivation prevents iMT stabilization at anaphase onset, while its overexpression favors spindle elongation in cells arrested in metaphase when cohesin is ectopically cleaved[93]. In parallel to Cdc14, Cdc5 drastically contributes to spindle elongation. We found that cells lacking the activity of both Cdc14 and Cdc5 arrest with a short spindle length, typical of metaphase cells, although molecularly, the cells are in anaphase as indicated by cohesin cleavage[63]. This result is in line with recent evidences indicating that mitotic kinases cooperate with Cdc14 to drive spindle elongation and other late mitotic events[27].

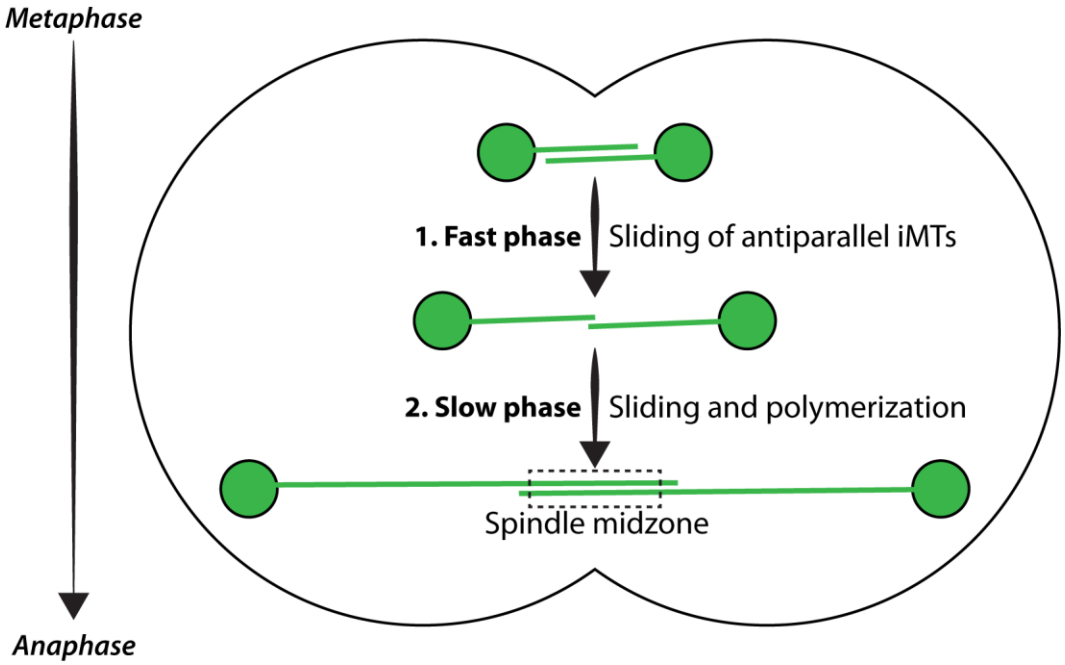

Figure 1.10. Interpolar microtubules in mitosis

1.3.6. Astral microtubules

In budding yeast, aMTs, which are present in every cell cycle phase (around 1-6 aMTs per cell), direct nuclear and spindle movements from the formation of the pre-division site in S phase until the end of mitosis[71,94,95]. In S-phase, the not yet separated SPBs contact the bud-emerging site, also called bud-neck, through few aMTs, and bring the nucleus in its proximity. During metaphase, as the bipolar spindle assembles, aMTs position the nucleus and the old-SPB in close proximity to the bud-neck and orient the spindle along the polarity axis. At anaphase onset, aMTs guide the segregation of old-SPBs to the daughter cell while keeping the new-SPB in the mother cell. In order to accomplish these complex tasks, aMTs need to generate a cortical pulling force and then direct this force where it is needed. This force is generated by two spindle positioning pathways and is affected by astral microtubule regulation established both at the SPBs and at the cellular cortex.

1.3.6.1. Spindle positioning pathways

In budding yeast, two main spindle positioning pathways exist[11]: the Kar9 and the Dyn1 pathways. In the first pathway, the Myosin motor protein Myo2 binds to aMT plus-end protein Bim1 via Kar9, a protein related to the Adenomatous Polyposis Coli (APC) in humans, and pulls the spindle toward the bud by moving on filamentous actin structures called actin cables. The second pathway involves the minus-end-directed motor protein Dyn1, which binds to the cellular cortex and pulls aMTs toward the bud thanks to its motor activity. The Dyn1 pathway can be further divided into two different branches, the canonical and the non-canonical pathway, depending on whether it requires the cortical receptor Num1 or not. While the Kar9 pathway acts in metaphase, the Dyn1 pathway is thought to be mostly active during anaphase. Indeed, the protein She1, which negatively affects both Dyn1 offloading to the cellular cortex and Dyn1 motor-activity, is active up to metaphase and is inhibited at anaphase onset[75]. However, the non-canonical Dyn1 actually acts prior to anaphase onset, and cells lacking Kar9 are still partially able to orient their spindle along the polarity axis in metaphase thanks to Dyn1 activity[38]. How Dyn1 is activated when She1 is inhibited is unclear. One interesting possibility comes from a recent study that has found that Dyn1 activity is promoted by aMT stabilization[96]: on the one hand, Kar9 inactivation is known to increase aMT length[20], and thus may promote Dyn1 activation in metaphase; on the other hand, activation of the non-canonical Dyn1 pathway occurs when aMTs contact the cortex bound protein Bud6, which stabilizes the connected aMTs, and thus may promote an in loco activation of the Dyn1 machinery.

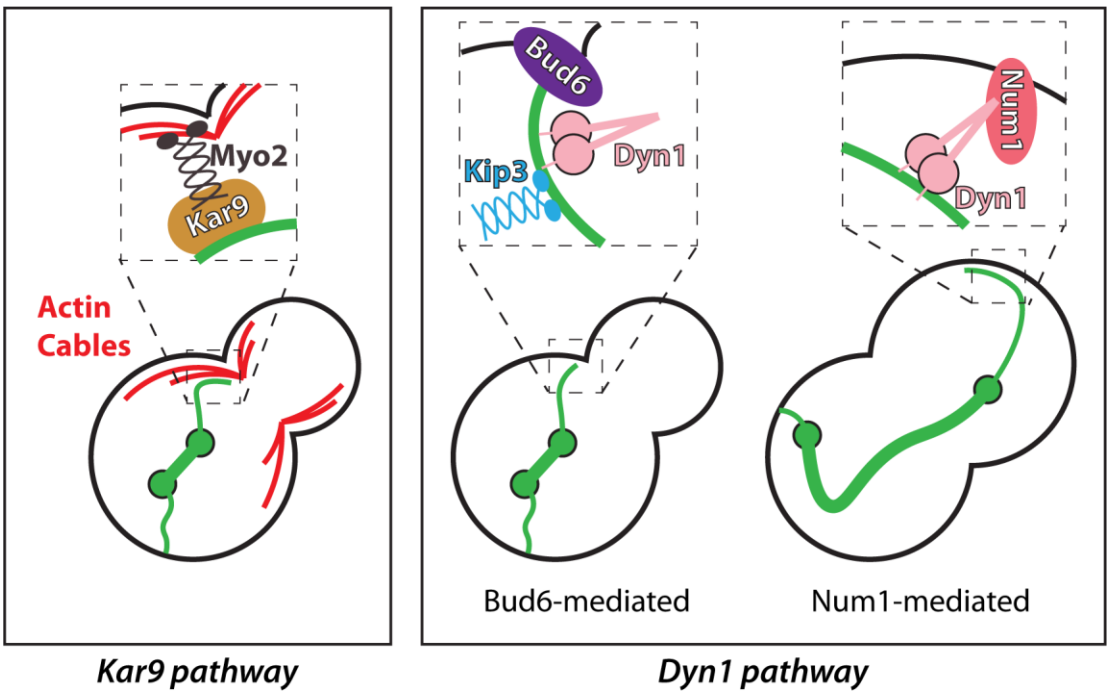

Figure 1.11. The two spindle positioning pathways

1.3.6.2. Astral microtubule regulation at the spindle pole bodies

Before anaphase onset, aMTs generated by the bud-directed SPB appear more numerous and longer than aMTs generated by the mother-directed SPB[97,98], thus favoring the connection of a single SPB to the bud cortex. Two different mechanisms have been proposed to generate this asymmetry, one relying on the different age of the two SPBs[78,99], the other involving SPB positioning over the bud[100].

In around 95% of *wild-type* cells[101], the bud-directed SPB corresponds to the old-SPB, which can nucleate aMTs more proficiently than the newly synthetized one, thus generating the aMT asymmetry. In support of this idea, γ-Tubulin and its outer plaque receptor Spc72 asymmetrically localize on the SPBs of short length spindles, being less abundant on the new-SPB until the spindle is longer than 1μm[78,99], thus suggesting the existence of a maturation lag between the two SPBs. This asymmetric localization is then responsible for the different nucleation capacities, since promoting γ-Tubulin and Spc72 symmetric localization disrupt aMT asymmetric behavior[99]. It was recently proposed that

this maturation lag may not be a mere consequence of the time required for the new SPB to build-up, but that it is actively promoted by Cdk-mediated phosphorylation of the scaffold protein Nud1 in order to set the order of SPB assembly[78]. Indeed, impairment of Cdk-activity abolishes Spc72 asymmetric localization and unifies aMT nucleation capacity[78]. Cells expressing Nud1 mutated in the seven Cdk-consensus sites show a partial impairment in Spc72 asymmetric localization, and prevent Nud1 phosphorylation through Cdk-mediated decrease of Spc72 binding efficiency *in vitro*[78]. Altogether, these results suggest that Cdk activity is polarized toward the old-SPB, which can phosphorylate Nud1 and other targets to promote Spc72, γ-Tubulin and aMT asymmetry. Supporting this idea, M-phase cyclin Clb4 preferentially localizes to the bud-directed old-SPB and aMTs[102,103], and Nud1 does not shuttle much between the two SPBs[100]. However, a clear experiment showing that Cdk activity is polarized toward the bud-directed old-SPB is still lacking. In addition, Cdk1 may also influence aMT dynamics by directly phosphorylating γ-Tubulin. Two independent phospho-proteomic analysis of purified SPBs[104] or isolated γTuSC[105] found many phosphorylated sites on the γ-Tubulin Tub4 that are important for aMT behavior. Cells expressing the Tub4 phospho-mimicking alleles of S74, S100, S360 and Y362 (*tub4-S74E*, *tub4-S100E*, *tub4-S360D* and *tub4-Y362E* cells) show abnormally long aMTs[105,106] independently of whether they are generated by the old or the new SPB[106]. Among these residues, S360 is highly conserved from yeast to humans, it is located on the Cdk consensus motif and has been shown to be directly phosphorylated by Cdk1 *in vitro*[104].

However, at least two observations argue against the idea that aMT asymmetry arises only from the different age of the two SPBs: first, in metaphase spindles longer than 1μm, aMTs are still asymmetric, although Spc72 and γ-Tubulin asymmetry is significantly reduced[78]; second, in *myo2* mutant cells, which randomly orient both SPBs on the mother-bud axis due to a defect in establishing the connection between cortex and aMTs, aMTs

of the bud-directed SPB are more numerous and longer than mother-directed aMTs, independently of age[100]. This result suggests that, in addition to the SPB age-dependent regulation of aMTs, also spatial signals control aMT behavior. The co-existence of age and spatial signals in the control of aMT dynamics is supported by the mechanism underlying the localization of the microtubule growth-promoting kinesin Kip2[53,73,107,108], which is recruited to the SPB in both an age- and position-dependent manner. In properly aligned spindles, Kip2 localization is strongly biased toward aMTs generated by the bud-directed old-SPB[73]. When SPB position is inverted, Kip2 localization is still biased toward aMTs of the old-SPB, even if it is directed toward the mother cell, the asymmetry, however, is less pronounced[73]. This multiple Kip2 regulation is probably due to the different kinases that are known to directly phosphorylate the protein itself: the yeast Glycogen Synthase Kinase 3 Mck1[107], which accumulates at the bud-cortex, Cdk, Dbf2 and Dbf20 kinases. Overall, Kip2 phosphorylation seems to prevents its random landing on the microtubule lattice in favor of the specific recruitment on the bud-directed old-SPB[73].

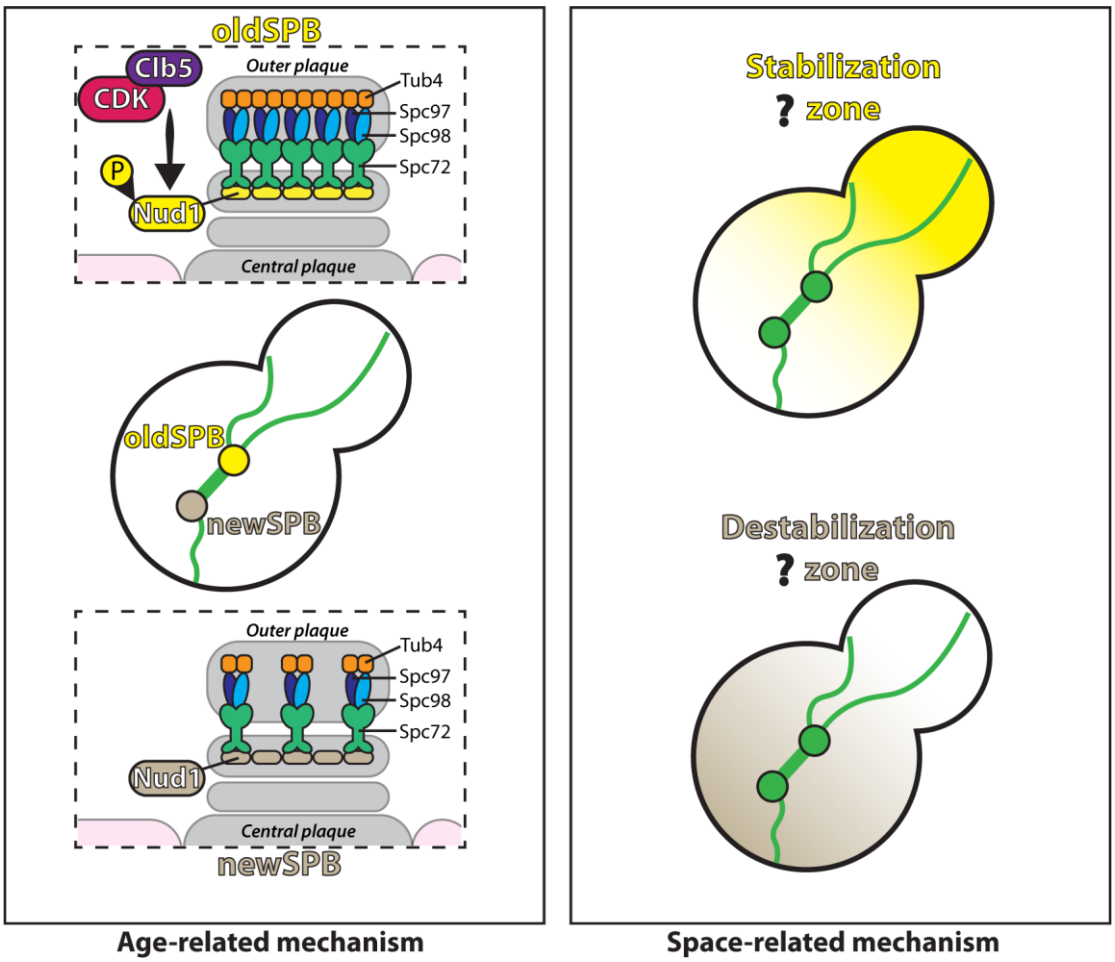

Figure 1.12. Mechanisms governing aMT asymmetry

1.3.6.2.1. Regulation of Kar9 localization

In addition to controlling aMT dynamics, SPBs act as platforms to regulate the localization of proteins associated with aMTs and that are involved in the spindle positioning process. One of these proteins is Kar9, which preferentially binds to the bud-directed old-SPB[98,102]. Kar9 is transported to aMT plus-ends by the kinesin motor protein Kip2[102], where it associates with Myo2[109]. Importantly, cells lacking Kar9 erroneously segregate the new-SPB in the daughter cell in around 40% of cases[101,110], indicating that Kar9 is a fundamental protein in the guidance of the non-random segregation of the two SPBs. Thus, it is not surprising that Kar9 localization is highly regulated, both in the preferential loading of Kar9 to the old-SPB and in the maintenance of this asymmetry. A recently described protein network called SPB Inheritance Network (SPIN) distinguishes

the old from the newly generated SPB that phosphorylates Nud1 during G1[111], when the new-SPB is not yet formed (for an in depth review on the SPIN see[83]). This phosphorylation event favors the association of the Bfa1-Bub2-Tem1 complex to the old-SPB, which in turn specifically recruits Kar9[111,112]. However, how this specific recruitment works is still unclear. Given that the Bfa1-Bub2-Tem1 complex acts as an inhibitor of the MEN cascade, an hypothesis is that its restriction on the old-SPB could polarize MEN activity on the new-SPB, which in turn could prevent Kar9 binding[83]. In support of this hypothesis, MEN inactivation negatively affects Kar9 asymmetry and consequently the non-random segregation of the two SPBs[110]. Furthermore, the MEN kinase Dbf2 directly phosphorylates Kar9, and mutations on the putative residues impair Kar9 specific localization on the old-SPB[110]. However, a direct proof that MEN activity is restricted on the new-SPB up to metaphase and that this restriction is involved in Kar9 asymmetry has yet to be shown. In addition to SPB-age, also spatial cues influence Kar9 localization. Indeed, transient depolymerization of microtubules by nocodazole treatment, which randomizes SPB age[113], induces the symmetric loading of Kar9 on both SPBs, followed by its re-localization on the bud-directed SPB[114]. In this re-localization process, polarity factors and the actin cytoskeleton play an important role[114], indicating that aMT-cortex interactions influence Kar9 localization. On the same line, in *kip2* delta cells, where SPB inheritance is partially perturbed (2% of *wild-type* cells segregate the new SPB into the bud [101], compared to 19% of *kip2 delta* cells[102]), Kar9 associates with the bud-directed SPB independently of its age[102]. Given the different nucleation capacity of the two SPBs in the early stages of mitosis[99], aMT-cortex interaction could promote the preferential binding of Kar9 to the old-SPB, representing an alternative mechanism to the SPIN-mediated SPB specification. Interestingly, the importance of one mechanism over the other correlates with the mechanism that generates aMT asymmetry. In the strain background where aMT polymerization is favored by the proximity of the SPB to the

bud-neck (rather than SPB age), Kar9 asymmetry is poorly altered by aMT-cortex interactions since it remains almost unaffected by Myo2 inactivation[100]. On the contrary, in the strain background where SPB-age intrinsically affects aMT asymmetry[99], Myo2 inactivation significantly affects Kar9 asymmetry[114]. These observations suggest that it is convenient for the cell to have the two mechanisms generating aMT- and Kar9 asymmetry working in parallel rather than on the same pathway.

Kar9 localization is also regulated by Cdk activity. Cdc28 associates with SPBs and aMTs[102], and its localization on aMTs requires Kar9, while its association with SPBs does not[102]. Inactivation of Cdc28, or usage of strains that lack the cyclin subunits Clb4 and Clb5, alone or in combination, increases the percentage of cells with symmetric Kar9 on the two SPBs[98,103,115,116], indicating that Cdk-Clb4 and Cdk-Clb5 regulate Kar9 localization. How is the localization of Kar9 regulated? It has been proposed that Cdk-Clb4 and Cdk-Clb5 regulate Kar9 asymmetry directly by phosphorylating serine 197 and serine 496, respectively. Indeed, while mimicking the phosphorylation on S197 partially rescues Kar9 localization defects observed in *clb4* delta cells, it does not affect *clb5* delta cells[115]. On the same line, mimicking the phosphorylation on S496 rescues Kar9 localization defects observed in *clb5* delta cells, but has no effect on *clb4* delta cells[115]. Phosphorylation of S197 reduces Kar9 affinity for the SPB-associated protein Stu2[51,115], suggesting that Cdk-Clb4-mediated phosphorylation of Kar9 could regulate its localization by modulating its binding affinity for the SPBs. However, a more complex situation emerged: S197 is probably one of the residues that are phosphorylated by Dbf2 and Dbf20 kinase[110], the MEN effector that is involved in Kar9 asymmetry, arguing that Cdk-Clb4 could not only directly phosphorylate Kar9, but even promote its MEN-mediated phosphorylation. Furthermore, while in *wild-type* cells Kar9 mostly localizes on SPBs and aMT plus-ends, *clb4* delta cells are characterized by a disperse localization of Kar9 on the entire aMT length, a phenotype that is not even recapitulated in cells

expressing Kar9 that is mutated in all of the Cdk consensus sites[117]. In addition, impairment of the activation of the SAC rescues Kar9 localization defects observed in *clb5* delta cells through MEN activation[116], suggesting that the effect of Cdk-Clb5 on Kar9 asymmetry could be mediated by SAC modulation, which in turn affects MEN activity. Altogether, these results point to that both Cdk-Clb4 and Cdk-Clb5 might regulate Kar9 localization by acting directly on Kar9 or indirectly by other means.

Finally, Kar9 is also regulated by the attachment of Small Ubiquitin-related Modifiers (SUMO). This post-translation modification called SUMOylation involves an enzymatic cascade that results in the formation of an isopeptide bond between the SUMO molecule and the substrate acceptor Lys residue[118]. Importantly, SUMOylation regulates several cellular processes such as DNA replication and repair, nuclear import/export and chromosome segregation[118]. Kar9 directly interacts with proteins of the SUMO pathway[119], and has been shown to be SUMOylated both *in vitro*[119] and *in vivo*[120]. Prevention of Kar9 SUMOylation, as well as disruption of its interaction with the SUMO machinery, results in symmetric localization of Kar9 and generates spindle orientation defects[119,120], indicating that SUMOylation of Kar9 directly affects its functions. Furthermore, SUMOylation of kinetochore-related proteins is involved in Kar9 regulation, first, because it is involved in the correct assembly of the spindle[120], the fundamental requirement for SAC inactivation that promotes Kar9 asymmetry, and secondly, because of its involvement in the control of Kar9 protein levels, which is fundamental for correct spindle positioning and chromosome segregation[121].

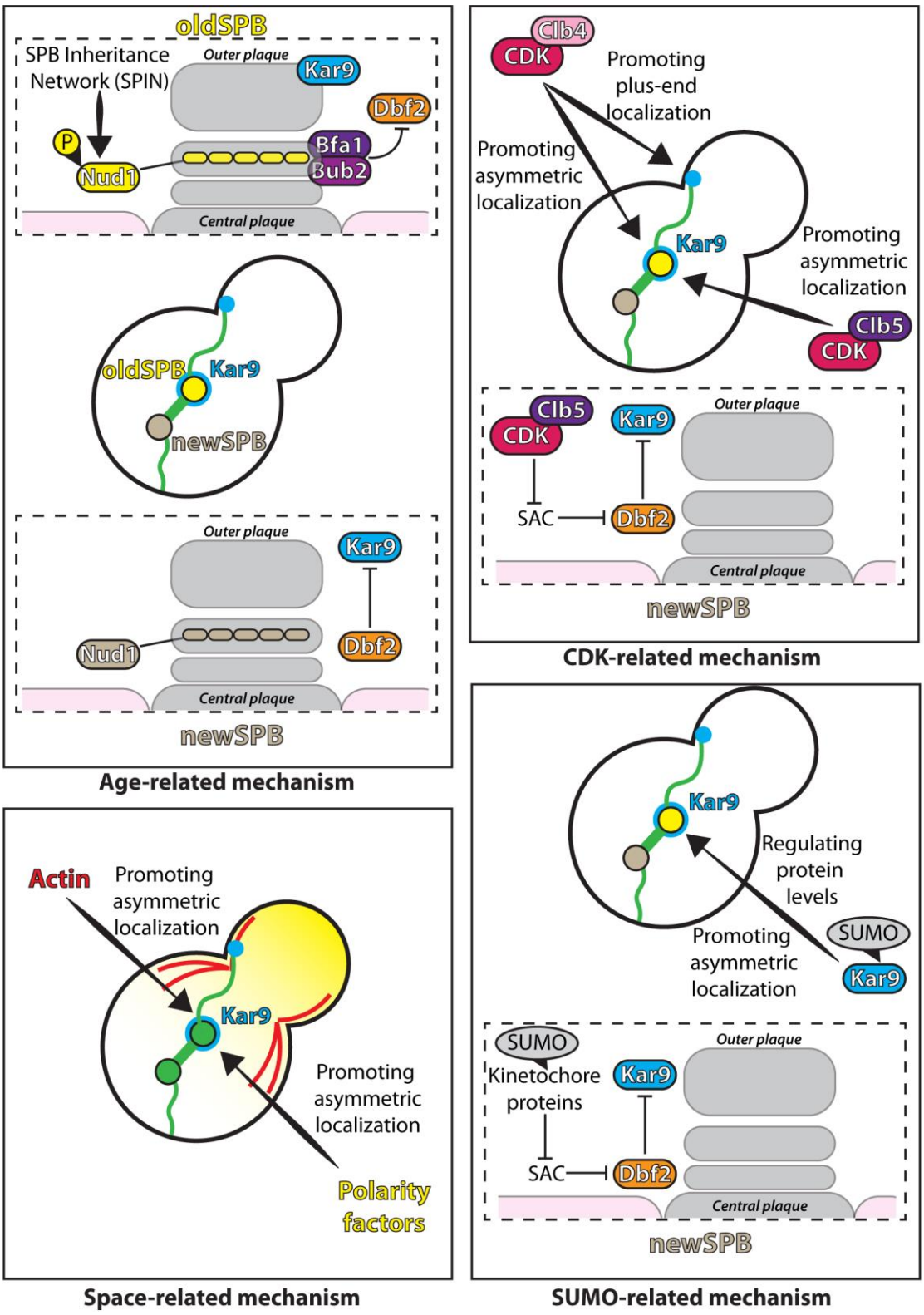

Figure 1.13. Mechanisms governing Kar9 asymmetric localization

1.3.6.2.2. Regulation of Dyn1 localization

Like Kar9, Dyn1 preferentially localizes to the bud-directed SPB[122,123]and is transported to aMT-plus ends by Kip2. Once there, Dyn1 generally binds to the plasma membrane receptor Num1 and pulls the spindle thanks to its minus-end-directed motor activity[124]. In order to correctly accomplish this task, Dyn1 asymmetric localization on bud-directed SPBs and aMTs is an essential prerequisite[123]. Different to Kar9, the establishment of Dyn1 asymmetry does not depend "*per se*" on the age of the SPB, as suggested by the unperturbed segregation of the old-SPB in the bud in *dyn1* cells[125] and by the almost complete randomization of age-dependent SPB segregation in *kar9* cells[101]. Instead, Dyn1 specific localization on the bud-directed SPB and aMTs relies on the interplay between the Cdk that is located on SPBs and cortical cues. Cdk acts in association with the M-phase cyclins Clb1 and Clb2, while cortical cues are provided by the bud-neck kinases Elm1, Hsl1 and Gin4, as indicated by the loss of Dyn1 asymmetry in *cdc28, clb1 clb2* and *elm1 hsl1 gin4* mutant cells[123]. In particular, Cdk activity seems to negatively affect Dyn1 attachment to the mother-directed SPB, as in *cdc28* and *clb1 clb2* mutant cells the amounts of Dyn1 on both SPBs (mother-directed SPB and bud-directed SPB) is as high as that on bud-directed SPB of *wild-type* cells[123]; in contrast, bud-neck kinases probably promote the specific recruitment of Dyn1 on the bud-directed SPB, as suggested by the low amounts of Dyn1 on both SPBs in *elm1 hsl1 gin4* mutant cells[123]. However, a clear characterization of the mechanism that generates Dyn1 asymmetry is still lacking. Cells lacking the outer plaque receptor Cnm67 recapitulate the phenotype of *clb1 clb2* cells, but cells expressing the non-phosphorylatable allele of *CNM67* mutated in the 8 putative Cdk motifs (Cnm67-8A) do not, arguing against its role in the process as a Cdk-target. Instead, *cnm67* mutant cells show a decreased amount of Clb2 on both SPBs[123], suggesting that it may act as a scaffold protein for Clb2 anchorage to the SPB. In conclusion, further research is required to clarify the mechanism of both Cdk- and bud-

neck kinases-mediated regulation of Dyn1 asymmetry, starting from identifying their target/s involved in the process.

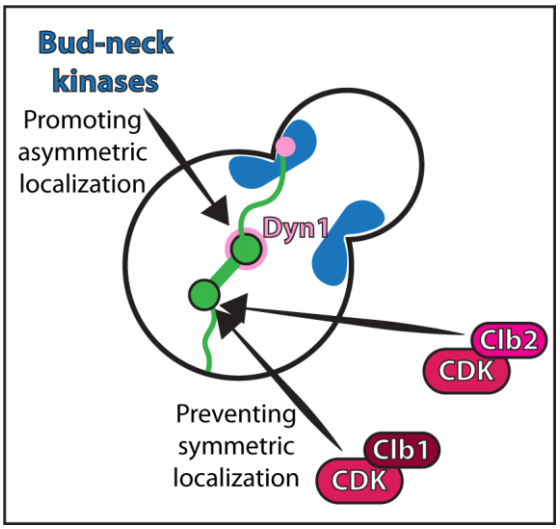

Figure 1.14. Mechanisms governing Dyn1 asymmetric localization

1.3.6.3. Astral microtubule regulation at the cellular cortex

In many different organisms, the cellular cortex acts as a fundamental platform for the regulation of various processes, such as organelle segregation, spindle positioning and cytokinesis. In budding yeast, the cascade of events that finely tunes the position of the spindle starts in late G1, when the pre-division site is selected based on the position of the division site of the previous cell cycle[126]. From this point on, the emerging bud-site will be recognized by different polarizing proteins that, following cell cycle progression, will achieve bud development. As the bud grows, some of these polarizing proteins lead to the compartmentalization of the cellular cortex, thus creating different structures, such as the bud-neck and the bud-tip, that will be recognized by different proteins involved in spindle positioning and that will add the spatial layer of regulation in the spindle positioning process. Furthermore, the localization of many spindle positioning proteins changes over time, thus connecting the spatial layer of regulation with the temporal one[103,127,128]. Similar to SPBs, the cellular cortex influences aMT behavior through the

regulation of proteins that bind to them and that control their dynamics. However, while SPB-mediated regulation often involves the whole population of aMTs generated by that particular SPB, cortex-mediated regulation is normally restricted to a single aMT that normally contacts the cortex for a short period of time. In budding yeast, three cortical proteins mediate aMT binding to the cellular cortex, and are thus involved in the regulation of aMT dynamics: the actin interacting protein Bud6, the actin motor protein Myo2 and the cortical receptor Num1.

1.3.6.3.1. Bud6-mediated

One of the first cortex-bound proteins that influences aMTs is the actin interacting protein Bud6, which was initially identified as a protein involved in the maintenance of budding patterns[129]. Bud6 has at least three fundamental roles in the regulation of spindle positioning. First, Bud6 directly binds and regulates aMTs. Already in G1, Bud6 localizes at the previous division site and promotes the interaction of aMTs with the cellular cortex[20,95]. Once the next division site has been selected, Bud6 accumulates at the tip of the emerging bud and attaches to the plus-end protein Bim1, favoring thus their stabilization[130]. The length of aMTs is then under the control of the kinesin motor protein Kip3, which associates with the growing aMT plus-end and triggers a catastrophe event [69,130], as suggested by the increased aMT length in *kip3* delta cells that relies on Bud6 [130]. When Dyn1 is present on the Bud6-attached plus-end (in around 30% of the Bud6/aMT connection events), a non-canonical version of the Dyn1 pathway (i.e., it does not require the plasma membrane protein Num1, but another unknown cortical receptor) generates a pulling force that brings the connected SPB closer to the emerging bud[130]. Importantly, as the bud grows, Bud6 detaches from the bud-tip and accumulates at the bud-neck, preventing aMT binding too far away from the mother cell compartment before anaphase onset[20,127]. Secondly, Bud6 is an important player of the Kar9 pathway. Bud6 acts as an actin nucleation-promoting factor[131] that together with the formins Bni1 and Bnr1

generates structures called actin cables, which are bundles of actin filaments that extend from the bud-neck to the bud-tip and that are essential for the Kar9 pathway[109,132]. Thirdly, in late anaphase, Bud6 forms a barrier at the bud-neck that depolymerizes aMTs that cross the division site[95]. Given the high Dyn1 activity present in anaphase, this barrier maintains the two segregated SPBs in the two different cellular compartments, preventing the generation of aneuploid cells.

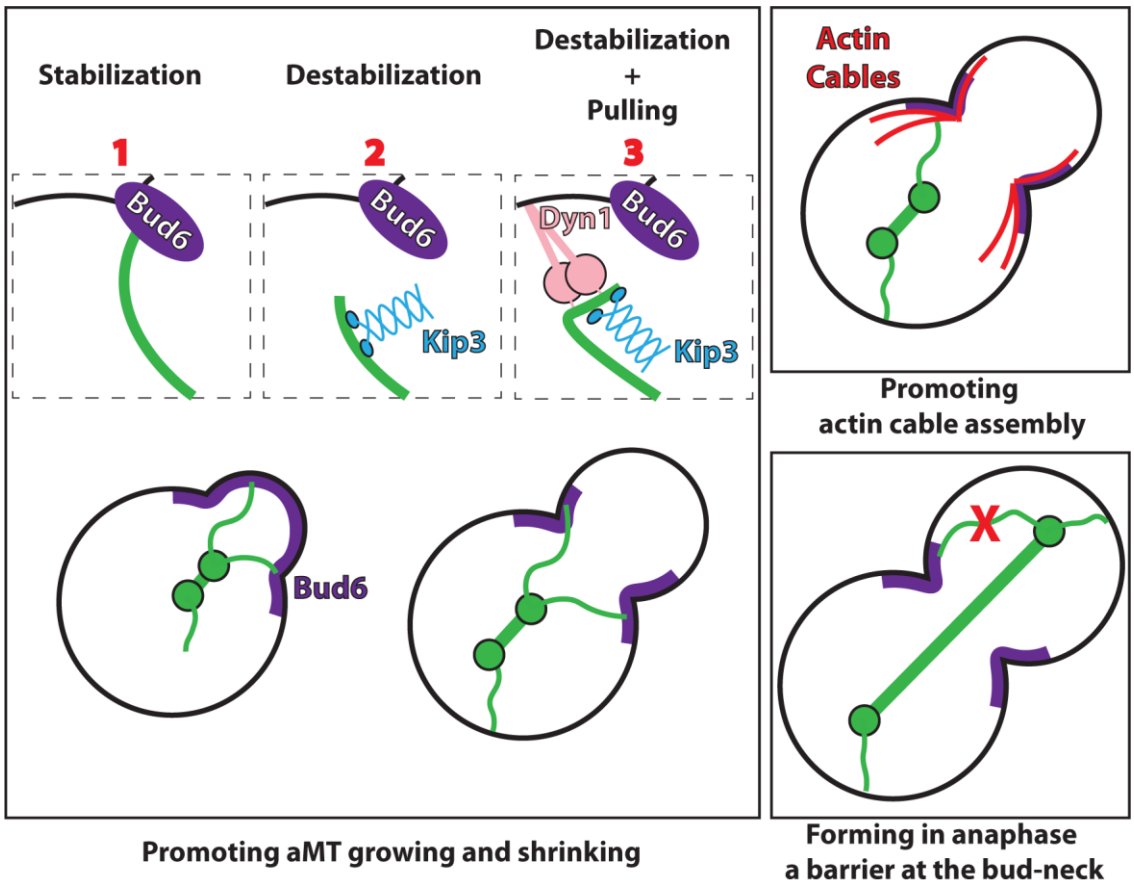

Figure 1.15. Bud6-mediated regulation of aMT dynamics

1.3.6.3.2. Myo2-mediated regulation

As mentioned above, aMTs associate with the actin cytoskeleton thanks to the plus-end protein Kar9, which directly binds Myo2. This motor protein maintains the spindle next to the bud-neck and orients it along the polarity axis until anaphase onset by moving onto actin cables, structures that are normally lacking in the mother cell cortex, thus providing

directionality to the Myo2-generated pulling force[133]. Similar to Bud6 re-localization from the bud-tip to the bud-neck, Myo2-mediated binding of aMTs to the bud-tip decreases in S phase thanks to Clb4-Cdk activity[102,103], probably preventing unscheduled entry of the spindle into the bud. However, it remains unclear whether Myo2-mediated movements on actin cables directly regulates aMT dynamics, and whether this regulation affects spindle orientation. Since Myo2 does not move on aMTs, it makes sense thinking that to actually generate the pulling force, either Myo2 should move faster than aMT polymerization or its binding to aMTs must somehow prevent their elongation. In line with this last hypothesis, *myo2* mutant cells, as well as other mutants of the Kar9 pathway, are characterized by abnormally long aMTs, suggesting that the Kar9 pathway somehow decreases aMT stability[20]. A seminal study[109] found that bud-directed aMTs decorated with Kar9 were often associated with shrinking events, suggesting that the Kar9 pathway could even promote aMT shortening. Furthermore, *KIP3* deletion is lethal in *dyn1* mutant cells[134], indicating that the depolymerizing kinesin Kip3 may be important for the correct functionality of the Kar9 pathway. However, this idea was never explored in depth, probably because Dyn1 resulted to play the major role in the generation of pulling forces coming from the shrinkage of cortically-bound aMTs[20]. In addition to a direct destabilization of the aMT plus-end bound to Myo2, the motor protein may alter aMT dynamics guiding the microtubule toward proteins that promote its depolimerization. In line with this, it has been reported the existence of a shrinking-promoting zone around the bud-neck that requires septin-dependent kinases and whose functionality positively affects Myo2-mediated spindle positioning[135]. In conclusion, further experiments are required to define if and how aMT binding to the actin cytoskeleton affects aMT dynamics.

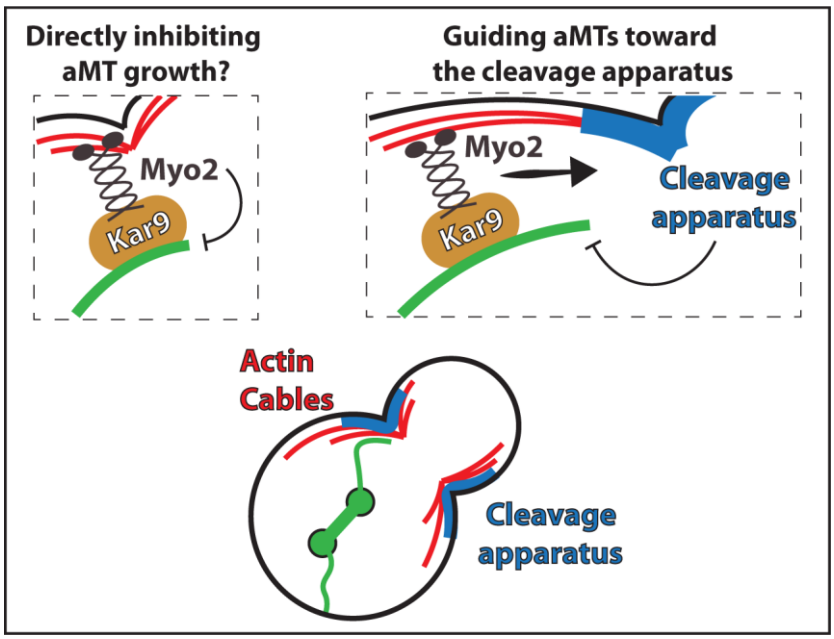

Figure 1.16. Myo2-mediated regulation of aMT dynamics

1.3.6.3.3. Num1-mediated regulation

Finally, the canonical Dyn1 receptor Num1 critically affects aMT behavior at the cellular cortex. Num1 localization is normally restricted to the mother cell until the onset of mitosis[128], thus preventing the activation of canonical dynein in small budded cells, where the non-canonical Dyn1 pathway is primarily active[130]. In addition to its Dyn1-binding role, Num1 attaches to different organelles and regulates their segregation to the newly formed cells, thus leading to the hypothesis that Num1 could form a complex cortical platform that comes in contact with Dyn1 and other organelles, such as mitochondria and the Endoplasmic Reticulum (ER). In support of this hypothesis, Num1 assembly in cortical clusters results critical for proper Dyn1 activation[136], and it requires the presence of mitochondria[137]. As such, cells that lack mitochondria or are impaired in their segregation to the bud show defects in Dyn1-mediated spindle positioning[137]. Once connected, Num1 promotes Dyn1 activity not only by attaching it to the cell cortex, but also by actively promoting its offloading and removing the dynein inhibitor Pac1[74]. In turn, cortically bound Dyn1 moves on aMTs, thus pulling the spindle toward the cortex.

It has been recently shown that this Dyn1-mediated pulling can be associated with aMT shrinkage depending on the type of Num1 bound to Dyn1[138]. In particular, this study found that two different pools of Num1 exist: one is located on the lateral bud cortex, requires the association with the ER (it relies on the presence of the ER tethering proteins Scs2 and Scs22), and does not generate aMT shrinkage; the other assembles at the bud tip, does not require the association with either the ER or mitochondria, and induces aMT shortening. Although the sole activity of the bud-tip-associated pool generates a sufficient pulling force to guide the spindle toward the bud, it decreases spindle oscillations between the mother and the bud in S phase-arrested cells, indicating that the presence of both pools increases the efficiency of the Dyn1 pathway[138]. An interesting question is how the canonical pathway induces aMT shrinkage. In the non-canonical Dyn1 pathway, aMT shrinkage is mainly mediated by Kip3 activity[130]. However, aMT shrinkage events mediated by the canonical Dyn1 pathway are unaffected by *KIP3* deletion, or the deletion of the other microtubule-depolymerizing motor Kar3[138], indicating that, in addition to the different cortical receptor, the two Dyn1 pathways do not even share the same aMT-depolymerizing mechanism. Instead, Dyn1 itself is directly involved in the aMT-shortening events of the canonical pathway. Indeed, Dyn1 destabilizes aMTs both *in vitro*[139] and *in vivo*[96]. Furthermore, the expression of a *DYN1* allele defective in ATP binding causes a loss in aMT shrinkage events at the bud-tip, although Dyn1-mediated aMT/bud-tip interactions last three times longer than in *wild-type* situation[138].

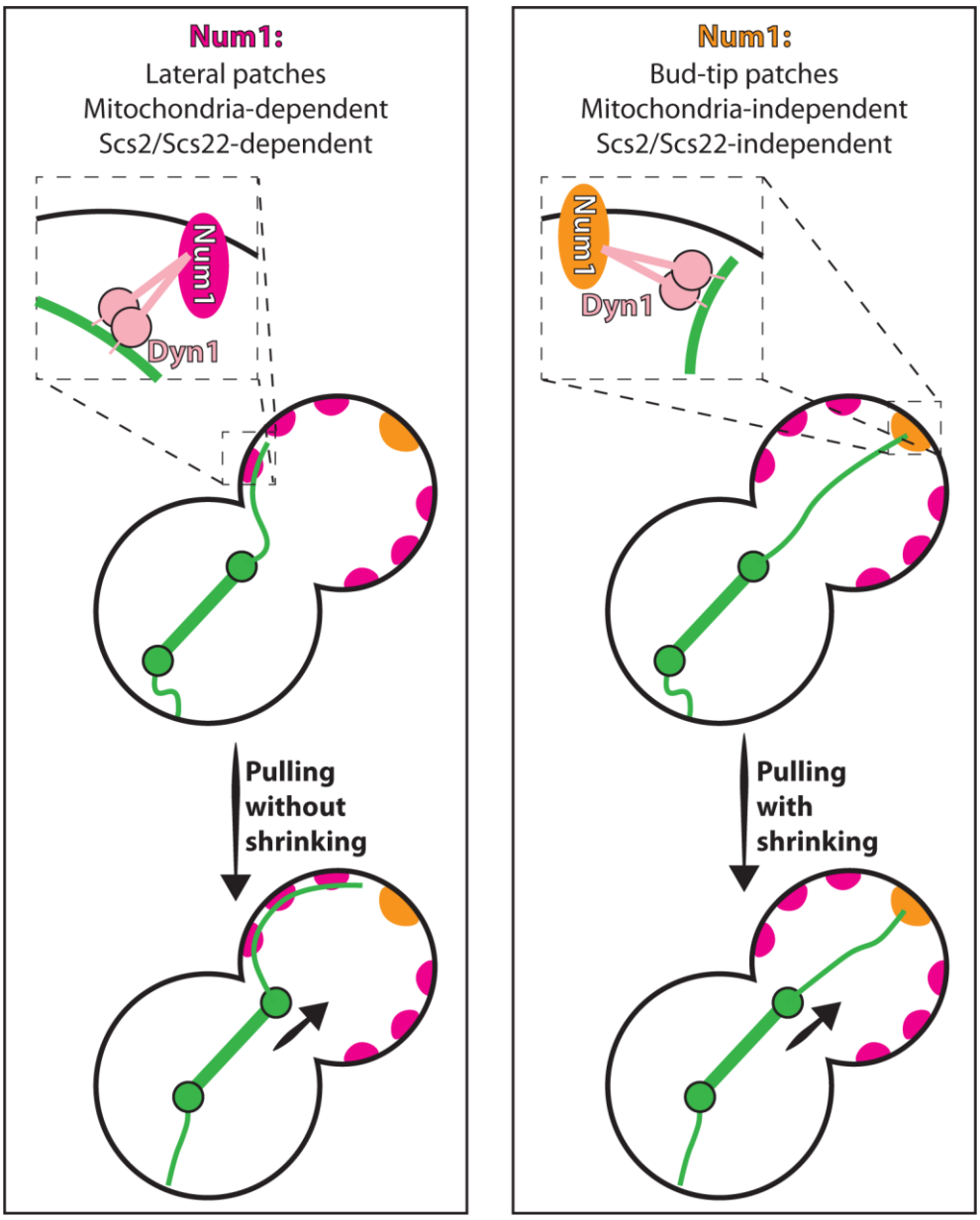

Figure 1.17. Num1-mediated regulation of aMT dynamics

2. MATERIALS AND METHODS

2.1. Strains and plasmid

All the *Saccharomyces cerevisiae* yeast strains used in this study are isogenic to the W303 (*ade2-1, can1-100, trp1-1, leu2-3,112,his3-11,15, ura3*) background except for the mating type tester strains Ry72 and Ry73. The majority of the strains were generated by dissecting sporulated heterozygous diploid strains obtained by crossing haploid strains of opposite mating type (see **section 2.4.1** for procedure). The relevant genotypes of the strains used are listed in **Table 2.1**.

The only plasmid used in this study is Rp345 (*Yiplac128/GAL-SCC1-R180D/R268D*), which contains the non cleavable form of Scc1 and was first published in ref. [30].

2.2. Media and growth conditions

2.2.1. Media for *Saccharomyces cerevisiae*

Yeast cells were grown in rich medium (YEP) or synthetic minimal medium (SC).

YEP: 1% yeast extract
2% bactopeptone
0.015% L-tryptophan
pH 5.4

YEP was supplemented with 300 µM adenine and either 2% glucose (YEPD), or 2% raffinose (YEPR) or 2% raffinose and 2% galactose (YEPRG) as carbon sources. For solid media 2% agar (DIFCO) was added to the medium.

SC: 0.15% yeast nitrogen base (YNB, DIFCO) without amino acids and ammonium sulfate.
0.5% ammonium sulfate
200 nM inositol

SC was supplemented with 2% glucose (SCD). For solid media 2% agar (DIFCO) was added to the medium.

All strains were grown at 23°C unless otherwise stated. Growth conditions for individual experiments are described in the corresponding figure legend.

2.2.2. Media for *Escherichia coli*

Bacterial cells were grown in Luria Broth (LB) medium.

LB: 1% bactotryptone (DIFCO)
0.5% yeast extract (DIFCO)
1% NaCl
pH 7.25

LB was supplemented with 50 µg/ml ampicillin (LB + amp). For solid media 2% agar (DIFCO) was added to the medium. All strains were grown at 37°C.

2.3. DNA-based procedures

2.3.1. *Escherichia coli* transformation

50 µl of fresh chemically competent Top10 cells (genotype: *F-mcrA Δ(mrr-hsdRMS-mcrBC) φ80lacZΔM15 ΔlacX74 nupG recA1 araD139 Δ(ara-leu)7697 galE15 galK16 rpsL(StrR) endA1 λ*) were thawed on ice for approximately 10 minutes prior to the addition of plasmid DNA or the ligation mixture. Cells were incubated with DNA on ice for 30 minutes and then subjected to a heat shock for 30-45 seconds at 37°C. After the heat shock, cells were returned to ice for 2 minutes. Finally, 950 µl of LB medium was added to the reaction tube. Cell suspension was incubated on a shaker at 37°C for 45 minutes before plating onto LB + amp plates. Plates were incubated overnight (ON) at 37°C.

2.3.2. Plasmid DNA isolation from *Escherichia coli* (mini prep)

Clones picked from individual colonies were used to inoculate 2 ml LB + amp and grown ON at 37°C. Next morning, bacterial cells were transferred to micro-centrifuge tubes and pelleted for 5 minutes at 8000 rpm. Minipreps were performed with the QIAprep Spin Miniprep Kit (Quiagen) following the manufacturer's instructions. Plasmids were eluted in 30µl of sterile double-distilled water (ddH_2O).

2.3.3. High efficiency LiAc-based yeast transformation

10X TE:	0.1 mM Tris, bring to pH 8.0 with HCl 10 mM EDTA pH 8
10X LiAc:	1 M LiAc, bring to pH 7.0 with acetic acid
1X TE/LiAc:	1X TE 1X LiAc
1X PEG/TE/LiAc:	1X TE 1X LiAc 40% PEG 4000

Yeast cells were grown ON in 50 ml of YEPD or of the appropriate medium allowing them to reach the stationary phase. Next morning the cell culture was diluted to OD_{600} = 0.2 and allowed to grow until it had reached an OD_{600} of 0.4-0.7. Cells were then harvested at 3000 rpm for 3 minutes and washed with 50 ml of ddH_2O. The pellet was then transferred to an eppendorf tube with 1 ml of ddH_2O and washed with 1 ml of 1X TE/LiAc solution. Cells were then resuspended in 250 µl of 1X TE/LiAc solution. 50 µl aliquots of competent cells were used for each transformation reaction and added with 300 µl of 1X PEG/TE/LiAc solution, 5 µl of 10 mg/ml single-stranded salmon sperm denatured DNA and "x" µl (max up to 10 µl) of DNA. After gentle mixing, the transformation reaction was incubated on a rotating wheel for 30 minutes at room

temperature (RT). Cells were heat-shocked at 42°C for 15 min and then centrifuged for 3 minutes at 3000 rpm. The pellet was resuspended in 200 µl of 1X TE and the cell suspension was plated on the appropriate auxotroph selective medium.

2.4. Yeast procedures

2.4.1. Tetrads dissection and analysis

Digestion mixture: 198 µl ddH_2O

2 µl of 10 mg/ml zymolase 100T (Seikagaka, Biobusiness)

Sporulation plates: 30 g K-Acetate

60 g Agar (DIFCO)

all amino acids at 1/4 of the normal concentration up to 3l with ddH_2O

MATa and *MATα* strains were mixed on solid medium, appropriate for the growth of both the haploids, and incubated ON at permissive conditions. The next day, cells from the cross mixture were streaked to single colonies on selective medium and incubated at the appropriate temperature, allowing for the selection of diploid cells. Single colonies grown under selective conditions were next amplified on rich media and let grow for 1 day. This step greatly increases the efficiency of sporulation. The next day diploids were patched onto sporulation plates to induce meiosis and sporulation by starvation. After 3-5 days, when diploids had efficiently sporulated and maturated, tetrads were dissected. To separate individual spores the wall of the ascus or tetrad was removed by enzymatic digestion. A toothpick full of tedrads was resuspended into the digestion mixture and the digestion mixture incubated at 37°C for 3 minutes. Next, 1 ml ddH_2O was added to dilute the mix and 20 µl were dripped in a line onto the appropriate agar plate. Individual tetrads were dissected using the Nikon dissection microscope. Spores were left to grow at 23°C

for 3-5 days. Colonies were replicated onto selective media plates to define their genotype.

2.4.2. G1 phase synchronization and release

Cells were grown ON in the appropriate medium at 23°C in a water shaking bath. The day after, cells were diluted to OD_{600} = 0.2 in fresh medium and let grow for 2 hrs. Cells were then diluted back to OD_{600} = 0.2 and added with 5 μg/ml α-mating factor synthetic peptide dissolved in ddH_2O (Primm). After 90 minutes of incubation, 2.5 μg/ml of α-factor was re-added to the culture. The G1 arrest was considered complete when more than 90% of the cells were unbudded. When the arrest was complete, cells were released from the G1 block. The α-factor was washed out by filtration, using between 5 to 10 volumes of fresh medium lacking the pheromone. Cells were next released into the appropriate fresh medium in the absence of the pheromone (REF Angelika synchronization procedures).

2.4.3. Regulation of gene expression

To regulate the expression of specific proteins we used yeast strains in which the encoding genes of the protein of interest were cloned under the control of inducible or repressible promoters, such as the *pGAL1-10* promoter[140] and the *pMET3* promoter[141] or placed under the control of the auxin-based degron system[142].

The *pGAL1-10* promoter is an inducible promoter that drives the expression of a fused-gene upon the addition of galactose (usually at 2%) to the growing media. Since the promoter is repressed by glucose, for the system to work, before the induction the cells have to grow on media supplemented with raffinose. In this PhD thesis, this system was used exclusively to overproduce proteins of interest.

The *pMET3* promoter is a repressible promoter that switches off the expression of *pMET3*-fused genes upon the addition of fresh methionine (usually 8 mM) to the growing

media. To maintain the promoter off it is recommended to re-add 4 mM methionine every hour. For the system to work, before the repression, the cells have to grow on methionine-free medium. This system was used to down-regulate the expression of essential genes in a timely regulated manner.

The Auxin Inducible Degron (AID) system allows for the rapid degradation of target proteins in response to auxin hormones. To use this system the cells must ectopically express the F-box transport inhibitor response 1 (Tir1) protein and the target protein has to be fused to the AID degron. To induce the degradation of the protein of interest 500µM of indole-3-acetic acid (IAA; a natural auxin) was added to the medium so that IAA could bind to Tir1 thereby promoting the interaction between Tir1 and the AID degron. This interaction is required for the recognition of the AID-fused protein by the degradation machinery.

2.4.4. Regulation of conditionally mutant genes

To conditionally modulate the expression of the genes of interest we implemented several strategies:

(i) Temperature sensitive alleles. These alleles are inactivated by incubating the cells carrying them at their restrictive temperature (usually 37°C).

(ii) ATP-analogue sensitive alleles. These alleles are inactivated by adding to the cells carrying them a specific inhibitor. In this study the *cdc5-as1* ATP-analogue sensitive allele[143] was inactivated by adding 5 µM CMK inhibitor (Accenda Tech) dissolved in DMSO to the medium. While the *cdc15-as1* ATP-analogue sensitive allele was inactivated by adding 5 µM Cdc15-as1 inhibitor (1NM-PP1 analogue 9) dissolved in DMSO to the medium.

2.4.5. Tubulin staining *via in situ* indirect immunofluorescence

0.1 M KPi buffer pH 6.4:	27.8 ml 1 M K_2HPO_4
	72.2 ml 1 M KH_2PO_4
	900 ml ddH_2O
Fixative solution:	3.7% formaldehyde in 0.1 M KPi
Sorbitol-citrate 1.2 M:	17.4 g Anhydrous KH_2PO_4
	7 g Citric acid
	218.64 g Sorbitol
	up to 1l with ddH_2O
PBS-BSA:	1% crude BSA (Sigma)
	0.04 M K_2HPO_4
	0.01 M KH_2PO_4
	0.15 M NaCl
	0.1% NaN_3
Digestion solution:	1.2 M sorbitol-citrate
	10% glusulase
	0.1 mg/ml zymolase 100T
DAPI mount solution:	0.04 M K_2HPO_4
	0.01 M KH_2PO_4
	0.15 M NaCl
	0.1% NaN_3
	0.05 µg/ml DAPI
	0.1% p-phenylenediamine
	90% glycerol

1 ml of a cell culture at OD_{600} = 0.2 - 0.4 was collected by centrifugation (1 minute at 13000 rpm) at RT and incubated ON at 4°C in 1 ml of the fixative solution. Cells were next pelleted and washed 3 times with 1 ml of 0.1 M KPi pH 6.4 followed by a wash with

1 ml of sorbitol-citrate solution. Cells were then resuspended in 200 µl of the digestion solution and incubated at 35°C in order to enzymatically digest the cell wall and obtain spheroplasts. Since spheroplasts are osmotically fragile and lyse in a hypotonic solution, to prevent cell lysis and maintain an isotonic environment this step is done in 1.2 M sorbitol. The low pH of the sorbitol buffer helps in slowing down the cells endogenous proteolytic activity. The digestion of the cell wall was next checked under an optical microscope by looking for spheroplasts formation as assessed by cells bursting when mixed with an equal volume of 1% SDS. When the digestion was complete, the spheroplasts were pelleted at 2000 rpm for 2 minutes and washed with 1 ml of sorbitol-citrate solution. The pellet was then resuspended in an appropriate volume of the sorbitol-citrate solution (spanning from 10 to 50 µl, depending on the pellet size) to achieve a proper concentration of cells on the slide well. 5 µl of spheroplasts were loaded on a 30-wells slide previously coated with 0.1% polylysine (Sigma). To further fix cells, the slide was put in cold methanol for 3 minutes, followed by 10 seconds in cold acetone. Next, cells were incubated for 60-90 minutes, in a humid dark incubation chamber, with the primary antibody (5 µl *per* well of a 1:100 rat anti-tubulin (Oxford-Biotechonology) dilution in PBS-BSA). After incubation, cells were washed 5 times with PBS-BSA and incubated with the secondary antibody (5 µl *per* well of a 1:100 FITC-conjugated anti-rat diluted in PBS-BSA) for 60 minutes. Cells were then washed 5 times with PBS-BSA and then added with 5 µl of DAPI mount solution. The slide was covered with a coverslip and sealed with nail polish.

2.4.6. Scoring of indirect immunofluorescence samples

To monitor cell cycle progression, IF slides were analysed with a Leica DMR HC BIOMED fluorescence microscope using a 100X immersion-oil objective. Cell cycle progression was scored by looking at nuclear and spindle morphologies. According to their nuclear and spindle morphology cells can be divided into three categories: (i)

interphase cells (cells in the G1, S, and G2 phases of the cell cycle), which typically contain one nucleus and 3-5 short cytoplasmic microtubules, without a clear spindle structure; (ii) metaphase cells, which contain an undivided nucleus closed to the bud-neck but exhibit a short and thick bipolar spindle; and finally (iii) anaphase/telophase cells which carry two separated nuclear masses and an elongated spindle.

2.4.7. Actin labelling by Phalloidin staining

PBS-T:	10% crude BSA (Sigma) 1% NaN_3 0.1% Triton
Phalloidin solution:	3.3 µM Phalloidin diluted in PBS-T
PBS+:	10% crude BSA (Sigma) 1% NaN_3

5 ml of a cell culture at OD_{600} = 0.2 - 0.4 were fixed for 45 minutes at RT by adding 10% formaldehyde directly into the medium of growth. Cells were next pelleted and washed 6 times with 1 ml of 0.1 M KPi pH 6.4, followed by a wash with 1 ml of PBS-T in order to partially permeabilize the yeast cell wall. Cells were subsequently incubated in the Phalloidin solution for 30 minutes in a dark chamber at RT, washed 3 times with the PBS+ solution and finally resuspended in 50 µl of PBS+. Cells can be stored at -20°C up to few days from the fixation, and when required can be visualized upon mixing the cellular suspension with a DAPI mount solution (1:3)

2.4.8. Collection of cellular samples for mass spectrometry analysis

To obtain around 200 µg of proteins for mass spectrometry analysis, for each cellular samples 5 ml of a cell culture at OD_{600} = 0.2 - 0.4 were collected and centrifuged for 2 minutes at maximum speed. The resulting pellet was washed with 1ml of ddH_2O, transferred to 2 ml Sarstedt tubes and frozen in liquid nitrogen to preserve protein

integrity. The samples were next sent to Prof. Gigy in dry ice and analysed by multiplexed Tandem Mass Tag (TMT) 10-plex-based strategy as described in ref. [144].

2.5. Image acquisition and data analysis

2.5.1. Astral microtubule and actin cytoskeleton analysis in fixed-cells

Images of stained cells were acquired with an upright LEICA DM6 B microscope with a 100X/1.40 oil UPlanSApo ∞/0.17/DFN 25 Olympus objective and Andor Zyla.4.2P camera using Leica Application Suite X software. Optimized z-stacks were taken to cover a thickness of 6.1 µm. Following acquisition images of actin-labelled cells were automatically deconvolved by the Huygens software. Their analysis was performed using the "Fiji Is Just ImageJ" (FIJI) software. aMT length was measured in three-dimensions using the FIJI plug-in "simple neurite tracer". Instead to properly score the aMT number, the presence of abnormal aMTs, the bud-neck/spindle angles and the actin cytoskeleton structures, Z-series were collapsed into a maximum-intensity two-dimensional projection using the Z-project function. The bud-neck was defined based on the DIC image of the cell.

2.5.2. Astral microtubule analysis in live-cells

50 µl of arrested cells carrying a GFP-tagged Tub1 fusion were collected at OD_{600} = 0.2 - 0.4 and loaded in a CellASIC ONIX plate for haploid yeast cells (Millipore). This allows to constantly add fresh medium to the culture and to prevent cellular movements during the image acquisition. Images were acquired every 10 seconds for a total of 10 minutes with Nikon Eclipse Ti inverted microscope with a with a 100X/1.40 oil Olympus objective and Andor Zyla sCMOS camera using the NIS software version 5.10.00. At each time-point, 17 z-stack images were taken (0.4 µm from each other,) covering a total thickness of 6.8 µm. Image acquisition was followed by a deconvolution process automatically performed by the Huygens software. Image analysis was performed using

FIJI. To reduce the complexity and the noise of the analysis, aMT length measurements were performed using the FIJI plug-in "simple neurite tracer" in maximum-intensity two-dimensional projection using the Z-project function. As described in ref. [145], different events were identified: (i) polymerization events - defined as an increase in microtubule length by at least 0.5 µm across a minimum of three time-points; (ii) depolymerization events - defined as a decrease in microtubule length by at least 0.5 µm across a minimum of three time-points; and (iii) pause events - defined as net changes in microtubule length less than 0.5 µm across a minimum of 3 timepoints. Next, different parameters were calculated[145,146]: (i) polymerization rates, by dividing the net change in length by the change in time for each growth event; (ii) depolymerization rates, by dividing the net change in length by the change in time for each shrinking event; (iii) catastrophe frequencies, by dividing the number of polymerization-to-depolymerization transitions by the total time of all growth events; (iv) rescue frequencies, by dividing the number of depolymerization-to-polymerization transitions by the total time of all shrinkage events; (v) microtubule dynamicity, by multiplying the sum of the absolute value of all length changes by the estimation of tubulin dimers contained in 1 µm of microtubule (1 µm = 1690 dimers)[147], and dividing the obtained value per the total duration of the image acquisition. aMT-cortex connection was evaluated based on the DIC image of the cell.

2.5.3. Statistical analysis

Depending on the experiment, P values were determined by unpaired Student's t-test or One-Way Anova - Tukey's multiple comparisons test using the GraphPad Software. P value of less than 0.05 was considered statistically significant ($* = P < 0.05$; $** = P < 0.01$; $*** = P < 0.001$; $**** = P < 0.0001$). In graphs, averages ± S.E.M. (Standard Error of the Mean) is normally shown.

Table 2.1. Yeast strains used in this study

Strain (Ry)	Relevant genotype	Origin
1	*MATa, ade2-1, leu2-3, ura3, trp1-1, his3-11,15, can1-100, GAL, psi+*	Visintin lab
72	*MATa*, (mating type tester strain)	Fink lab
73	*MATalpha*, (mating type tester strain)	Fink lab
1112	*MATa, cdc15::CDC15-as1(L99G)::URA3*	Visintin lab
1223	*MATa, pMET3-CDC20::URA3, CDC14-3HA*	Visintin lab
1574	*MATa, cdc14-1*	Visintin lab
1602	*MATa, cdc14-1, cdc5-as1(L158G)*	Visintin lab
2143	*MATa, cdc14-1, cdc5-as1(L158G), pds1::URA3*	Visintin lab
2446	*MATa, cdc5-as1(L158G)*	Visintin lab
3201	*MATa, pMET3-CDC20::URA3, cdc14-1, cdc5-as1(L158G)*	Visintin lab
3204	*MATa, pMET3-CDC20::URA3, cdc14-1*	Visintin lab
3209	*MATa, pMET3-CDC20::URA3, cdc5-as1(L158G), CDC14-3HA*	Visintin lab
3256	*MATa, cdc14-1, cdc5-as1(L158G), ura3::pAFS125-TUB1p-GFPTUB1::URA3*	Visintin lab
3346	*MATa, cdc14-1, cdc5-as1(L158G), bub2::HIS3*	Visintin lab
3771	*MATa, cdc14-1, cdc5-as1(L158G), mad2::URA3, rad9::LEU2*	Visintin lab
4853	*MATa, ura3::pADH1-OsTIR1-9MYC::URA3, CDC20-aid::KanMX*	Visintin lab
4936	*MATa, cdc5-as1(L158G), ura3::pADH1-OsTIR1-9MYC::URA3, CDC20-aid::KanMX*	Visintin lab
7545	*MATa, kar9::HIS5, ura3::pADH1-OsTIR1-9MYC::URA3, DYN1-aid:KanMX, CDC20-aid::KanMX*	This Thesis
7589	*MATa, cdc5-as1(L158G), kar9::HIS5*	This Thesis
7620	*MATa, leu2::pTEF1-osTIR::LEU2, DYN1-aid:KanMX, kar9::HIS5, cdc15-as1(L99G)::URA3*	This Thesis
7623	*MATa, leu2::pTEF1-osTIR::LEU2, DYN1-aid:KanMX, cdc15-as1(L99G)::URA3*	This Thesis

Strain (Ry)	Relevant genotype	Origin
7626	*MATa, kar9::HIS5, cdc15-as1(L99G)::URA3*	This Thesis
7694	*MATa, leu2::pTEF1-osTIR::LEU2, DYN1-aid:KanMX, kar9::HIS5, cdc5-as1(L158G)*	This Thesis
7697	*MATa, leu2::pTEF1-osTIR::LEU2, DYN1-aid:KanMX, cdc5-as1(L158G)*	This Thesis
7702	*MATa, cdc5-as1(L158G), leu2::pTEF1-osTIR::LEU2, kar9::HIS5, CDC20-aid::KanMX*	This Thesis
7732	*MATa, leu2::pTEF1-osTIR::LEU2, CDC20-aid::KanMX, ura3::pAFS123-TUB1p-GFPTUB1::URA3*	This Thesis
7746	*MATa, leu2::pTEF1-osTIR::LEU2, DYN1-aid:KanMX, kar9::HIS5, CDC20-aid::KanMX, cdc5-as1(L158G)*	This Thesis
7749	*MATa, leu2::pTEF1-osTIR::LEU2, DYN1-aid:KanMX, CDC20-aid::KanMX, cdc5-as1(L158G)*	This Thesis
7873	*MATa, leu2::pTEF1-osTIR::LEU2, CDC20-aid::KanMX*	This Thesis
8210	*MATa, pGAL-SCC1(R180D,R268D)*	This Thesis
8969	*MATa, pMET3-CDC20::URA3, cdc14-1, cdc5-as1(L158G), pds1::URA3*	This Thesis
9128	*MATa, cdc14-1, cdc5-as1(L158G), esp1-1*	This Thesis
9131	*MATa, cdc14-1, esp1-1*	This Thesis
9134	*MATa, cdc5-as1(L158G), esp1-1*	This Thesis
9237	*MATa, ura3::pADH1-OsTIR1-9MYC::URA3, CDC20-aid::KanMX, cdc12-6*	This Thesis
9291	*MATa, leu2::pTEF1-osTIR::LEU2, CDC20-aid::KanMX, clb5::URA3*	This Thesis
9294	*MATa, leu2::pTEF1-osTIR::LEU2, CDC20-aid::KanMX, kip1::HIS3*	This Thesis
9490	*MATa, esp1-1*	This Thesis
9512	*MATa, esp1-1, cdc15-as1(L99G)::URA3*	This Thesis
9516	*MATa, leu2::pTEF1-osTIR::LEU2, CDC20-aid::KanMX, cdc15-as1(L99G)::URA3*	This Thesis
9877	*MATa, leu2::pTEF1-osTIR::LEU2, CDC20-aid::KanMX, dbf4-1*	This Thesis
9880	*MATa, leu2::pTEF1-osTIR::LEU2, CDC20-aid::KanMX, alk2::HIS3*	This Thesis

Strain (Ry)	Relevant genotype	Origin
9883	*MATa, leu2::pTEF1-osTIR::LEU2, CDC20-aid::KanMX, alk2::HIS3, alk1::KanMX*	This Thesis
10025	*MATa, leu2::pTEF1-osTIR::LEU2, CDC20-aid::KanMX, acm1::KanMX*	This Thesis

3. RESULTS

The phosphatase Cdc14 and the polo-like kinase Cdc5 are two essential promoters of mitotic exit, as indicated by the telophase arrest - elongated spindle and segregated nuclei - typical of both *cdc14* and *cdc5* single mutant cells[148]. Cdc14 triggers mitotic exit by promoting CDK inhibition - via degradation of mitotic cyclins and accumulation of the CDK inhibitor Sic1 - and by reversing CDK-mediated phosphorylation events[22], while Cdc5 plays a central role in the activation of the phosphatase. Cdc5 is the only shared component of both the FEAR and the MEN: the two signaling cascades that drive Cdc14 activation in early and late anaphase, respectively[24,148]. Cdc14 activation is not the only role attributed to Cdc5, mounting evidences indicate that Cdc5, as well as other late mitotic kinases, cooperate with Cdc14 to orchestrate late mitotic events[27], one of them being spindle elongation. Indeed, FEAR-released Cdc14 and Cdc5 redundantly promote spindle elongation at anaphase onset, as indicated by the observation that their concomitant inactivation results in cells arresting with short bipolar spindles and undivided nuclei, albeit having cleaved cohesin[63]. Spindle elongation is a process that relies on drastic changes in spindle microtubule dynamics, often driven by modulation of MAPs and motor proteins. In line with this general view, the kinesin-5 motor Cin8 is a key target of both Cdc14 and Cdc5, which remove CDK-mediated phosphorylation and phosphorylate Cin8 on residues that are not targeted by CDK (probably promoting its activity), respectively[63,149]. The aim of this PhD thesis was to elucidate the mechanisms underlying microtubule regulations that occur at anaphase onset, taking advantage of the peculiar phenotype of *cdc14 cdc5* double mutant cells.

3.1. Are spindle microtubules altered in *cdc14 cdc5* double mutant cells?

cdc14 cdc5 double mutant cells arrest in what we define as “mini anaphase”, a condition that morphologically resembles metaphase but in which cells have short spindles and undivided nuclei although, molecularly, the cells are in anaphase, as indicated by the

completion of the metaphase to anaphase transition assessed by cohesin cleavage[63]. The primary defect of these cells is an erroneous anaphase spindle elongation[63]. We reasoned that this phenotype might underlie alterations in mitotic spindle microtubules; as such, we probed spindle microtubules in *cdc14 cdc5* double mutant cells and compared them with those of *wild-type* cells. Within the mitotic spindle, three kinds of microtubules are recognized, namely: interpolar microtubules (iMTs), kinetochore microtubules (kMTs) and astral microtubules (aMTs). To assess spindle microtubule morphology, we used different imaging techniques: iMTs and kMTs were analyzed by electron microscopy (EM), as fluorescence microscopy is not sufficient to distinguish between these two types of microtubules; while aMTs, which can be easily visualized by fluorescence microscopy, were assessed by indirect immunofluorescence (IF).

3.1.1. *cdc14 cdc5* double mutant cells show proper iMTs and kMTs, but abnormally stable aMTs

In order to assess spindle microtubule morphology, *wild-type* and *cdc14 cdc5* cells were arrested in G1 at the permissive conditions for the *cdc14* and *cdc5* mutant alleles, and synchronously released into the next cell cycle in restrictive condition (see **sections 2.4** for details). We followed the cell cycle progression by probing nuclear and spindle morphology. Nuclear and spindle analysis allows us to assess the synchrony of the cell population and to morphologically classify the cells into two groups: metaphase-like (an undivided nucleus and a short, thick bipolar spindle) and anaphase (a bilobate nucleus and an elongated spindle). As expected, *wild-type* cells complete an entire cell cycle, while *cdc14 cdc5* cells arrest with a metaphase-like morphology (**figure 3.1a**). Based on this scoring, we selected the appropriate time points for the microtubule analysis. For *wild-type* cells, samples were processed when the vast majority of the population was either in metaphase (around 60% of cells at 60 minutes from the G1 release) or anaphase (around 75% of cells at 100 minutes from the release). For the *cdc14 cdc5* mutants,

samples were processed at their terminal phenotype (140 minutes from the release), as indicated by the prolonged metaphase-like morphology (around 100% of double mutant cells reached a metaphase-like morphology at 100 minutes from the G1 release and remained arrested for longer than 40 minutes – the time required for *wild-type* cells to go from the metaphase peak to the anaphase peak). Interestingly, at a first glance, we did not notice any obvious defect in the central spindle morphology, while aMTs seemed anomalous (**figure 3.1b**). The EM analysis of iMTs and kMTs was performed in collaboration with Prof. Mark Winey at the University of Boulder in Colorado. Electron micrographs of serial thin sections of yeast cells were prepared by high-pressure freezing and freeze substitution, and spindles were assembled using three dimensional (3-D) reconstruction, as described in depth by Prof. Winey and colleagues[9]. We found that iMTs and kMTs of *cdc14 cdc5* cells were structurally undistinguishable from their *wild-type* counterpart (**figure 3.1c**; note that the different spindle length arises from the protracted arrest, as previously described[63]). The IF analysis of aMTs was performed and aMT length and number, two "*bona fide*" indicators of aMT stability, were measured in one hundred cells per condition. In particular, we compared *cdc14 cdc5* cells with both metaphase- and anaphase-like *wild-type* cells (**figure 3.1d**), and found that in double mutant cells, both aMT length and number were drastically increased (on average, 4 µm and 4.6 aMT per cell in *cdc14 cdc5* cells, compared with 2 µm and 1.6 aMT per cell and 2.7 µm and 3.1 aMT per cell in *wild-type* metaphase- and anaphase-like cells, respectively). Of note, we also noticed that *wild-type* anaphase cells show more and longer aMTs than the metaphase counterpart. Altogether, these results indicate that *cdc14 cdc5* double mutant cells carry morphologically proper iMTs and kMTs, but are characterized by anomalously stable aMTs. Intrigued by the peculiar aMT phenotype of *cdc14 cdc5* cells, we decided to focus our attention on this class of spindle microtubules since little is known about their regulation during mitotic progression.

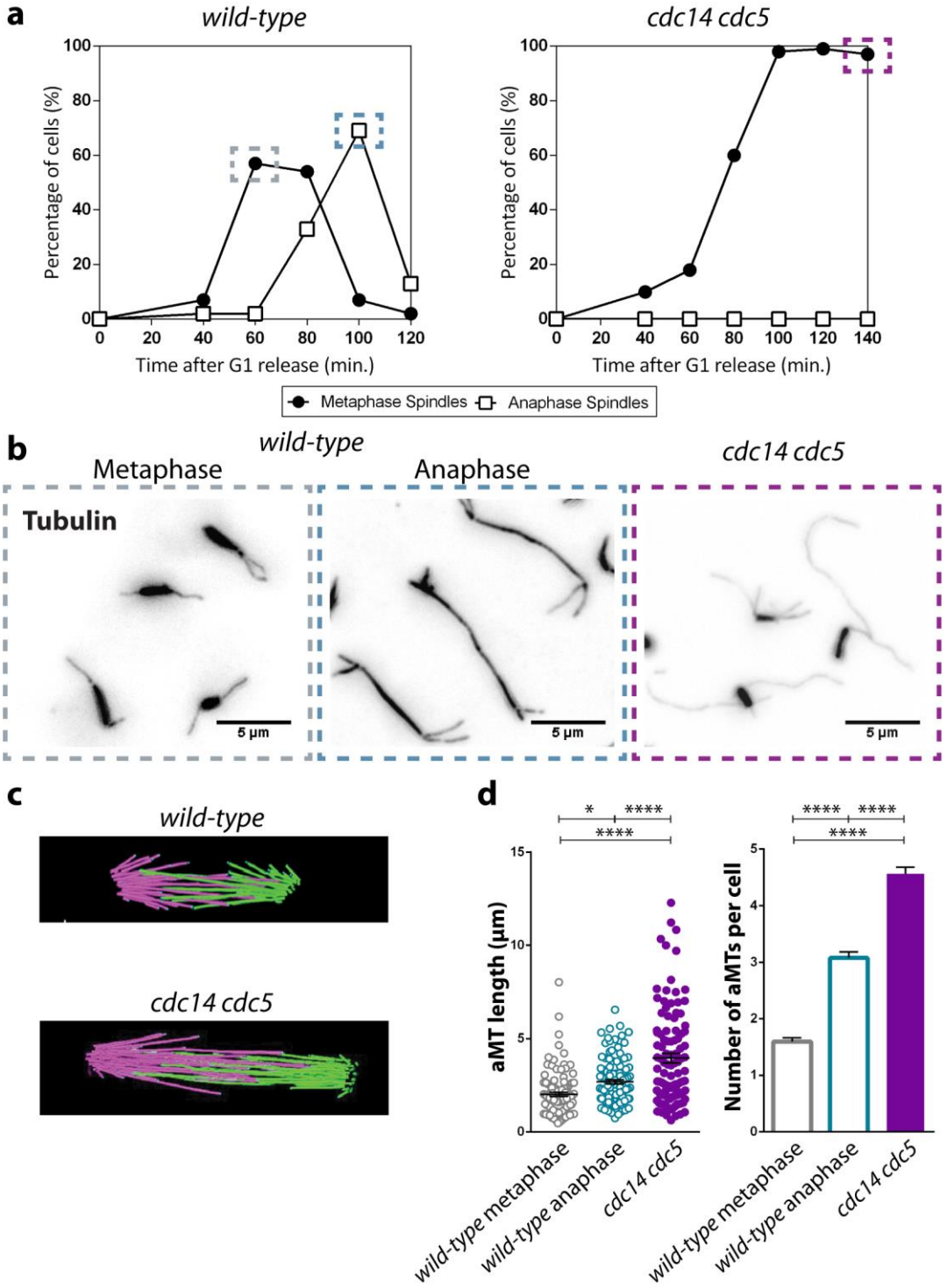

Figure 3.1. *cdc14-1 cdc5-as1* cells are characterized by stable aMTs. *wild-type* (Ry1) and *cdc14-1 cdc5-as1* (Ry1602) cells were arrested in G1 by α-factor in YEPD at 23°C and then released in fresh YEPD media supplemented with CMK at 37°C to inactivate the *cdc5-as1* and *cdc14-1* allele, respectively. (**a**) To probe spindle microtubules at the appropriate cell cycle phase, cells were collected at the indicated time-points and scored for metaphase (closed circles) and anaphase (open squares) spindles. The subsequent analyses were performed for *wild-type* cells at the metaphase (grey box, 60 minutes after the release) and anaphase (grey-green box, 100 minutes after the release) peaks and the *cdc14-1 cdc5-as1* cells at their terminal arrest (purple box, 140 minutes after the release). (**b**) Representative images of the time-points analyzed are shown. (**c**) 3-D reconstruction of a *wild-type* early anaphase and a *cdc14-1 cdc5-as1* spindle obtained by EM analysis. (**d**) Quantification of aMT length and number in cells of the indicated genotype (n=100; mean +/- SEM is shown;*=p<0.05 - ****=p<0.0001) is shown.

3.2. What is the mechanism underlying the aMT phenotype of *cdc14 cdc5* cells?

Different hypotheses can be formulated to explain the aMT phenotype of *cdc14 cdc5* double mutant cells, it can be a consequence of: (i) the activation of a cell cycle checkpoint; (ii) a protracted arrest with a short length spindle; (iii) the inactivation of either or both Cdc14 and Cdc5; (iv) a molecular event taking place at anaphase onset; (v) a combination of the possibilities mentioned above. To elucidate the molecular mechanisms that generate the aMT phenotype of *cdc14 cdc5* cells, we took advantage of the "*almost-magical*" potential of yeast genetic.

3.2.1. aMT phenotype of *cdc14 cdc5* double mutant cells is not due to the activation of a cell cycle checkpoint

Several checkpoints supervise the later stages of mitosis, including the Spindle Assembly Checkpoint (SAC), the DNA Damage Response (DDR) and the Spindle Positioning Checkpoint (SPoC). None of these checkpoints is responsible for the spindle elongation defect of *cdc14 cdc5* cells[63], however, it is not clear whether they impact on aMT dynamics. To assess whether the activation of any of these checkpoints is responsible for the aMT phenotype of double mutant cells, checkpoint responses were abrogated in a *cdc14 cdc5* background. In particular, we used *mad2*, *rad9* and *bub2* mutants to impair SAC, DDC and SPoC-mediated surveillance mechanisms, respectively. To this aim, c*dc14 cdc5*, c*dc14 cdc5 mad2 rad9* and c*dc14 cdc5 bub2* mutant cells were synchronized in G1 and aMTs were analyzed at the terminal arrest. Of note, all these strains arrest in "mini-anaphase"[63] (**figure 3.2a**). We found that in all checkpoint defective cells, aMTs remained as stable as in *cdc14 cdc5* double mutant cells, as typified by aMT length and number (**figure 3.2a** and **3.2b**), thus indicating that none of the tested checkpoints is responsible for the aMT phenotype of *cdc14 cdc5* cells.

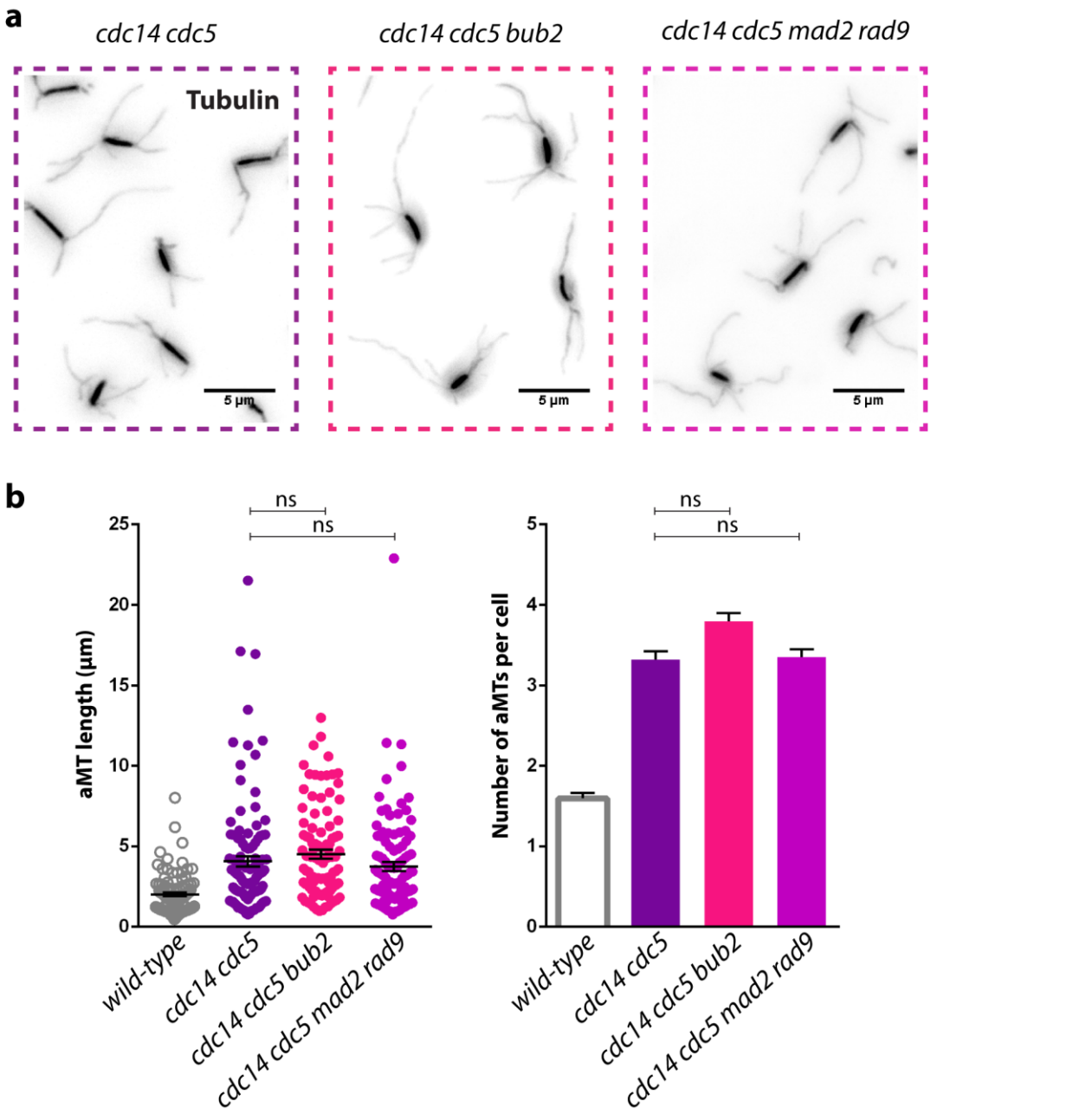

Figure 3.2. The aMT phenotype of *cdc14-1 cdc5-as1* cells is not a consequence of SPoC, SAC or DDR activation. *Wild-type* (Ry1), *cdc14-1 cdc5-as1* (Ry1602), *cdc14-1 cdc5-as1 bub2*Δ (Ry3346) and *cdc14-1 cdc5-as1 mad2*Δ *rad9*Δ (Ry3771) cells were arrested in G1 by α-factor in YEPD at 23°C and then released in fresh YEPD media supplemented with CMK at 37°C to inactivate the *cdc5-as1* and the *cdc14-1* allele, respectively. The aMT analysis was performed in *wild-type* cells at the metaphase peak (60 minutes after the release) and in *cdc14-1 cdc5-as1*, *cdc14-1 cdc5-as1 bub2*Δ and *cdc14-1 cdc5-as1 mad2*Δ *rad9*Δ cells at their terminal arrest (160 minutes after the release). (**a**) Representative images of the time-points analyzed are shown. (**b**) Quantification of aMT length and number in cells of the indicated genotype (n=100; mean +/- SEM) is shown.

3.2.2. aMT phenotype of *cdc14 cdc5* double mutant cells is not due to the protracted arrest with a short bipolar spindle

Having excluded a role for cell cycle checkpoints in the generation of the anomalous aMTs observed in double mutant cells, we then assessed whether this phenotype was a consequence of a protracted arrest with a short bipolar spindle. To test this hypothesis, we compared aMT length and number of *cdc14 cdc5* arrested cells with the ones of metaphase arrested cells, which arrest with a similar short bipolar spindle (**figure 3.3a**)[63]. To achieve the metaphase arrest, we took advantage of the *CDC20-AID* mutant allele, which prevents the activation of the ubiquitin-ligase Anaphase Promoting Complex/Cyclosome (APC/C) by inducing the degradation of its activator subunit Cdc20 upon Auxin addition to the growth media. We found that, although slightly more stable than *wild-type* (non-arresting) metaphase cells, aMTs of *cdc20* cells did not reach the length and number of *cdc14 cdc5* cells (**figure 3.3b** and **3.3c**) (on average, 4 µm and 3.3 aMT per cell in *cdc14 cdc5* cells, compared with 2.6 µm and 2.6 aMT per cell in *cdc20* cells). This result indicates that a protracted arrest, although altering aMT dynamics, is not sufficient to explain the aMT phenotype of *cdc14 cdc5* arrested cells.

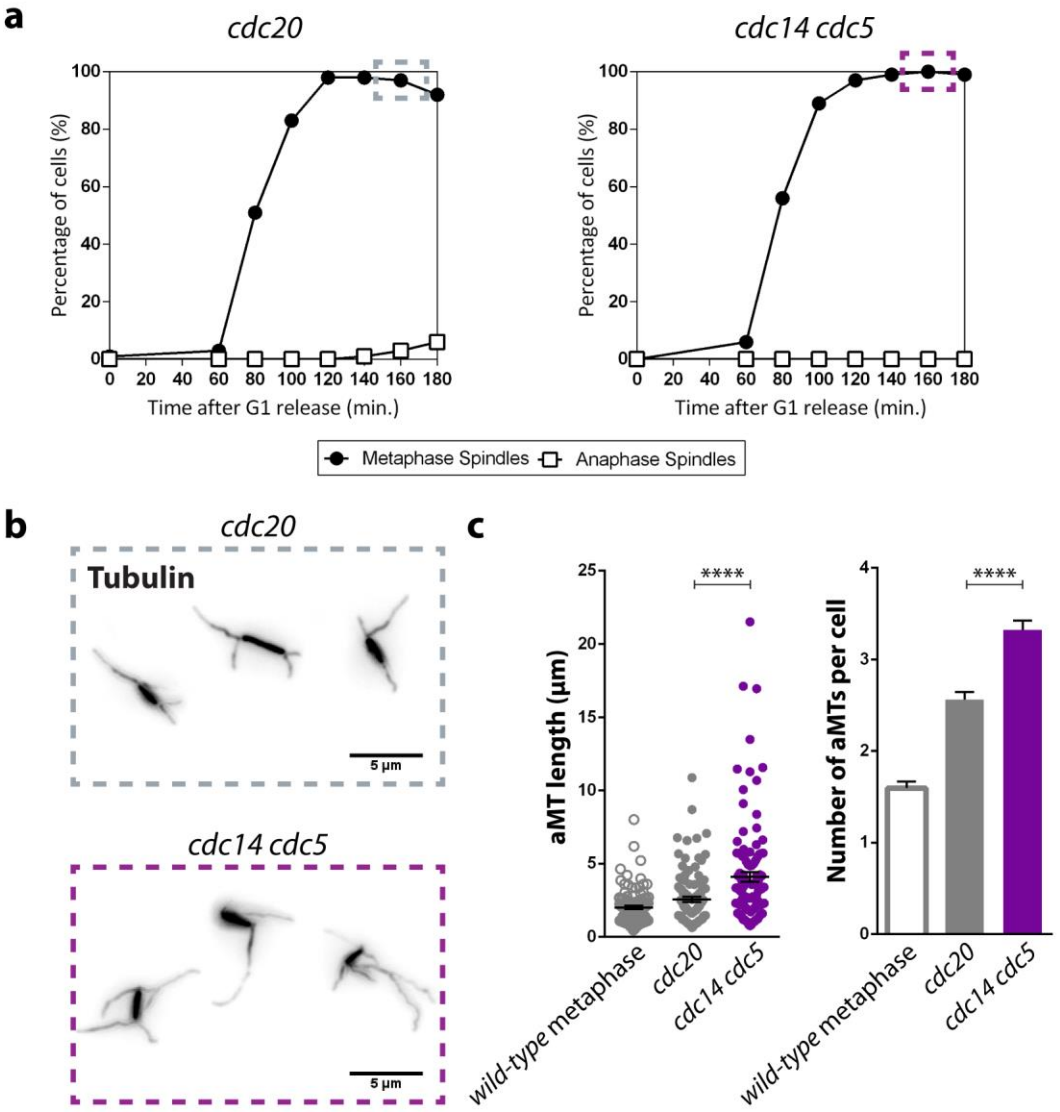

Figure 3.3. The aMT phenotype of *cdc14-1 cdc5-as1* cells is not a consequence of a protracted arrest with a short bipolar spindle. *cdc20-AID* (Ry4853) and *cdc14-1 cdc5-as1* (Ry1602) cells arrested in G1 by α-factor in YEPD at 23°C were released at 37°C in fresh YEPD media supplemented with CMK, to inactivate the *cdc14-1* and the *cdc5-as1* alleles, respectively. Auxin was added to deplete the Cdc20-AID protein. (**a**) To make sure to carry out the aMTs analysis in cells that stayed at their terminal arrest for the same amount of time, we monitored cell cycle entry and progression by means of the appearance of metaphase (closed circles) and anaphase (open squares) spindles. Since both strains proceeded into the cell cycle with similar kinetics prior to arresting with a metaphase-like morphology, the aMT analysis was performed for each strain160 minutes after the release. (**b**) Representative images of the time-points analyzed are shown. (**c**) Quantification of aMT length and number in cells of the indicated genotype (n=100; mean +/- SEM is shown; ****=p<0.0001) is shown.

3.2.3. The concomitant inactivation of Cdc14 and Cdc5 is not sufficient to generate the aMT phenotype of *cdc14 cdc5*, but an anaphase molecular feature is required

Since the aMT phenotype of *cdc14 cdc5* cells does not result from the activation of a cell cycle checkpoint or from a protracted arrest with short bipolar spindles, we wondered whether it might be directly linked to Cdc14 and/or Cdc5 inactivation or whether it involves a molecular event that takes place at the metaphase to anaphase transition. To discriminate between the two hypotheses, the best experiment would be to compare aMTs of *cdc14 cdc5* cells with those of another mutant that arrests in "mini-anaphase" with potentially active Cdc14 and Cdc5. Unfortunately, to the best of our knowledge, such a mutant does not exist. However, given that metaphase arrested cells do not recapitulate the aMT phenotype of double mutant arrested cells, they represent a perfect platform for assessment of whether the removal of Cdc14 and Cdc5 is sufficient to stabilize aMTs. To this aim, we inactivated Cdc14 and Cdc5, alone or in combination, in *cdc20* mutant cells. For this analysis, we had to use the *pMET-CDC20* mutant allele[141], as combining *cdc14* and *cdc5* with all of the other *cdc20* mutant alleles available in the laboratory (i.e., *cdc20-1*, *cdc20-3*, *CDC20-AID*) is synthetically lethal[63]. We arrested *pMET-CDC20*, *pMET-CDC20 cdc14*, *pMET-CDC20 cdc5*, *pMET-CDC20 cdc14 cdc5*, and *cdc14 cdc5* cells in G1 using minimal growth medium lacking methionine at the permissive conditions for both *cdc14* and *cdc5* mutant alleles. Cells were then released in complete growth medium supplemented with methionine to suppress CDC20 expression[29] at the restrictive conditions for *cdc14* and *cdc5* alleles and, at their terminal arrest, the aMT morphology was evaluated (**figure 3.4a** and **3.4b**). We found that all of the metaphase arrested strains carried less stable aMTs than double mutant cells (on average, 3.6 µm and 3.5 aMT per cell in *cdc14 cdc5* cells, compared with 1.9 µm and 2.7 aMT per cell in *pMET-CDC20* cells, 2.3 µm and 2.4 aMT per cell in *pMET-CDC20 cdc14*, 2.4 µm and 2.4 aMT per cell in *pMET-CDC20 cdc5, and* 2.8 µm and 2.4 aMT per cell in *pMET-CDC20 cdc14 cdc5*),

thus indicating that Cdc14 and Cdc5 inactivation is not sufficient "*per se*" to stabilize aMTs, but that an additional molecular feature of anaphase is required.

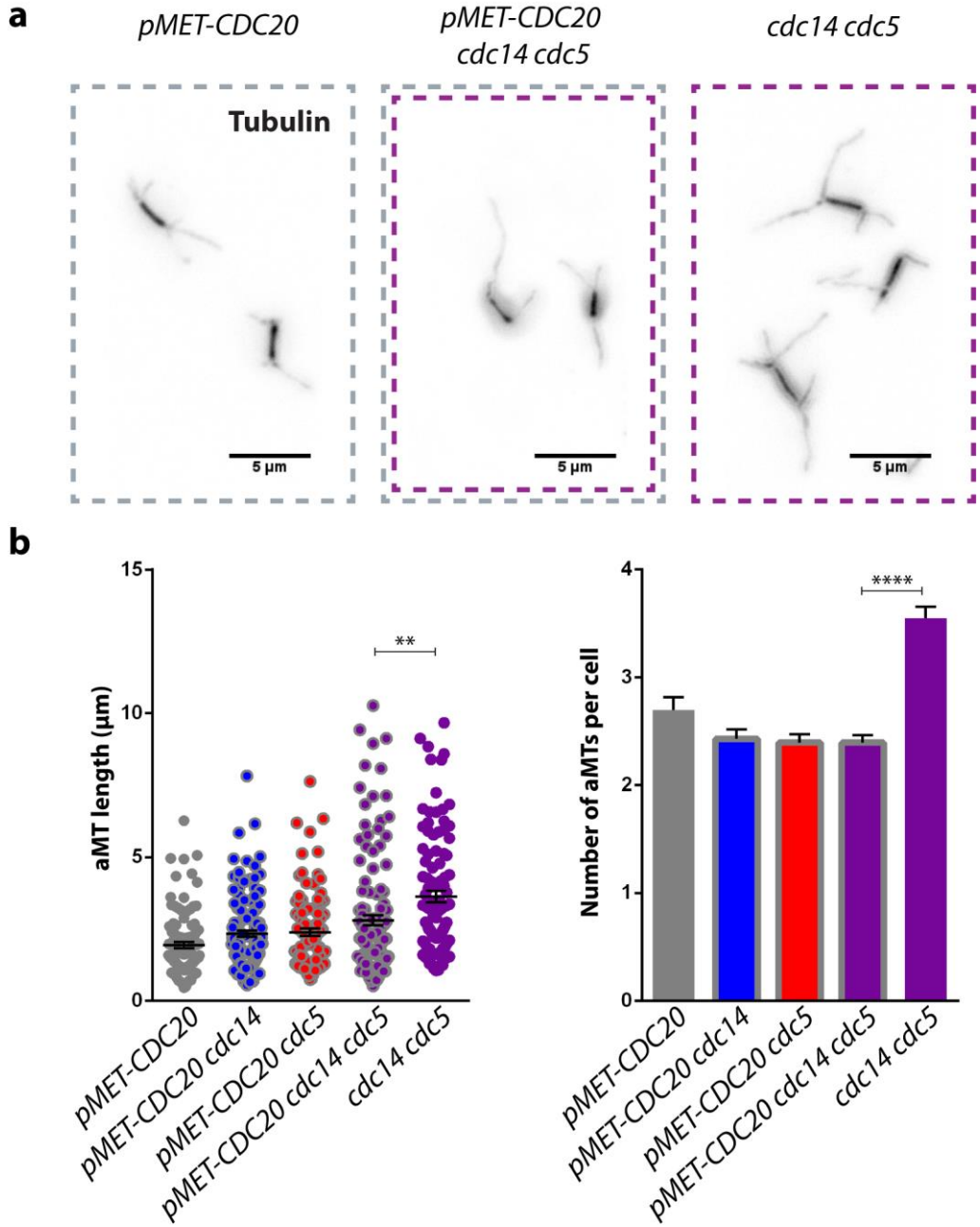

Figure 3.4. Cdc14 and Cdc5 concomitant inactivation in metaphase is not sufficient to generate the aMT phenotype of *cdc14-1 cdc5-as1* cells. *pMET-CDC20* (Ry1223), *pMET-CDC20 cdc14-1* (Ry3204) *pMET-CDC20 cdc5-as1* (Ry3209) *pMET-CDC20 cdc14-1 cdc5-as1* (Ry3201) and *cdc14-1 cdc5-as1* (Ry1602) cells were arrested in G1 by α-factor in synthetic complete medium lacking methionine (SC-Met) and released at 37°C in YEPD medium added with CMK and methionine to inactivate *cdc14-1* and the *cdc5-as1* allele, respectively and to repress the expression of *CDC20*. The aMT analysis was performed at the terminal arrest of each mutant strain (160 minutes after the release). (**a**) Representative images of the time-points analyzed are shown. (**b**) Quantification of aMT length and number in cells of the indicated genotype (n=100; mean +/- SEM is shown; **=P<0.01 - ****=P<0.0001) is shown.

However, these results do not exclude a role for the two proteins in anaphase. Therefore, to test whether Cdc14 and Cdc5 activities are required in anaphase, we analyzed aMTs of *cdc15* cells, which arrest in anaphase with long length spindles and segregated nuclei due to an impairment in exit from mitosis[148], and compared them with aMTs of *cdc14 cdc5* arrested cells (**figure 3.5a** and **3.5b**). Clear predictions can be made regarding the expected phenotypes: if Cdc14 and Cdc5 activities do not affect aMT dynamics, aMTs of *cdc15* cells should resemble those of *cdc14 cdc5* double mutant cells; vice versa, if Cdc14 and/or Cdc5 play a role in the process, *cdc15* cells should carry less stable aMTs. We found that, although aMTs of *cdc15* arrested cells are almost as numerous as those of *cdc14 cdc5* cells, they do not reach a length comparable to that of double mutant cells (on average, 4 µm in *cdc14 cdc5* cells, compared with 2.1 µm in *cdc15* cells), thus indicating that Cdc14 and/or Cdc5 inactivation is a necessary condition to elicit the aMT phenotype of *cdc14 cdc5* cells. To test the single contribution of Cdc14 and Cdc5, we analyzed aMTs of *cdc14* and *cdc5* single mutant cells, which arrest with long length spindles and bilobed nuclei, and found no difference between the two strains and *cdc15* cells (**figure 3.5a** and **3.5b**), thus indicating that Cdc14 and Cdc5 have to be concomitantly inactivated to stabilize aMTs. Altogether, these results suggest that an anaphase molecular feature is required to stabilize aMTs at anaphase onset, while Cdc14 and Cdc5 redundantly counteract this stabilization.

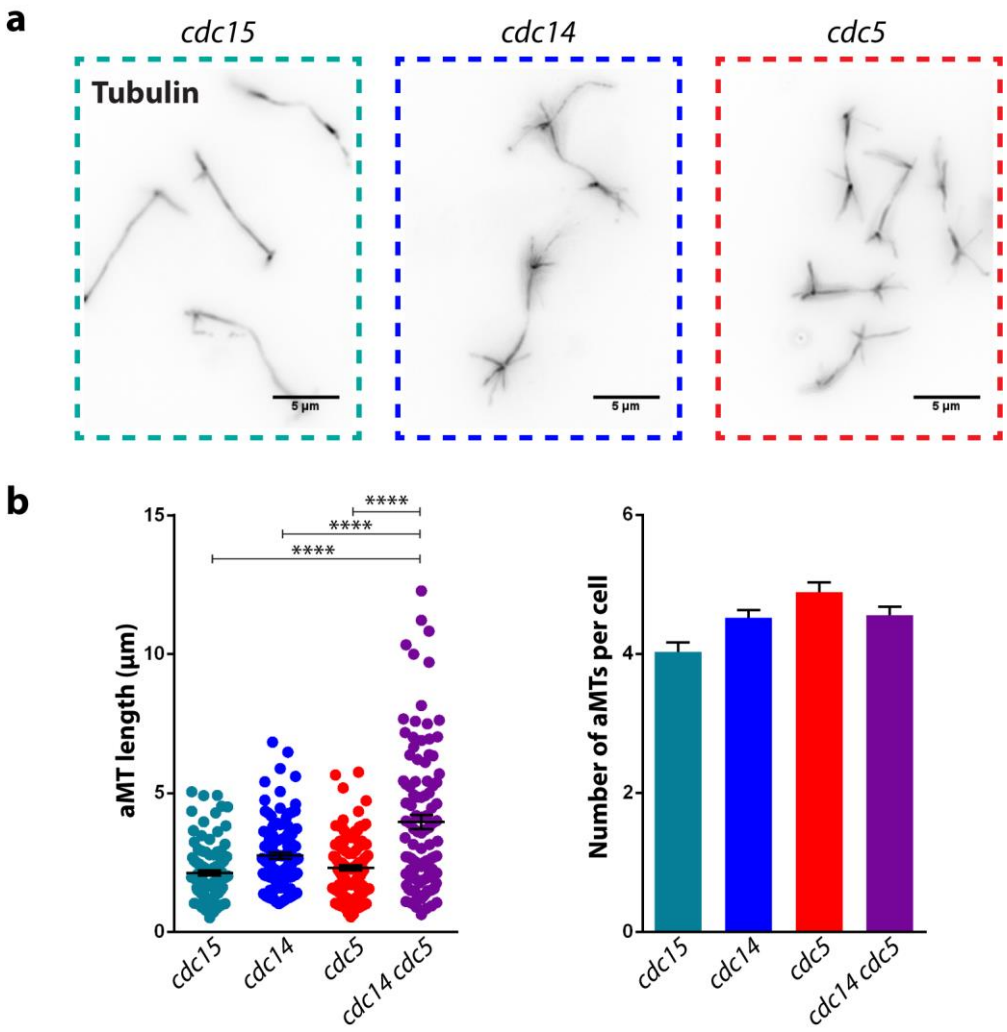

Figure 3.5. Cdc14 and Cdc5 concomitant inactivation in anaphase is necessary to generate the aMT phenotype of *cdc14-1 cdc5-as1* cells. *cdc15-as1* (Ry1112), *cdc14-1* (Ry1574), *cdc5-as1* (Ry2446) and *cdc14-1 cdc5-as1* (Ry1602) cells arrested in G1 by α-factor in YEPD at 23°C were released at 37°C in fresh YEPD media containing 1NM-PP1 analogue 9 and CMK, to inactivate the *cdc14-1,* the *cdc15-as1*, and the *cdc5-as1* alleles, respectively. The aMT analysis was performed at the terminal arrest of each mutant strain (180 minutes after the release). (**a**) Representative images of the time-point analyzed are shown. (**b**) Quantification of aMT length and number in cells of the indicated genotype (n=100; mean +/- SEM is shown; ****=p<0.0001) is shown.

3.3. What is the anaphase molecular signature involved in aMT stabilization?

Beside Cdc14 and Cdc5 inactivation, aMT stabilization requires an event that takes place at the metaphase to anaphase transition. To unveil this requirement at the molecular level, we decided to first identify its nature and then to dig deeper to elucidate the key targets.

3.3.1. APC/C^{Cdc20} activation is sufficient to stabilize aMTs at anaphase onset

The metaphase to anaphase transition – conventionally defined by cohesin cleavage – is composed of three critical and distinct events: (i) APC/C^{Cdc20} activation; (ii) Separase/Esp1 activation, consequently to APC/C^{Cdc20}-mediated degradation of Securin/Pds1; and (iii) Esp1-mediated cleavage of the cohesin subunit Scc1. It is worth noticing that each step corresponds to a different molecular status. The "*almost magical*" potential of yeast genetics allows us to appreciate the consequences of each individual step, taking advantage of appropriate mutant strains that are specifically impaired in the completion of each stage. In particular: (i) in APC/C mutant cells (e.g., *cdc20* cells), APC/C^{Cdc20} substrates are present, separase is inactive and cohesin is bound to chromatin; (ii) in separase mutant cells (e.g., *esp1* cells), APC/C^{Cdc20} substrates are removed, separase is inactive and cohesin is bound to chromatin; (iii) in cells expressing an uncleavable allele of Scc1 (*scc1R180DR268D)*, namely *scc1nc* cells[29,30], APC/C^{Cdc20} substrates are removed, separase is active but cohesin remains bound to chromatin; and finally (iv) in anaphase cells (e.g., *cdc15*) APC/C^{Cdc20} substrates are removed, separase is active and cohesin is removed from chromatin. The latter is also the molecular status of *cdc14 cdc5* double mutant cells. To identify the critical step of the metaphase to anaphase transition required for aMTs regulation, we first decided to compare aMTs of *cdc20*, *esp1*, *scc1nc*, and *cdc14 cdc5* cells. However, we noticed that different to *cdc20* and *cdc14 cdc5* cells, *esp1* and *scc1nc* cells eventually disassembled their short bipolar spindle (**figure 3.6a**). We hypothesized that this behavior is probably due to the combination of nuclear movement into the bud and low CDK activity, typical of cells with an active APC/C^{Cdc20-}

[32]. These events promote the activation of the MEN and ultimately the release of Cdc14 from the nucleolus, resulting in spindle disassembly and mitotic exit[32]. With this caveat in mind, we performed a preliminary analysis, assessing aMTs of the four mutant strains at the time point prior to spindle disassembly of *esp1* and *ssc1nc* cells (black box in **figure 3.6a)**. We found that both *esp1* and *scc1nc* cells carried more and longer aMTs than *cdc20* cells, similar to *cdc14 cdc5* double mutant cells (**figure 3.6b** and **3.6c**) (on average, 2.3 µm and 2.4 aMT per cell in *cdc20* cells, compared with 3 µm and 2.8 aMT per cell in *esp1* cells, 3 µm and 3.2 aMT per cell in *scc1nc* cells, and 3 µm and 3.1 aMT per cell in *cdc14 cdc5* cells). Since we showed that aMT stabilization requires that *cdc14 cdc5* cells are in anaphase, and based on the observation that the four strains enter and progress through the cell cycle with similar kinetics, we speculate that the APC/C^{Cdc20} was potentially active in *esp1* and *ssc1nc* cells, hence suggesting that its activation is sufficient to stabilize aMTs.

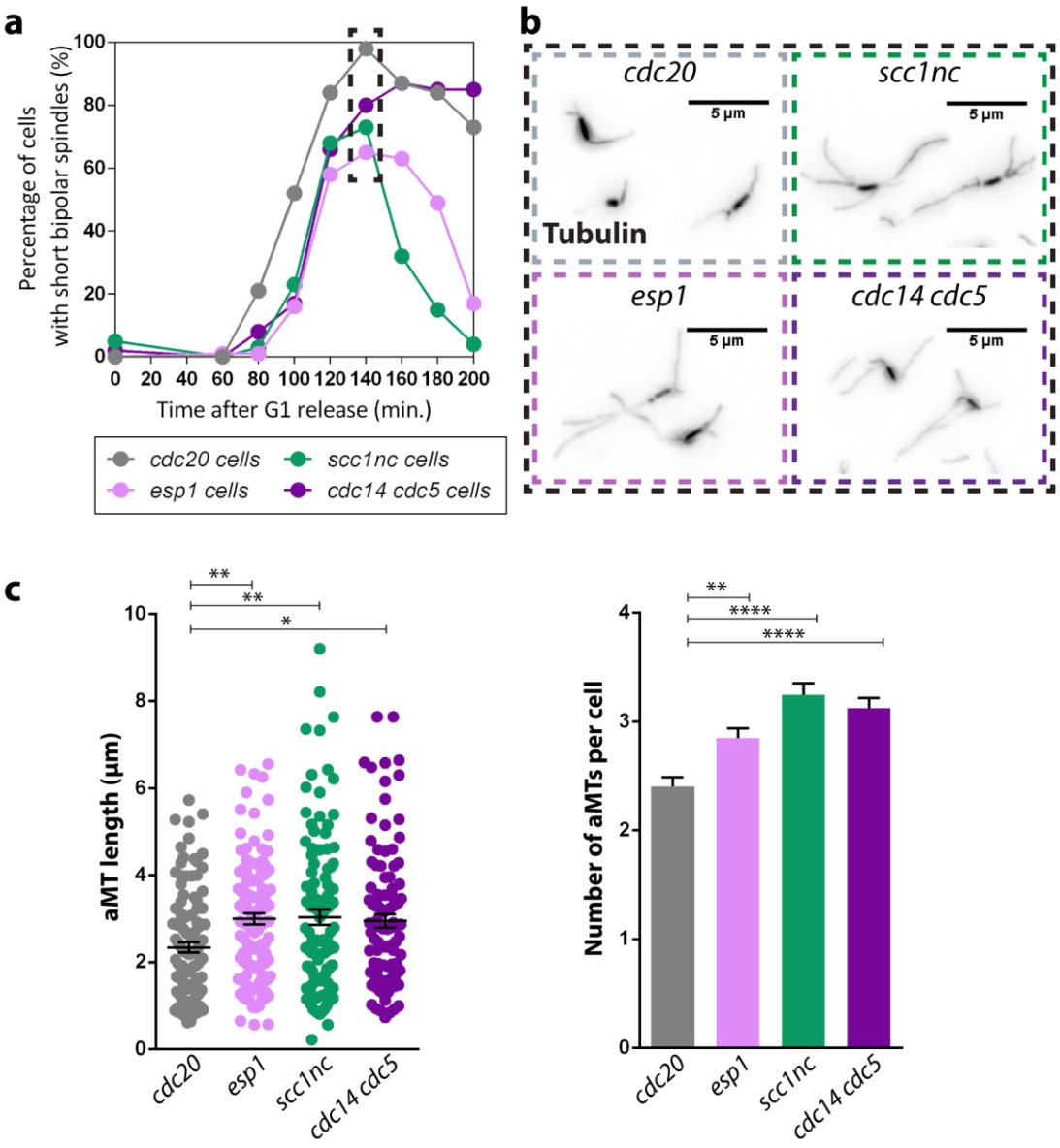

Figure 3.6. APC/C^{Cdc20} activation is necessary to stabilize aMTs. *cdc20-AID* (Ry4853), *esp1-1* (Ry9490), *pGAL-SCC1nc* (Ry8210) and *cdc14-1 cdc5-as1* (Ry1602) cells arrested in G1 by α-factor in YEPR at 23°C were released at 37° in fresh YEPR media supplemented with 2% galactose to inactivate the *esp1-1* and the *cdc14-1* alleles and to express the *SCC1nc* allele. Auxin and CMK were also added to deplete the Cdc20-AID protein to inactivate the *cdc5-as1* allele, respectively. Cells were incubated at 37° to inactivate both the *esp1-1* and the *cdc14-1* alleles. (**a**) Cells were collected at the indicated time-points to determine the percentage of cells with short bipolar spindles. (**b**) Representative images of the time-points analyzed are shown. (**c**) Quantification of aMT length and number in cells of the indicated genotype (n=100; mean +/- SEM is shown;*=p<0.05 - **=p<0.01 - ****=p<0.0001) is shown. Note that in both *esp1-1* and *pGAL-SCC1nc* cells, spindles collapse soon after reaching a bipolar conformation. The aMT analysis was performed before this spindle collapse (black box; after 140 minutes from the release).

To further validate this result, we assessed aMTs at the terminal arrest of *esp1* cells preventing spindle collapse. To this end, we decided to: (i) prevent nuclear movement into the bud by disrupting spindle pulling forces, via *DYN1* deletion; (ii) impair MEN activity by inhibiting Cdc15 and Cdc5 – two of its essential components – taking advantage of *cdc15* and the *cdc5* mutant alleles; and (iii) inactivate Cdc14 thanks to the *cdc14* mutant allele. We found that, compared to *esp1* mutant cells, a higher number of *esp1 dyn1*, *esp1 cdc15*, *esp1 cdc5,* and *esp1 cdc14* cells retain the bipolar spindle conformation during the protracted arrest (**figure 3.7a**), thus supporting the idea that nuclear movement into the bud and low CDK activity are responsible for the spindle collapse observed in cells with an active APC/C^{Cdc20}. However, we noticed that Cdc14 inactivation was more effective than Cdc15, Cdc5 or Dyn1 impairment in retaining the bipolar spindle morphology in *esp1* arrested cells, hence suggesting that even a MEN-independent pool of Cdc14 contributes to the spindle collapse. Importantly, we found that aMTs of *esp1 cdc15* arrested cells resemble those of double mutant cells (on average, 4 µm and 3.5 aMT per cell in esp1 cdc15 cells and 4.1 µm and 3.4 aMT per cell in *cdc14 cdc5* cells), with no clear synergistic effect observed upon Cdc14 and Cdc5 inactivation (**figure 3.7b** and **3.7c**). Altogether, these data indicate that: (i) the activation of the APC/C^{Cdc20} is the first step of a molecular cascade that generates the anaphase molecular signature, which is necessary and sufficient to elicit the aMT phenotype of *cdc14 cdc5*; (ii) this signature does not involve separase activation or cohesin cleavage; and (iii) up to cohesin cleavage, Cdc14 and Cdc5 concomitant inactivation is a dispensable condition. This last observation is very puzzling, because it implies that Cdc14 and Cdc5 requirement for aMT modulation differs according cell cycle phase. However, this is in line with the timing of Cdc14 activation, which remains inactive up to metaphase and is activated only at anaphase onset.

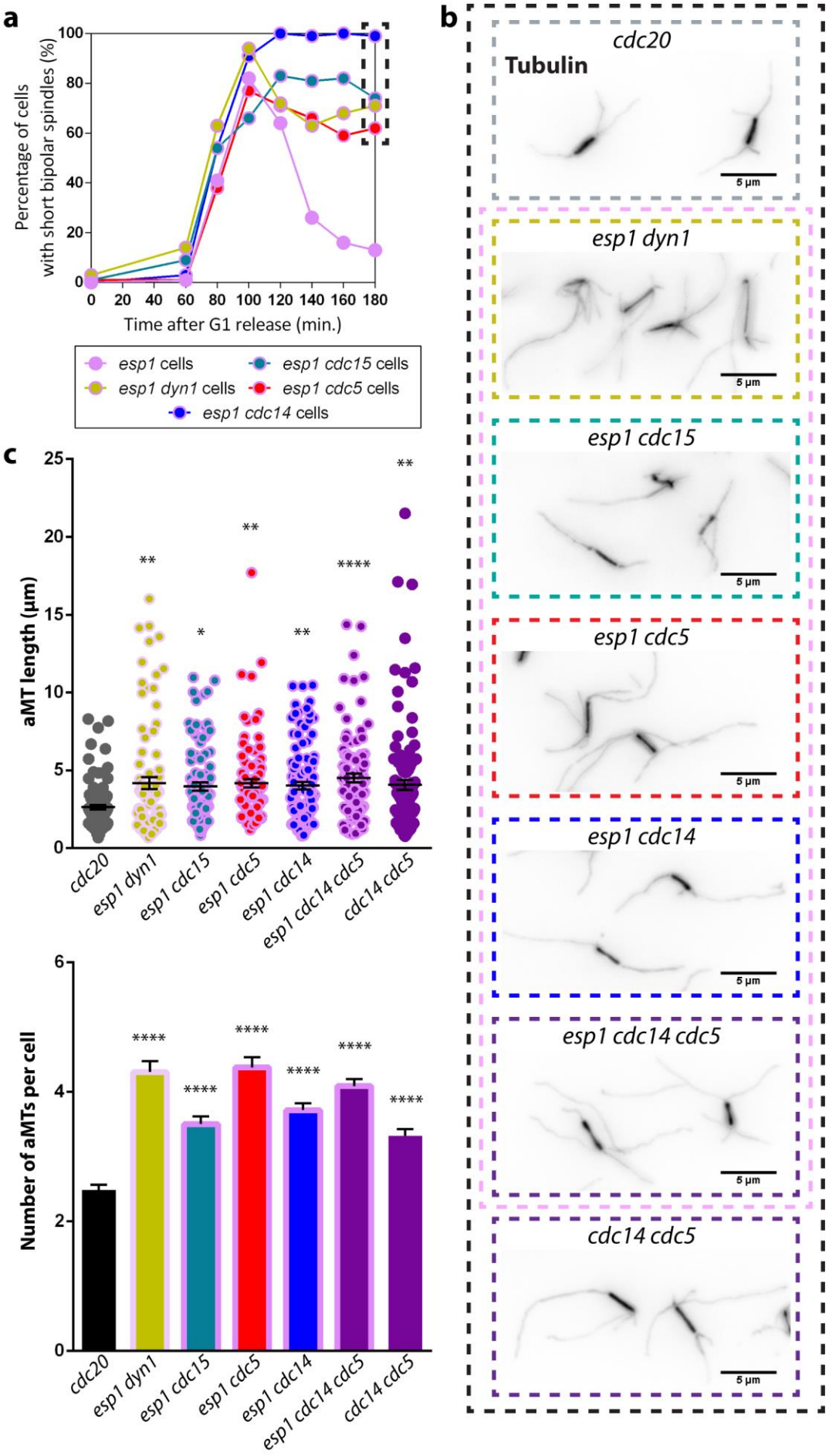
a
Percentage of cells with short bipolar spindles (%)
Time after G1 release (min.)
esp1 cells
esp1 dyn1 cells
esp1 cdc14 cells
esp1 cdc15 cells
esp1 cdc5 cells
b
cdc20
Tubulin
esp1 dyn1
esp1 cdc15
esp1 cdc5
esp1 cdc14
esp1 cdc14 cdc5
cdc14 cdc5
5 µm
c
aMT length (µm)
Number of aMTs per cell
cdc20
esp1 dyn1
esp1 cdc15
esp1 cdc5
esp1 cdc14
esp1 cdc14 cdc5
cdc14 cdc5

(Previous page) Figure 3.7. APC/C^{Cdc20} activation is sufficient to stabilize aMTs. *esp-1* (Ry9490), *esp1-1 dyn1*Δ (Ry9516), *esp1-1 cdc15-as1* (Ry9512), *esp1-1 cdc5-as1* (Ry9134) *esp1-1 cdc14-1* (Ry9131), *esp1-1 cdc14-1 cdc5-as1* (Ry9128) and *cdc14-1 cdc5-as1* (Ry1602) cells arrested in G1 by α-factor in YEPD at 23°C were released in fresh YEPD media at 37° to inactivate both the *esp1-1* and the *cdc14-1* alleles, and supplemented with 1NM-PP1 analogue 9 and CMK to inactivate the *cdc15-as1* and *cdc5-as1* alleles, respectively. (**a**) Cells were collected at the indicated time-points to determine the percentage of cells with short bipolar spindles. (**a**) Representative images of the time-points analyzed are shown. (**b**) Quantification of aMT length and number in cells of the indicated genotype (n=100; mean +/- SEM is shown; **=p<0.01 - ****=p<0.0001) is shown. Note that the mutant strains analyzed retain an increase percentage of cells with a short bipolar spindle, in respect to the *esp1-1* cells. The aMT analysis was performed at the terminal arrest of each mutant strain (black box; 180 minutes after the release).

3.3.2. Anaphase molecular signature characterization by a candidate approach

Having identified the activation of the APC/C^{Cdc20} as the essential requirement for astral microtubule stabilization, we moved to: (i) search for its substrate(s), whose degradation is necessary for the process; and (ii) unveil the downstream effector(s) whose activity may be directly or indirectly impacted by the removal of the APC/C^{Cdc20} substrate.

3.3.2.1. The individual degradation of known APC/C^{Cdc20} targets is not sufficient to stabilize aMTs

To unveil the APC/C^{Cdc20} substrate(s) that affect aMT dynamics and, consequently, may be part of the signaling cascade that leads to astral microtubule stabilization, we initially proceeded with educated guesses. We tested the consequences of inactivating: (i) the anaphase inhibitor Pds1 and (ii) additional APC/C^{Cdc20} targets, some of which have been already connected to the regulation of aMT dynamics and functions[78,122,150].

3.3.2.1.1. The removal of Pds1 or Clb5 does not affect aMT dynamics

In budding yeast, securin Pds1 is the critical APC/C^{Cdc20} target whose removal is sufficient to trigger entry into anaphase[151,152]. As such, we wondered whether Pds1, in addition to its anaphase inhibitory activity, also represses aMT stability up to metaphase. To test this hypothesis, we set out to analyze metaphase arrested cells lacking Pds1, reasoning that if securin is the APC/C ^{Cdc20} involved in aMT stabilization, then the aMTs

should resemble those of mini-anaphase arrested cells. However, *cdc20 pds1* cells proficiently elongate their spindle, possibly altering aMT dynamics. Given that impairment of Cdc14 and Cdc5 activities does not affect aMTs in metaphase, we avoided this caveat by preventing spindle elongation and inactivating the two proteins in *pMET-CDC20 pds1* cells, and found that *pMET-CDC20 cdc14 cdc5 pds1* cells retain unstable aMTs, comparable to aMTs in *pMET-CDC20 cdc14 cdc5* cells (**figure 3.8a** and **3.8b**). This result indicates that the removal of Pds1 is not sufficient to stabilize aMTs and thus points toward other APC/C^{Cdc20} targets. Among the targets, cyclins represent ideal candidates. More specifically, the S-phase cyclin Clb5, which is entirely removed upon APC/C^{Cdc20}-mediated ubiquitination, and the M-phase cyclin Clb2, which is only partially degraded at anaphase onset. The degradation of the two cyclins lowers CDK activity, a reduction that is essential in higher eukaryotes to allow progression into anaphase[17], and in budding yeast to trigger mitotic exit[32]. We wondered whether, instead of Pds1, cyclins are the critical targets of APC/C^{Cdc20}-mediated aMT stabilization. However, Clb2 levels remain high in *cdc14 cdc5* cells[63], and as such we excluded that its degradation is involved in the aMT phenotype of the double mutant cells. We then evaluated the role of the S-phase cyclin by analyzing aMTs of metaphase arrested cells lacking Clb5 (*cdc20 clb5* cells), and found that they resembled those of *cdc20* mutants (**figure 3.9a** and **3.9b**). These results indicate that the individual degradation of either securin or cyclins is not sufficient to explain the role of APC/C^{Cdc20} in aMT stabilization. Since we cannot exclude that the concomitant degradation of the two APC/C^{Cdc20} targets is the required condition to stabilize aMTs, we analyzed also other known APC/C^{Cdc20} targets.

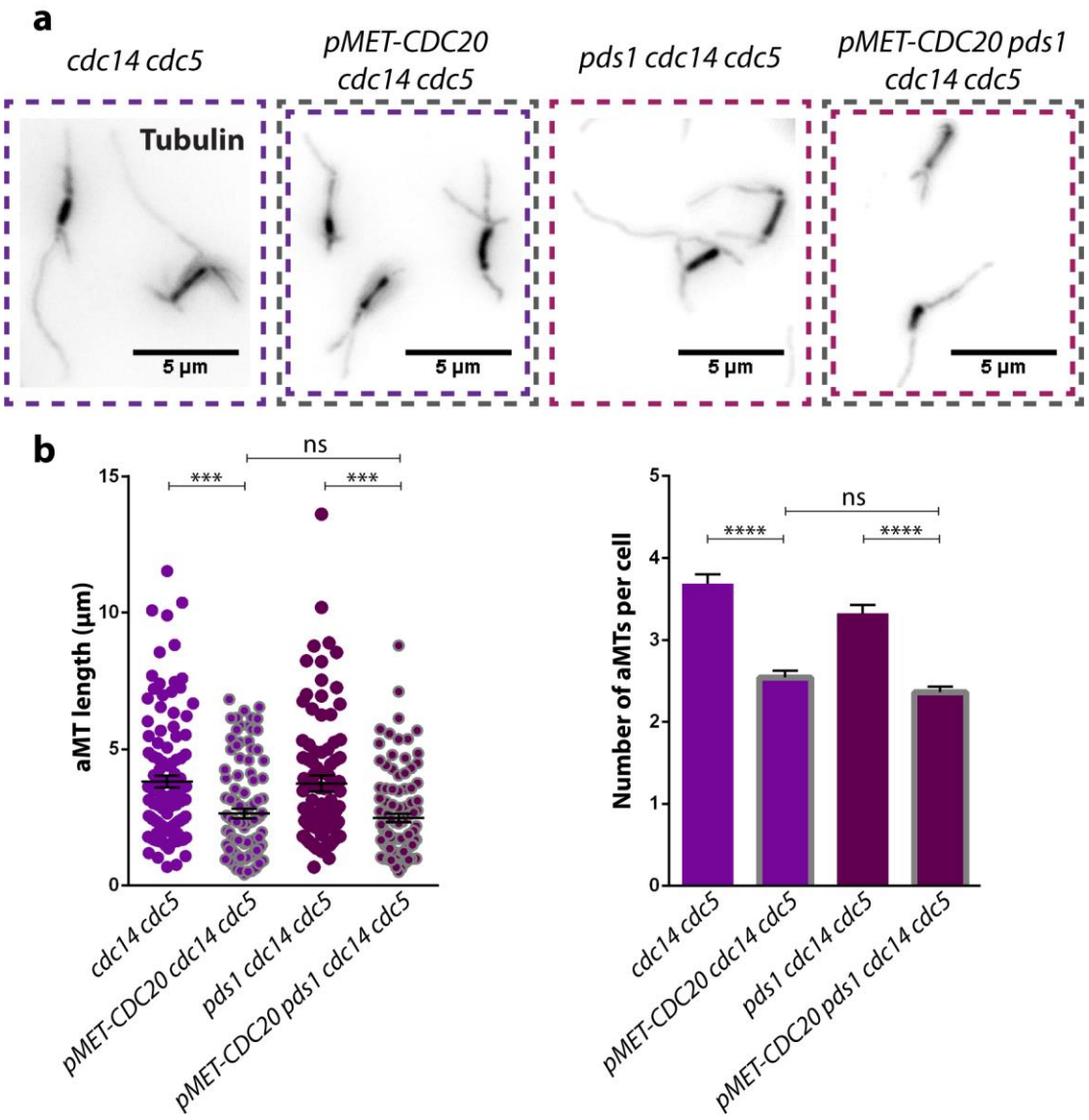

Figure 3.8. Pds1 degradation *per se* does not affect aMTs stability. *cdc14-1 cdc5-as1* (Ry1602), *pMET-CDC20 cdc14-1 cdc5-as1* (Ry3201), *pds1*Δ *cdc14-1 cdc5-as1* (Ry2143), and *pMET-CDC20 pds1*Δ *cdc14-1 cdc5-as1* (Ry8969) cells arrested in G1 by α-factor in synthetic complete medium lacking methionine (SC-Met) were released in YEPD medium added with methionine and CMK to repress the expression of *CDC2*0 and to inactivate the *cdc5-as1* allele. The culture was incubated at 37°C, to inactivate the *cdc14-1* allele. The aMT analysis was performed at the terminal arrest of each mutant strain (180 minutes after the release). (**a**) Representative images of the time-points analyzed are shown. (**b**) Quantification of aMT length and number in cells of the indicated genotype (n=100; mean +/- SEM is shown;***=p<0.001 - ****=p<0.0001) is shown.

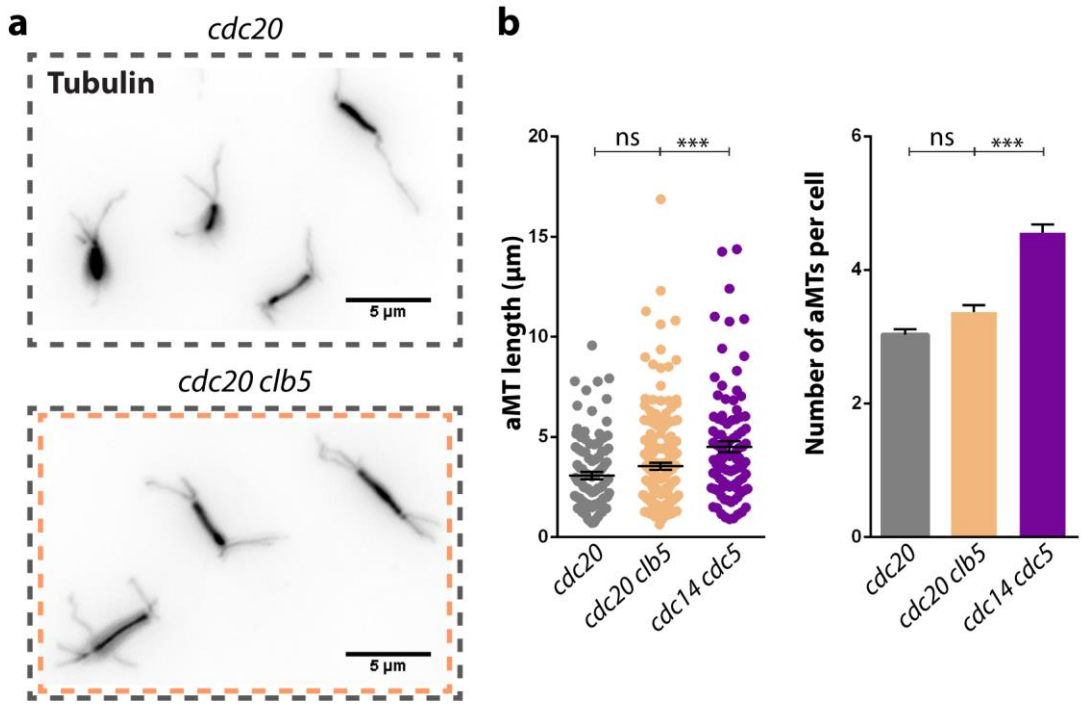

Figure 3.9. Clb5 removal does not affect aMTs. *cdc20-AID* (Ry7873), *cdc20-AID clb5*Δ (Ry9291), and *cdc14-1 cdc5-as1* (Ry1602) cells arrested in G1 by α-factor in YEPD at 23°C were released at 37°C in fresh YEPD media supplemented with Auxin and CMK, to inactivate the *cdc14-1* allele, to deplete the Cdc20-AID protein and to inactivate the *cdc5-as1* allele, respectively. The aMT analysis was performed at the terminal arrest of each mutant strain (180 minutes after the release). (**a**) Representative images of the time-point analyzed are shown. (**b**) Quantification of aMT length and number in cells of the indicated genotype (n=100; mean +/- SEM is shown;***=p<0.001) is shown.

3.3.2.1.2. The removal of Kip1, Alk2, Acm1 or Dbf4 is not sufficient to stabilize aMTs

At least four other APC/C^{Cdc20} targets exist: (i) the kinesin motor protein Kip1[60]; (ii) the Haspin-like kinase Alk2[153]; (iii) the APC/C^{Cdh1} inhibitor Acm1[154]; and (iv) the DNA replication-promoting kinase Dbf4[155]. Of note, both Alk2 and Acm1 are indirectly linked to aMT functions, as their depletion affects nuclear or spindle positioning[150,156]. Given that *KIP1*, *ALK2* and *ACM1* are non-essential genes, we assessed the effect of their deletion in *cdc20* arrested cells, but found no change in aMT morphology, even when a possible compensatory effect of Alk2-paralog Alk1 was prevented by depleting both kinases simultaneously (**figure 3.10a** and **3.10b**). To test the role of the essential protein Dbf4, we took advantage of its thermo-sensitive allele *dbf4-1*, which allows the inactivation of the protein by increasing the temperature of the medium to 37°C. *cdc20* and *cdc20 dbf4* cells were released from G1 at the permissive temperature for the *dbf4* allele, and Dbf4 was inactivated upon reaching the metaphase arrest. For the analysis, we probed aMTs after 90 minutes into the arrest, and found that their length and number was unaltered by Dbf4 inactivation (**figure 3.10a** and **3.10b**). Altogether, these results suggest that the individual degradation of the APC/C^{Cdc20} targets tested so far is not sufficient to stabilize aMTs, and point to a combined degradation of two or more candidates or toward a currently unknown APC/C^{Cdc20} target.

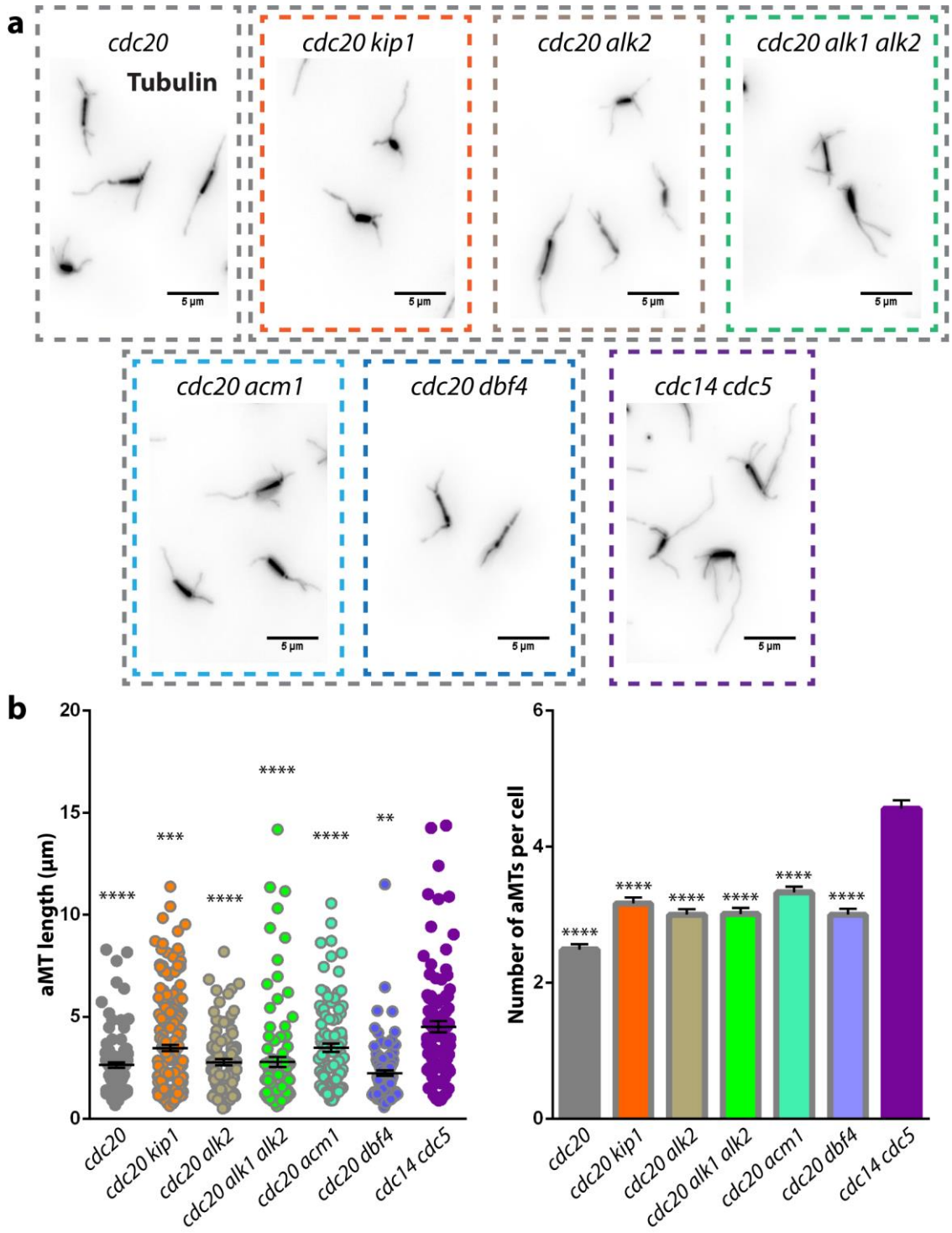

Figure 3.10. Kip1, Alk2, Acm1 or Dbf4 removal does not affect aMTs. *cdc20-AID* (Ry7873), *cdc20-AID kip1*Δ (Ry9294), *cdc20-AID alk2*Δ (Ry9880), *cdc20-AID alk*Δ*1 alk2*Δ cells (Ry9883), *cdc20-AID acm1*Δ cells (Ry10025), *cdc20-AID dbf4-1* cells (Ry9877), and *cdc14-1 cdc5-as1* cells (Ry1602) arrested in G1 by α-factor in YEPD at 23°C were released at 37°C in fresh YEPD media supplemented with CMK, to inactivate the *cdc14-1* and the *cdc5-as1* alleles, respectively. Auxin was added to deplete the Cdc20-AID protein. *cdc20 dbf4-1* cells were moved to 37°C only upon reaching metaphase (assessed by quick DAPI staining), in order to inactivate Dbf4 only after S-phase completion. The aMT analysis was performed at the terminal arrest of each mutant strain (180 minutes after the release, which corresponds to 90 minutes after reaching a metaphase-like morphology). (**a**) Representative images of the time-points analyzed are shown. (**b**) Quantification of aMT length and number in cells of the indicated genotype (n=100; mean +/- SEM is shown; **=p<0.01 - ***=p<0.001 - ****=p<0.0001) is shown.

3.3.2.2. Stabilization of aMT dynamics in *cdc14 cdc5* cells does not arise from the modulation of a specific kinetic parameter of plus-end dynamics

In budding yeast, microtubule turn over takes place exclusively at the plus-ends, while minus-ends remain anchored to the SPB and poorly exchange tubulin dimers[94]. Indeed, several MAPs and motor proteins alter aMT morphology, affecting the kinetics of plus-end dynamic instability[44,96,146]. To investigate whether the aMT phenotype of double mutant cells arises from an alteration of microtubule plus-end dynamics, we measured aMT length over time in *cdc20* and *cdc14 cdc5* cells carrying a GFP-tagged Tub1 fusion by live-cell imaging[145]. In particular, *cdc20* and *cdc14 cdc5* cells were released from G1 at the restrictive conditions for their mutant alleles, time-lapse z-series images were acquired upon reaching the terminal phenotype (**figure 3.11a**), and their aMT length was measured over time (**figure 3.11b**). Similar to what we found in our previous experiments performed on fixed-cells, also in this case, aMTs in *cdc14 cdc5* cells had a longer maximal length than those of *cdc20* cells (**table 3.1**; on average, 5 µm and 3.3 µm in *cdc14 cdc5* and *cdc20* cells, respectively). Along the same line, the mean aMT length at which both rescue and catastrophe events occur were drastically increased in *cdc14 cdc5* cells (on average, 2.5 µm/4.7 µm in *cdc14 cdc5* cells and 1.4 µm/2.6 µm in *cdc20* cells). To assess whether these changes reflect the modulation of specific properties of plus-end dynamics, we measured different microtubule kinetic parameters[96,117,146]. In particular, based on changes in aMT length over time, we calculated microtubule dynamicity - an estimation of tubulin exchange rate, equivalent to the number of tubulin dimers gained or lost per second[147] - and identified polymerization, depolymerization and pausing events[145]. Finally, by analyzing aMT length during each specific event, we extrapolated polymerization and depolymerization rates, rescue and catastrophe frequencies, and the time spent in the growing or shrinking phases[145]. We found that none of the calculated parameters specifically changes between *cdc20* and *cdc14 cdc5* arrested cells (**table 3.1**).

However, a similar trend in *cdc14 cdc5* cells can be observed - a slight increase in microtubule dynamicity, linked to an increment in both growing and shrinking rates and time spent growing instead of shrinking and pausing. These results support that measurements of aMT length in fixed cells properly reflect aMT stability, but suggest that the aMT phenotype of double mutant cells is not due to the alteration of a specific plus-end dynamic property.

Table 3.1. Parameters of aMT dynamics

	cdc20	*cdc14 cdc5*	
Rates (µm/min.)			
Growing	1,883+/-0,1223	1,974+/-0,1037	*p*=0,5774
Shrinking	2,203+/-0,1624	2,297+/-0,3630	*p*=0,8414
Frequency (event/min.)			
Rescue	0,2483+/-0,0276	0,2387+/-0,0215	*p*=0,7844
Catastrophe	0,2759+/-0,0345	0,2445+/-0,0252	*p*=0,4629
Total times (%)			
Growing	21,03+/-2,147	26,44+/-3,022	*p*=0,2019
Shrinking	21,03+/-3,465	19,08+/-2,772	*p*=0,6625
Pausing	57,93+/-4,201	54,48+/-4,124	*p*=0,5783
Dynamicity (subunit/sec)	39,39+/-1,843	43,28+/-2,555	*p*=0,2752
Length at rescue (µm)	1,374+/-0,2969	2,505+/-0,4925	*p*<0.1
Length at catastrophe (µm)	2,633+/-0,3348	4,682+/-0,5983	*p*<0.01
Maximum length (µm)	3,310+/-0,3806	5,016+/-0,4550	*p*<0.1

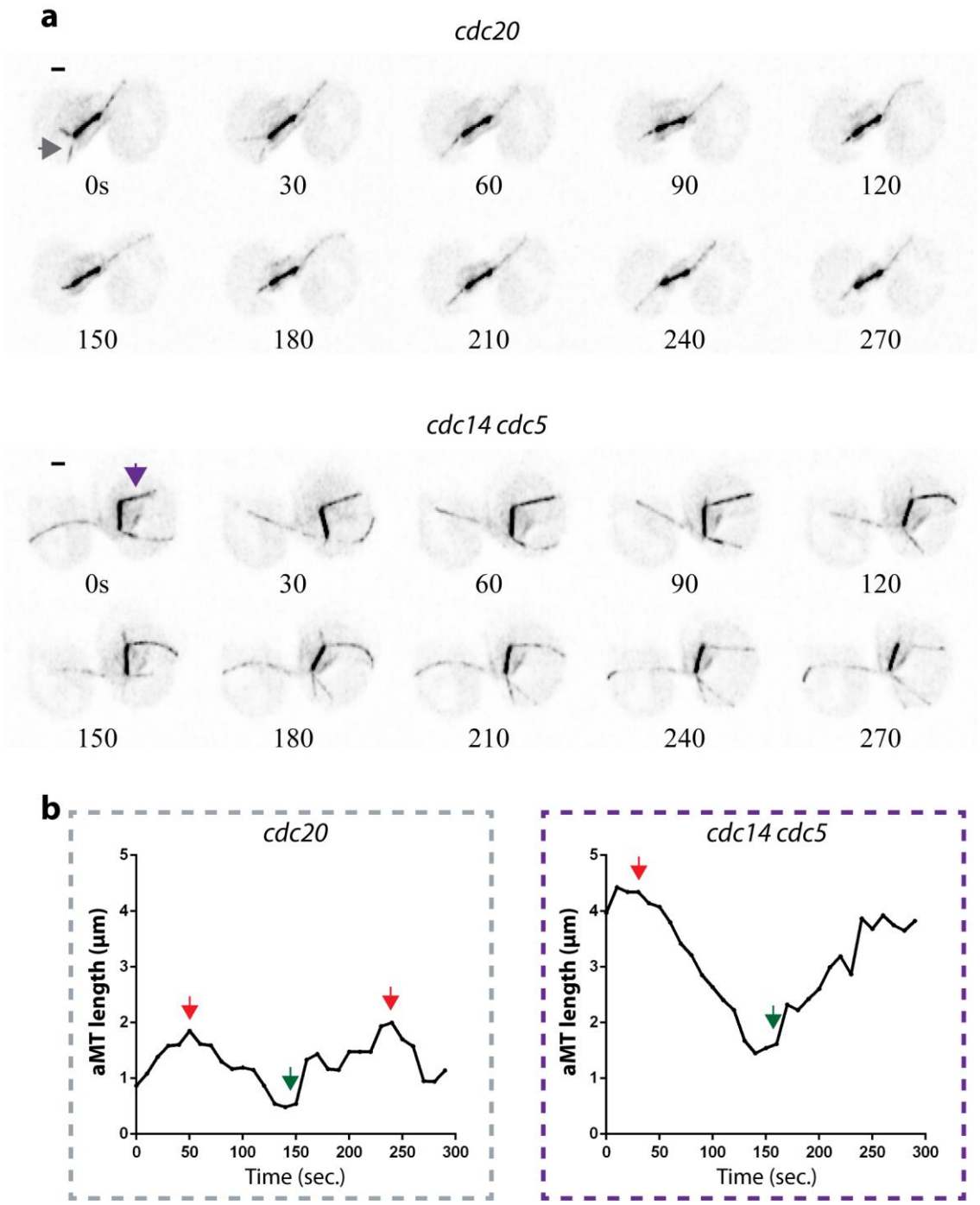

Figure 3.11. Investigating aMT dynamics by live cell-imaging. *cdc20-AID* (Ry7732) and *cdc14-1 cdc5-as1* (Ry3256) cells carrying a *TUB1-GFP* fusion were arrested in G1 by α-factor in YEPD at 23°C and then released at 37°C in fresh YEPD media supplemented with CMK, to inactivate the *cdc14-1* the *cdc5-as1* alleles, respectively. Auxin was added to deplete the Cdc20-AID protein. To analyze aMT dynamics over time, when cells reached the terminal phenotype they were transferred in a CellASIC ONIX plate and z-stack time-lapse images of spindle microtubules were acquired. To maintain the arrest, cells were incubated at 37°, and perfused with fresh media supplemented with the above mentioned compounds for the entire length of the experiment. (**a**) Representative time-lapse images of *cdc20-aid* and *cdc14-1 cdc5-as1* cells are shown. Scale bar = 1 µm (**b**) The length of each aMT was measured over-time and plotted; two representative graphs are shown. The two aMTs plotted are highlighted by a grey and a purple arrow in **a**. The occurrence of catastrophe and rescue events is indicated in the graphs with a red and a green arrow, respectively.

3.3.2.3. aMT stabilization, typical of *cdc14 cdc5* cells, may arise from the alteration of aMT-cortex connection dynamics

The regulation of aMT dynamics often occurs at the cellular cortex, where different proteins bind to aMTs and promote either their growth or shrinkage. We wondered whether the increased aMT stability seen in the double mutant cells reflects changes in the dynamics of aMT-cortex interactions. To test this hypothesis, we analyzed the behavior of aMTs at the cellular cortex in *cdc20* and *cdc14 cdc5* arrested cells carrying a GFP-tagged Tub1 fusion by live-cell imaging, in this case, measuring the time that each individual aMT spends contacting the cellular cortex (examples are shown in **figure 3.12a**). We found that aMTs of *cdc14 cdc5* cells remain bound to the cellular cortex drastically longer than aMTs of *cdc20* cells (**figure 3.12b**; on average, aMTs of *cdc14 cdc5* and *cdc20* cells remain close to the cortex during 77% and 39% of the analyzed time, respectively), thus indicating that the dynamics of aMT-cortex connections are altered in the double mutant cells. As aMTs normally detach from the cellular cortex following a catastrophe event, we hypothesized that the cortex-mediated aMT shrinkage machinery might be impaired in *cdc14 cdc5* cells. In budding yeast, two proteins are known to promote aMT shrinkage at the cellular cortex: the minus-end directed motor protein Dyn1, which promotes aMT shortening alone[96] or in combination with the microtubule-depolymerizing motor protein Kip3[130], and the microtubule binding protein Kar9, which associates with cortex-mediated shrinking events[109] and guides aMTs toward a destabilization zone located at the bud-neck[135]. To assess whether impairment of cortex-mediated aMT shrinkage results in the stabilization of aMTs in cells arrested with short bipolar spindles, we concomitantly inactivated Dyn1 and Kar9 pathways in *cdc20* cells by combining the *DYN1-AID* mutant allele with *KAR9* deletion[38]. We found that aMTs of *cdc20 kar9 dyn1* cells are as stable as those of *cdc14 cdc5* cells (**figure 3.13a** and **3.13b**). Altogether, these results suggest that the aMT stabilization observed in double

mutant cells may reflect an alteration of the aMT shrinkage machinery located at the cellular cortex.

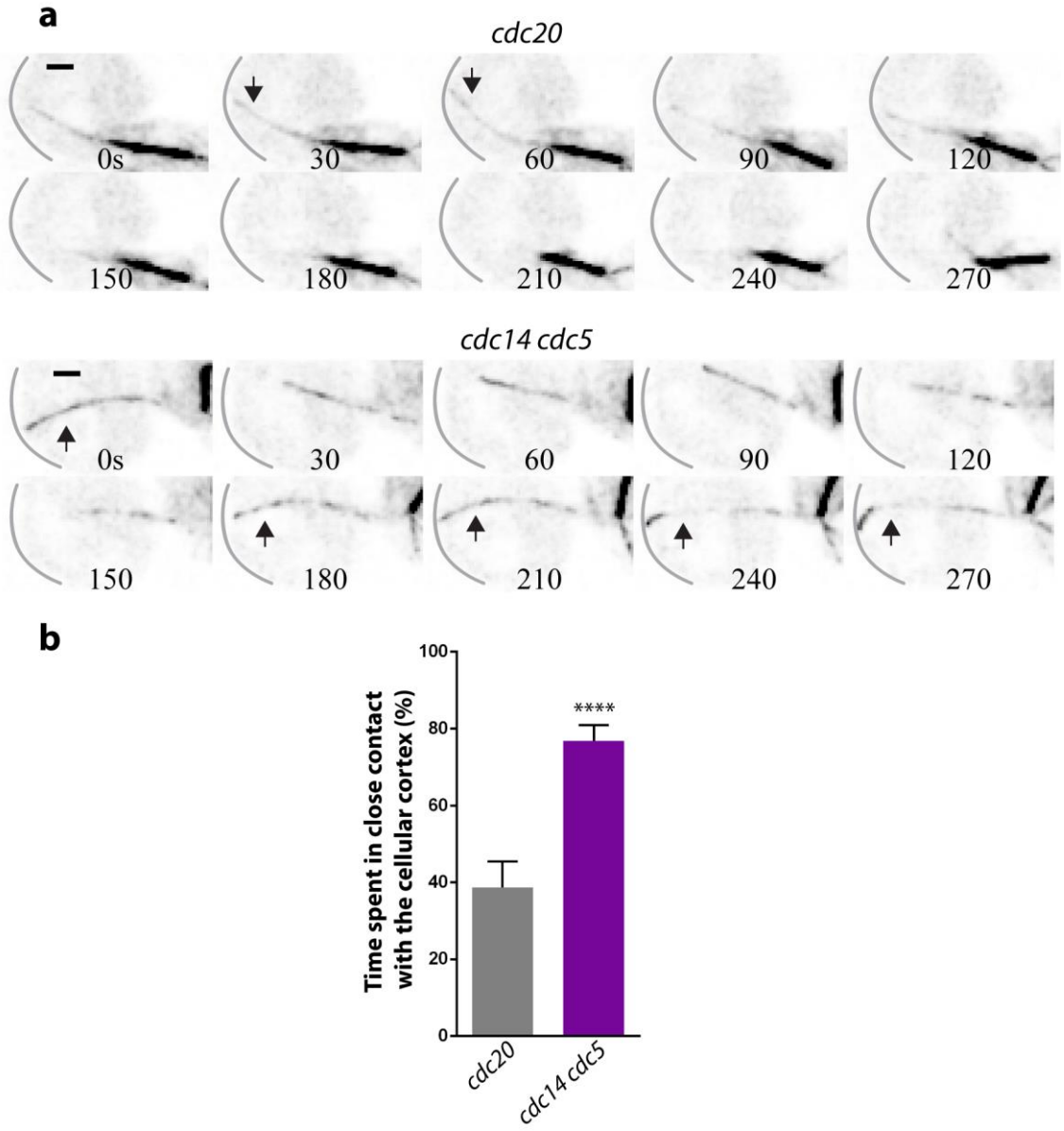

Figure 3.12. *cdc14-1 cdc5-as1* cells show an altered aMT/cortex interaction. *cdc20-AID* (Ry7732) and *cdc14-1 cdc5-as1* (Ry3256) cells carrying a *TUB1-GFP* fusion treated as in figure 3.11 were analyzed at their terminal arrest for aMT/cortex interaction dynamics. The plasma membrane was visualized by DIC images of the cells. (**a**) Two examples of aMTs contacting the cellular cortex (indicated with a grey line) are shown. Black arrows indicate when the analyzed aMT is contacting the cortex. (**b**) Quantification of the time that each aMT spends contacting the cortex over the total time (n=15; mean +/- SEM is shown; ****=p<0.0001) is shown.

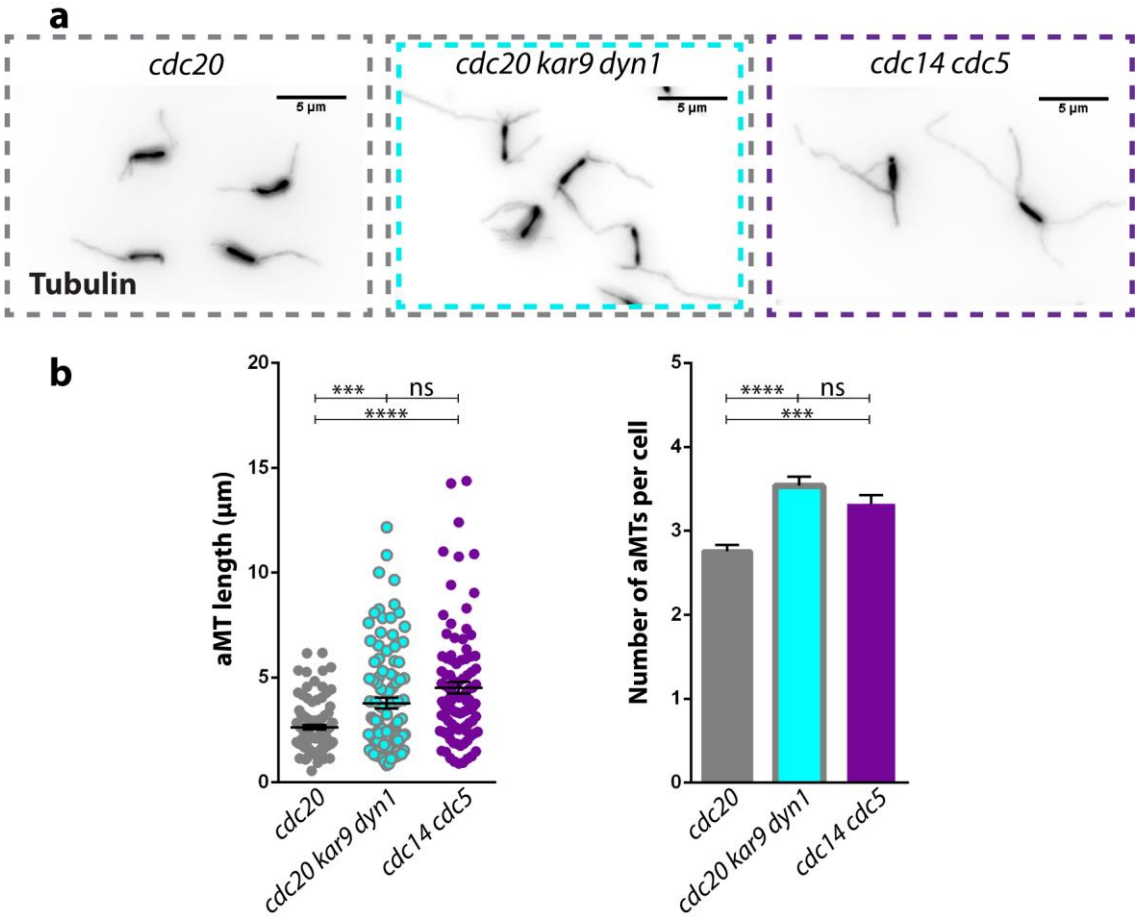

Figure 3.13. Affecting aMT/cortex interactions alters aMT dynamics. *cdc20-AID* (Ry7873), *cdc20-AID kar9*Δ *dyn1-AID* (Ry7545), and *cdc14-1 cdc5-as1* (Ry1602) cells were arrested in G1 by α-factor in YEPD at 23°C and then released at 37°C in fresh YEPD media supplemented with CMK, to inactivate the *cdc14-1* and the *cdc5-as1* alleles, respectively. Auxin was added to deplete the Cdc20-AID and Dyn1-AID proteins. The aMT analysis was performed at the terminal arrest of each mutant strain (180 minutes after the release). (**a**) Representative images of the time-poinst analyzed are shown. (**b**) Quantification of aMT length and number in cells of the indicated genotype (n=100; mean +/- SEM is shown;***=p<0.001 - ****=p<0.0001) is shown.

3.3.2.4. Alterations in the actin cytoskeleton or in the septin ring do not generate the aMT phenotype of *cdc14 cdc5* cells

Given that the aMT morphology of *cdc14 cdc5* cells is phenocopied by the concomitant inactivation of Kar9 and Dyn1 pathways in *cdc20* arrested cells, we wondered if the phenotype of double mutant cells arises from the impairment of the two pathways. If this is the case, either two different components or a common element of the Kar9 and Dyn1 pathways should be altered in *cdc14 cdc5* cells. We first searched for a common requirement of the two pathways. To function properly, both pathways rely on the actin

cytoskeleton: on the one hand, Kar9 binds to the actin motor protein Myo2, which moves along actin in order to pull the spindle toward the bud; on the other hand, Dyn1 activity is promoted by mitochondria[137], whose segregation relies on actin[157]. As such, we tested the possibility that the actin cytoskeleton might be altered in *cdc14 cdc5* cells by comparing its structure in the double mutant cells with that of *cdc20* arrested cells. Two actin structures can be recognized in budding yeast, namely cables and patches. Actin cables are filamentous structures located around the bud-neck and are used by Myo2 and other actin motor proteins to direct their movements, while actin patches are punctate bodies mostly involved in the endocytic process. We evaluated whether the actin staining could clearly distinguish between these two structures by analyzing the actin cytoskeleton of a *wild-type* strain growing exponentially, and found that both structures can be visualized in dividing cells (**figure 3.14a**). We then compared the actin cytoskeleton of *cdc14 cdc5* arrested cells with that of *cdc20* and *cdc15* cells, used here as controls of metaphase and anaphase arrest, respectively. Both mutant strains were synchronized in G1, released at the restrictive conditions for the mutant alleles, and the appropriate time-point at which to perform actin staining was selected based on nuclear and spindle morphologies. We found no clear differences between the actin cytoskeleton of *cdc20* or *cdc15* arrested cells and that of *cdc14 cdc5* arrested cells (**figure 3.14b**), thus indicating that double mutant cells carry unaltered actin structures.

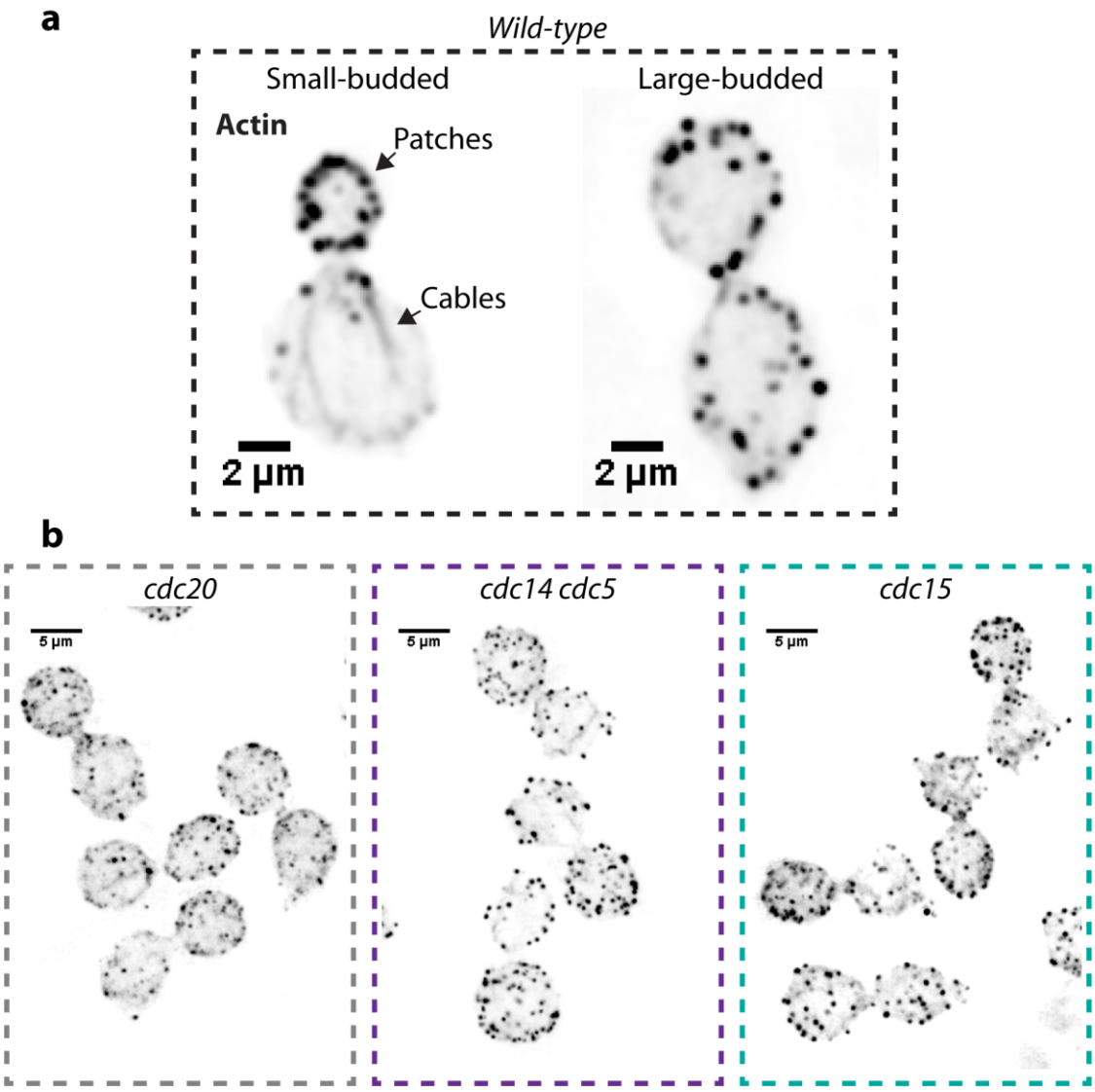

Figure 3.14. The actin cytoskeleton is unaltered in *cdc14-1 cdc5-as1* cells. (**a**) Exponentially growing *wild-type* cells (Ry1) were probed for their actin cytoskeleton. Two examples (a small-budded and a large-budded cell) are shown. The black arrows indicate actin patches and cables. (**b**) *cdc20-AID* (Ry4853), *cdc14-1 cdc5-as1* (Ry1602) and *cdc15-as1* (Ry1112) cells arrested in G1 by α-factor in YEPD at 23°C were released at 37° in fresh YEPD media supplemented with CMK and 1NM-PP1 analogue 9 to inactivate the *cdc14-1*, the *cdc5-as1*, and the *cdc15-as1* alleles, respectively. Auxin was added to deplete the Cdc20-AID protein. The actin cytoskeleton was assessed at the terminal arrest of each mutant strain (180 minutes after the release). Representative images of the time-points analyzed are shown.

Besides the actin cytoskeleton, another common feature of both Kar9 and Dyn1 pathways is the septin ring. The septin ring is a proteinaceous structure that is formed around the bud-neck and is involved in several cellular processes, such as cellular polarization and cytokinesis. Regarding the two pathways, the septin ring mediates aMT capture and shrinkage at the bud-neck upon Kar9-mediated transport of aMTs to its proximity[135] and fosters Dyn1 activity, promoting both Dyn1 localization on the bud-directed SPB[123] and the polarization of the Dyn1 cortical receptor Num1 toward the bud-cortex[19]. To test whether alterations in the septin ring may account for the aMT stabilization seen in *cdc14 cdc5* cells, we evaluated the effects of its inactivation in *cdc20* arrested cells, taking advantage of the thermo-sensitive allele of the septin Cdc12 (*cdc12-6*), which induces the disassembly of the septin ring when the growth medium temperature is raised to 37°C. We found that *cdc20 cdc12* cells retain unstable aMTs (**figure 3.15a** and **3.15b**), similar to the ones of *cdc20* arrested cells, thus indicating that impairment of septin is not sufficient to stabilize aMTs. Altogether, these results suggest that neither alterations in the actin cytoskeleton nor in the septin ring structure account for the aMT phenotype of *cdc14 cdc5* cells.

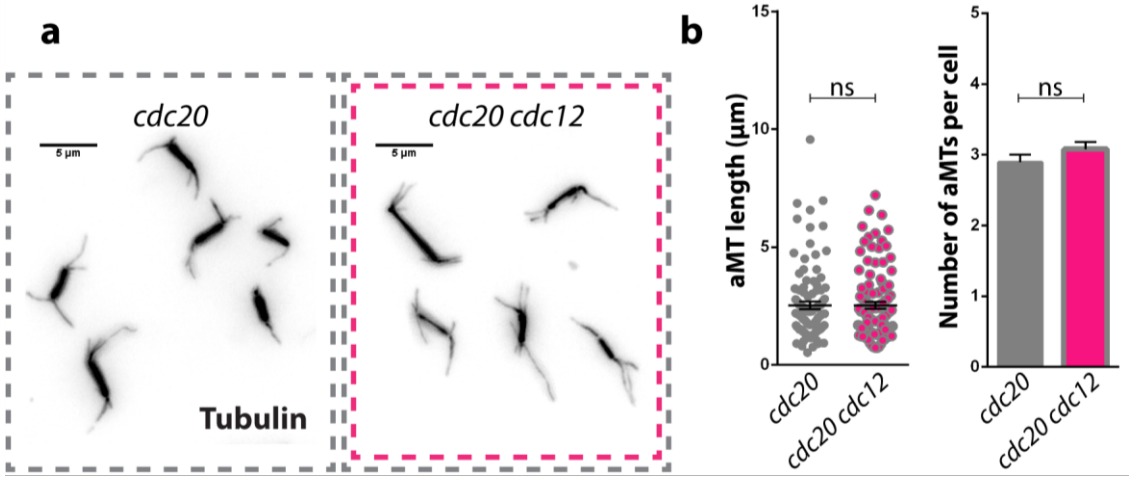

Figure 3.15. Disrupting the septin ring does not impact on aMT length and number. *cdc20-AID* (Ry4853) and *cdc20-AID cdc12-6* (Ry9237) cells were arrested in G1 by α-factor in YEPD at 23°C and then released at 37°C in fresh YEPD media supplemented with Auxin, to inactivate the *cdc12-6* allele and to deplete the Cdc20-AID protein, respectively. The aMT analysis was performed at the terminal arrest of each mutant strain (180 minutes after the release). (**a**) Representative images of the time-points analyzed are shown. (**b**) Quantification of aMT length and number in cells of the indicated genotype (n=100; mean +/- SEM is shown) is shown.

3.3.2.5. Spindle elongation "*per se*" does not alter aMT length

Up to now, our candidate approach allowed us to link the aMT stabilization that follows APC/C^{Cdc20} activation at anaphase onset to alterations in aMT/cortex interaction dynamics. Subsequently, we moved our educated guesses toward a yet unresolved issue in the stabilization process, that is, the role of Cdc14 and Cdc5. Our results suggest that the concomitant inactivation of Cdc14 and Cdc5 is not required to stabilize aMTs, at least as long as cohesin remains uncleaved, but the aMT length of *cdc15*, *cdc14* and *cdc5* cells clearly indicates that it is required afterwards. This situation recalls the role of Cdc14 and Cdc5 in promoting spindle elongation, and indeed spindle length is a clear difference between *cdc14 cdc5* arrested cells and all the other mutants tested that arrest in anaphase. We then wondered whether the inactivation of Cdc14 and Cdc5 promotes aMT stabilization by preventing spindle elongation. Given that the impairment of aMT-cortex connection dynamics stabilizes aMTs, we took advantage of *kar9 dyn1* double mutant cells to test the possibility that spindle elongation negatively affects aMT stabilization. In particular, we compared aMTs of *cdc20 kar9 dyn1* cells with *cdc15 kar9 dyn1* cells, which arrest with short and long bipolar spindles, respectively. We found that the abrogation of aMT-shrinkage events at the cellular cortex promotes aMT elongation independently of spindle length (**figure 3.16a** and **3.16b**) – as indicated by the similar (and even increased) fold-change in aMT length due to Kar9 and Dyn1 inactivation in *cdc20* and *cdc15* cells, 1.4 and 1.68, respectively – thus indicating that spindle elongation "*per se*" does not prevent aMT stabilization.

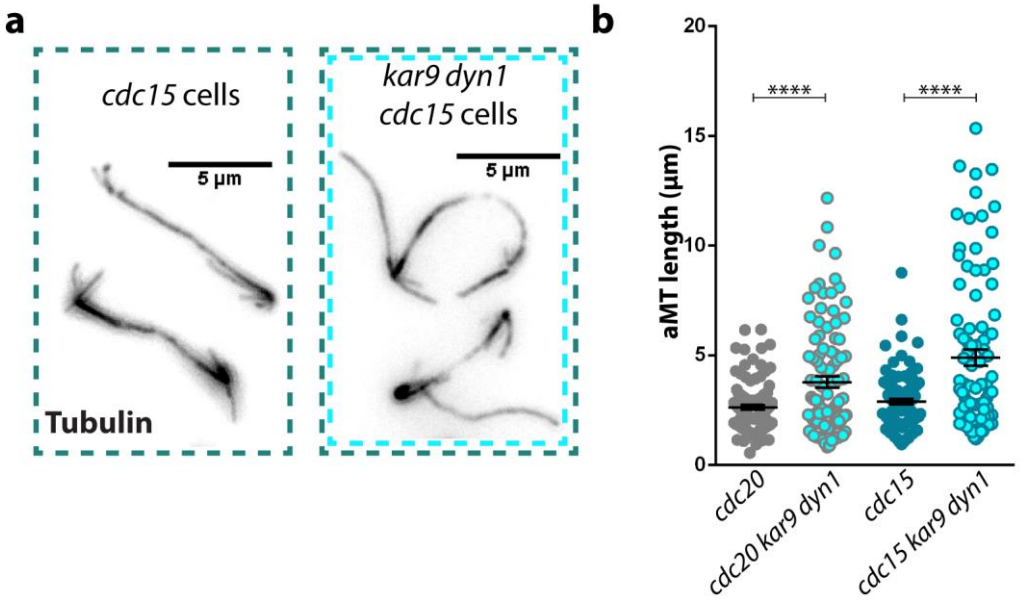

Figure 3.16. Affecting aMT/cortex interactions increases aMT stability independently to spindle length. *cdc20-AID* (Ry7873), *cdc20-AID kar9*Δ *dyn1-AID* (Ry7545), *cdc15-as1* (Ry1112) and *cdc15-as1 kar9*Δ *dyn1-AID* (Ry7620) cells arrested in G1 by α-factor in YEPD at 23°C were released in fresh YEPD media supplemented with 1NM-PP1 analogue 9 and Auxin, to inactivate the *cdc15-as1* allele and to deplete the Cdc20-AID/Dyn1-AID proteins, respectively. The aMT analysis was performed at the terminal arrest of each mutant strain (180 minutes after the release). (**a**) Representative images of the time-points analyzed are shown. (**b**) Quantification of aMT length and number in cells of the indicated genotype (n=100; mean +/- SEM is shown; ****=p<0.0001) is shown.

3.3.3. Anaphase molecular signature characterization by a proteome-wide approach

Besides the candidate approach, we investigated the mechanisms that govern aMT modulation at the metaphase to anaphase transition by interrogating, in particular, the proteome and phospho-proteome of: (i) *cdc20* cells, which typify metaphase and carry unstable aMTs; (ii) *cdc14 cdc5* cells, which arrest in "mini-anaphase" and show stable aMTs; and (iii) *cdc15* cells, which arrest in anaphase with an intermediate aMT phenotype. This approach allowed us to characterize aMT regulation in an unbiased way and, more broadly, to unveil overall microtubule regulation that occurs at anaphase onset. The analysis was performed in collaboration with Prof. Steven Gygi at the Harvard Medical School in Boston, using a multiplexed Tandem Mass Tag (TMT) 10-plex-based strategy as described by Prof. Gygi and colleagues[144]. The 10-plex technology allowed us

to increase the confidence of the screening, as we examined the proteome and phospho-proteome of *cdc20* and *cdc14 cdc5* cells in three biological replicates, and that of *cdc15* cells was examined in two biological replicates. The workflow was similar to the experiments performed up to now: first, *cdc20*, *cdc14 cdc5*, and *cdc15* cells were arrested in G1 at the permissive conditions of the four mutant alleles; secondly, cells were synchronously released into the cell cycle, followed by monitoring nuclear- and spindle morphology; finally, at the time-point of their terminal arrest, cells were collected and analyzed using the 10-plex technology. With this approach, we quantified the abundance of 4641 proteins and identified 5324 phosphosites. At a first glance, the TMT strategy allowed a highly conservative phosphosite assessment, as suggested by the fact that the vast majority of the identified sites were already reported in other phospho-proteomic screenings[158–161]. A comprehensive analysis of the several pathways that are differently modulated in the three mutant strains is still ongoing. However, a user-friendly software allowed us to interrogate the data to some extent and answer rather specific questions.

3.3.3.1. Proteome analysis revealed other possible APC/C^{Cdc20} substrates

Given that APC/C^{Cdc20} activation is the required step to stabilize aMTs, but none of its tested targets singularly affects aMT dynamics, we interrogated the proteomes by searching for proteins whose degradation kinetics typifies that of APC/C^{Cdc20} targets, being relatively high in metaphase (*cdc20* cells) and less abundant in anaphase (*cdc14 cdc5* and *cdc15* cells). Our top hits resulted to be the already proposed targets that we tested in the candidate approach, thus supporting this filtering approach to identify new APC/C C^{Cdc20} substrates (**figure 3.17**). The only exception is Clb5, which together with many other cyclin subunits has not been identified at all in the proteomic analysis, probably due to the high sequence similarity among the cyclin family members. Indeed, when a sequenced peptide belongs to more than one protein, it is directly discarded. With this approach, we identified four possible targets that resemble the interrogated pattern,

although less clearly than the already tested candidates: the 3-phosphoglycerate dehydrogenase Ser3; the high-affinity glucose transporter Hxt4; the ammonium transmembrane transporter Mep2; and finally, the protein of unknown function Tma10. To our knowledge, no obvious connection exists between these four proteins and aMTs. Altogether, these results support the sensitivity of the proteomic screen, as the vast majority of the already known APC/C^{Cdc20} targets emerged, and provide other possible candidates to be validated.

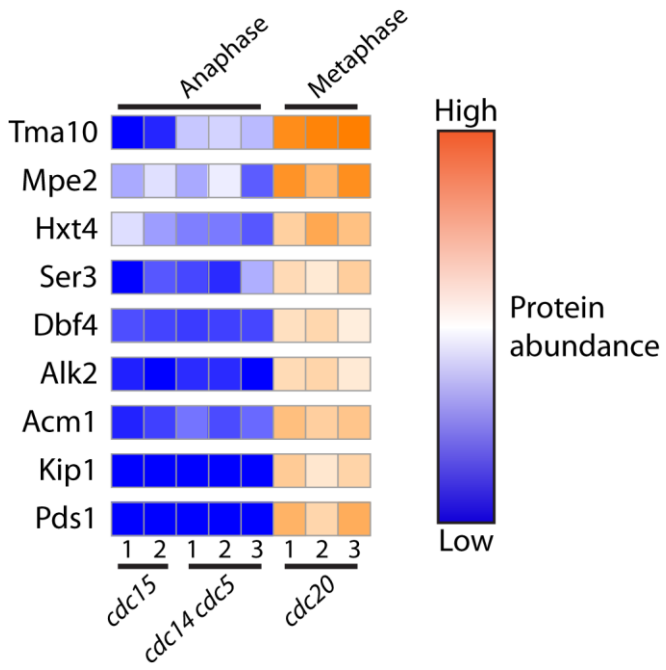

Figure 3.17. Potential unknown APC/C^{Cdc20} targets are identified by proteomic analysis. *cdc15-as1* (Ry1112), *cdc14-1 cdc5-as1* (Ry1602) and *cdc20-AID* (Ry4853) cells arrested in G1 by α-factor in YEPD at 23°C were released at 37°C in fresh YEPD media supplemented with 1NM-PP1 analogue 9 and CMK, to inactivate the *cdc14-1*, the *cdc15-as1* and the *cdc5-as1* alleles, respectively. Auxin was added to deplete the Cdc20-AID protein. At the terminal arrest, a phospho-proteome analysis of the three different mutants was performed. The proteomic data obtained were filtered for proteins that show a pattern of abundance reminiscent to that of APC/C^{Cdc20} targets - high in metaphase (*cdc20-AID* cells) and low in anaphase (*cdc14-1 cdc5-as1* and *cdc15-as1* cells). The top 9 hits of this filtering and their abundance profile for each strain (2 replicates for *cdc15-as1* cells, 3 replicates for both *cdc14-1 cdc5-as1* and *cdc20-AID* cells) are shown.

3.3.3.2. Phospho-proteome analysis revealed several possible downstream effectors of anaphase aMT stabilization

In budding yeast mitosis, microtubules are known to be regulated by phosphorylation and dephosphorylation events on motor proteins and MAPs. For this reason, we interrogated the phospho-proteomes of *cdc20*, *cdc14 cdc5* and *cdc15* cells to obtain hints on the downstream effector(s) of anaphase-induced aMT stabilization. We started the analysis by examining five kinesin motor proteins (Cin8, Kip1, Kip2, Kip3, and Kar3), the single minus-end directed protein Dyn1, and four MAPs (Bim1, Bik1, Ase1, and Stu2), all of which have been reported to affect aMT dynamics[20,44,59,146]. Of note, all of these proteins are equally abundant in the three mutant strains except for Kip1, which, being an APC/C^{Cdc20} substrate, shows an abundance pattern that is typical of the ubiquitin ligase targets. We found that Cin8, Kip2, Bik1, Bim1, Ase1, and Stu2 showed at least one residue with a different phosphorylation status between metaphase, mini-anaphase and anaphase arrested cells (**figure 3.18**), and as such might be implicated in aMT modulation at anaphase onset. Given that the activity of these proteins is often modulated by microtubule-cortex interaction[20,130,138], we extended our analysis to proteins that mediate the connection, among which the cortical receptor Num1 and the actin motor protein Myo2, which mediate microtubule/cortex interactions of the Dyn1 and the Kar9 spindle positioning pathways, respectively, showed at least one residue that is phosphorylated differently in the analyzed conditions (**figure 3.18**). These results indicate that different proteins that affect aMT dynamics are phosphorylated or dephosphorylated at anaphase onset, and consequently may account for aMT stabilization.

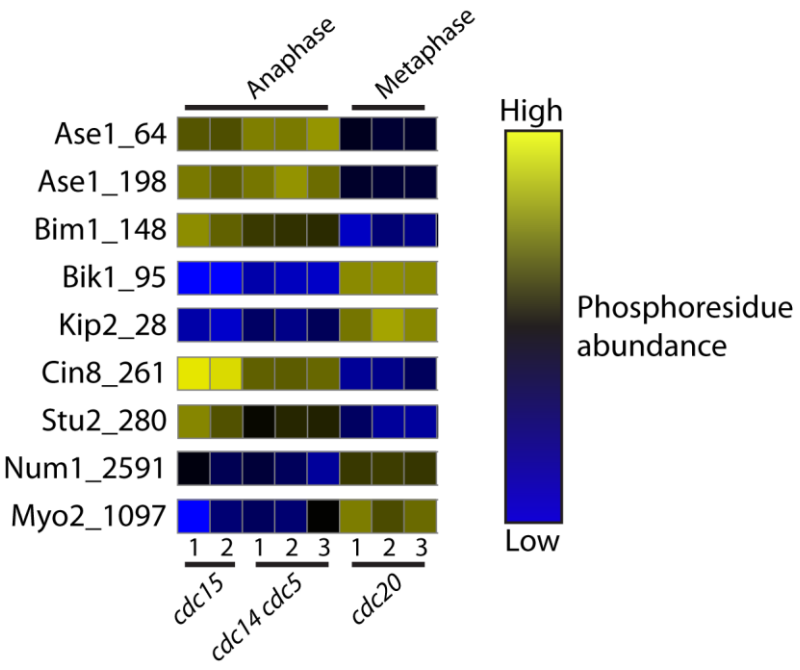

Figure 3.18. Putative proteins involved in aMT stabilization at anaphase onset are identified by phospho-proteomic analysis. *cdc15-as1* (Ry1112), *cdc14-1 cdc5-as1* (Ry1602) and *cdc20-AID* (Ry4853) cells arrested in G1 by α-factor in YEPD at 23°C were released at 37°C in fresh YEPD media supplemented with 1NM-PP1 analogue 9 and CMK to inactivate the *cdc14-1*, the *cdc15-as1* and the *cdc5-as1* alleles, respectively. Auxin was added to deplete the Cdc20-AID protein. At the terminal arrest, a phospho-proteome analysis of the three different mutants was performed. The phospho-proteomic data obtained were filtered for proteins involved in the regulation of aMT dynamics first and next for carrying phospho-residues whose phosphorylation status changes between metaphase (*cdc20-AID* cells) and anaphase (*cdc14-1 cdc5-as1* and *cdc15-as1* cells). The residues obtained and their abundance profiles are shown for each strain (2 replicates for *cdc15-as1* cells, 3 replicates for both *cdc14-1 cdc5-as1* and *cdc20-AID* cells).

3.4. Does the regulation of aMT stability have any physiological impact?

In budding yeast, aMTs anchor the spindle to the cellular cortex and guide its positioning during the whole mitotic process. In metaphase, aMTs contribute to spindle orientation along the mother/bud axis, a process that requires a tight equilibrium of forces generated at the cortex. During anaphase, aMTs drive the segregation of the bud-directed SPBs in the daughter cell and maintain the two SPBs in different cellular compartments until cells exit from mitosis. Given that our results point to that aMTs remain highly dynamic up to metaphase and are stabilized at anaphase onset, we wondered whether and how this modulation may affect their functionality.

3.4.1. aMT instability and Cdc5 activity guide proper spindle orientation

When the spindle is short, aMTs are known to contribute to proper spindle orientation along the mother/bud axis. During our analyses we noticed that aMTs of *cdc14 cdc5* cells exhibit an anomalous phenotype (**figure 3.19a** and **3.19b**): while the vast majority of metaphase arrested cells are characterized by proper aMTs (aMTs originating from the bud-directed SPB enter the bud, while the others point to the mother cell cortex), *cdc14 cdc5* arrested cells show an increased percentage of abnormal aMTs (aMTs originating from two different SPBs that point to the same direction or aMTs originating from a single SPB that point to different directions; on average, 19% of *cdc20* cells and 58% of *cdc14 cdc5* cells show anomalous aMTs).

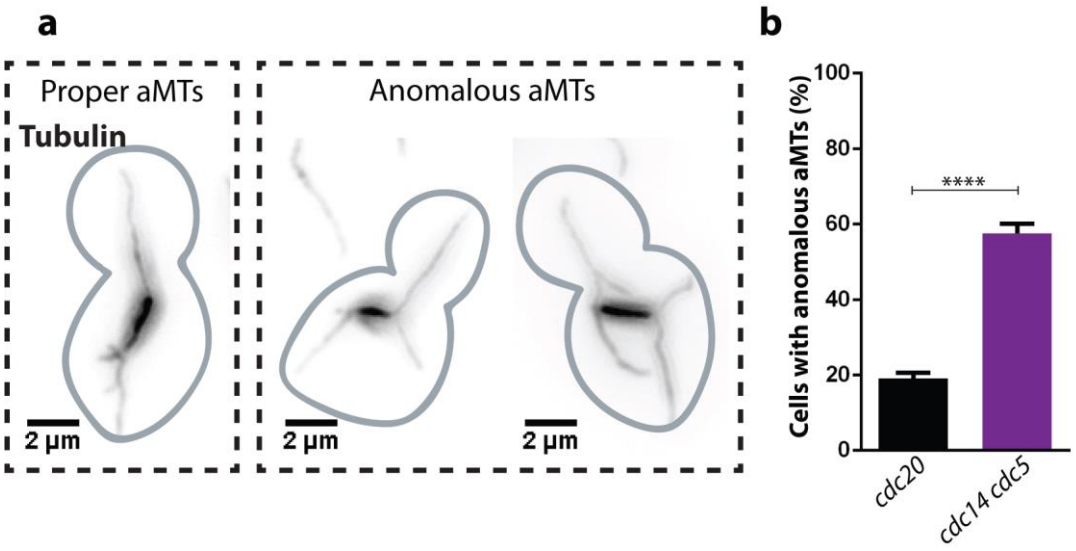

Figure 3.19. *cdc14-1 cdc5-as1* cells carry anomalous aMTs. (**a**) Examples of cells with proper or anomalous aMTs are shown. Are defined as proper aMTs, those aMT that when generated by opposite SPBs direct towards the two different cellular compartments (mother and daughter cell) with the aMT emanating from the same SPB going towards the same compartment . Are defined as anomalous aMTs those aMT that when generated by opposite SPBs direct toward the same cellular compartment and when generated by the same SPB move toward the two different compartments. (**b**) *cdc20-AID* (Ry4853) and *cdc14-1 cdc5-as1* (Ry1602) cells arrested in G1 by α-factor in YEPD at 23°C were released at 37°C in fresh YEPD media supplemented with CMK, to inactivate the *cdc14-1* and the *cdc5-as1* alleles, respectively. Auxin was added to deplete the Cdc20-AID protein. The analysis was performed at the terminal arrest of each mutant strain (160 minutes after the release). (**a**) Representative images of the time-points analyzed are shown. (**b**) The percentage of cells carrying anomalous aMTs for the indicated genotype (n=100; mean +/- SEM is shown; ****=p<0.0001) is shown.

To assess whether this aMT phenotype could highlight a functional defect in spindle orientation, we probed spindle orientation by measuring the angle between the bud-neck and the spindle (**figure 3.20a**). The more the angle is close to 90°, the more the spindle is correctly oriented toward the polarity axis, while the more the angle is close to 0°, the more the spindle is misoriented. As reported in the literature, we found that most *wild-type* metaphase cells, as well as cells arrested in metaphase, correctly orient their spindle along the polarity axis (**figure 3.20b**). On the contrary, *cdc14 cdc*5 cells randomly orient their spindle – as indicated by the mean bud-neck/spindle angle of 45° (**figure 3.20b**). To assess whether the phenotype observed was due to the protracted arrest with stable aMTs, or rather a consequence of Cdc14 and Cdc5 inactivation, we repeated the same analysis in *esp1 cdc15* cells, which carry stable aMTs and active Cdc14 and Cdc5, and *cdc20 cdc14*, *cdc20 cdc5* and *cdc20 cdc14 cdc5* cells, which carry unstable aMTs and inactive Cdc14 and/or Cdc5. We found that all of these mutants arrested with properly oriented aMTs and spindles (**figure 3.20b**), thus indicating that neither aMT stability nor Cdc14 and Cdc5 inactivation are "per se" sufficient to generate the spindle orientation defect typical of *cdc14 cdc5* double mutant cells. We then wondered whether both aMT stabilization and Cdc14 and/or Cdc5 inactivation were required to generate the defect. To test this possibility, we analyzed aMT orientation in *esp1 cdc14*, *esp1 cdc5* and *esp1 cdc14 cdc5* cells, which combine both aMT stabilization and Cdc14 and/or Cdc5 inactivation. We found that both *esp1 cdc5* and *esp1 cdc14 cdc5* cells show spindle orientation defects (**figure 3.20b**), pointing to that concomitant aMT stabilization and Cdc5 inactivation generate the spindle orientation defect of *cdc14 cdc5* cells. Altogether, these data indicate that proper spindle orientation requires aMT instability, typical of metaphase cells, and Cdc5 activity, and that only the impairment of both aMT instability and Cdc5 activity results in a spindle orientation defect.

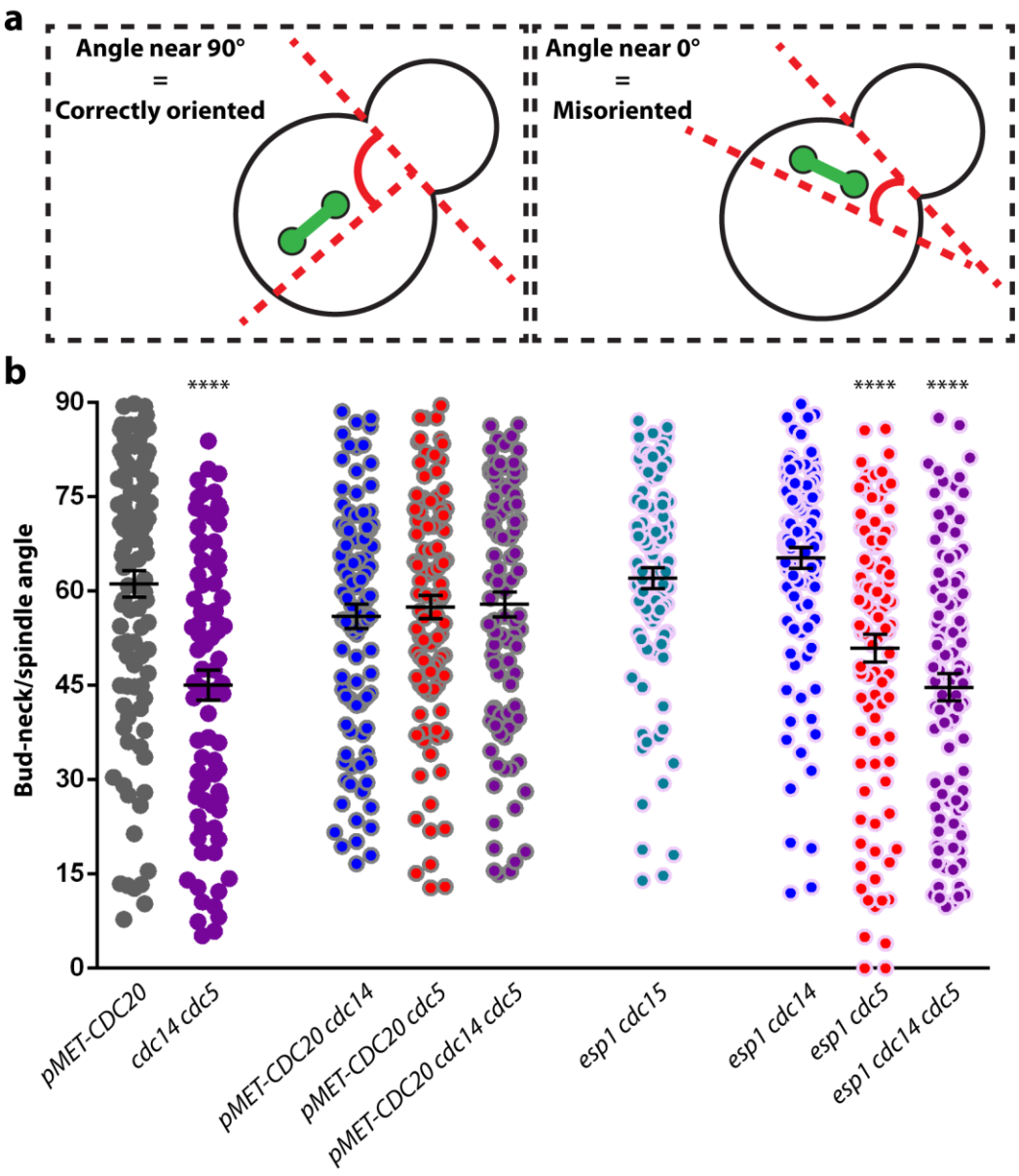

Figure 3.20. aMT instability and Cdc5 activity are required for proper spindle orientation. (**a**) Schematic representation of the bud-neck/spindle angle, indicator of spindle orientation along the polarity axis is shown. The more the angle is close to 90°, the more the spindle is correctly oriented, while *vice versa* the more it is near 0°, the more the spindle is misoriented. A mean angle of 45° indicates the randomization of the orientation process. (**b**) Bud-neck/spindle angles were determined in *pMET-CDC20* (Ry1223), *cdc14-1 cdc5-as1* (Ry1602), *pMET-CDC20 cdc14-1* (Ry3204) *pMET-CDC20 cdc5-as1* (Ry3209), *pMET-CDC20 cdc14-1 cdc5-as1* (Ry3201), *esp1 cdc15-as1* cells (Ry9512), *esp1-1 cdc5-as1* cells (Ry9134) *esp1-1 cdc14-1* cells (Ry9131) and *esp1-1 cdc14-1 cdc5-as1* cells (Ry9128) cells arrested at their terminal phenotype (180 minutes after the release) (n=100; mean +/- SEM is shown; ****=p<0.0001 – cells were compared to *pMET-CDC20* cells as control).

3.4.2. Cdc5 works in parallel with both Kar9 and Dyn1 pathway to regulate spindle orientation and positioning

Several connections between aMT stability and the modulation of forces generated at the cortex have already been proposed[20,72,96]. However, no clear mechanism is directly linked to Cdc5, although the PLK1 – the human homologue of Cdc5 – has been already implicated in spindle orientation[162]. For this reason, we decided to investigate the role of the kinase in both the spindle orientation and the positioning processes. As mentioned above, two main pathways generate the cortex-mediated pulling forces and in parallel guide spindle orientation and positioning: the Kar9 and Dyn1 pathways. In metaphase arrested cells, single inactivation of one of these two pathways results only in a mild orientation defect, while their concomitant impairment induces random spindle orientation (**figure 3.21**). We took advantage of this genetic interaction to understand how Cdc5 controls spindle orientation by performing a genetic analysis that combines *kar9* and *dyn1* mutant cells with Cdc5 inactivation in metaphase arrested cells. We expected that, if Cdc5 was part of the Kar9 pathway, it should generate random spindle orientation only in *dyn1* mutant cells, and vice-versa. Unexpectedly, we found that Cdc5 inactivation results in random spindle orientation in both *kar9* and *dyn1* single mutant cells (**figure 3.21**), thus suggesting that Cdc5 works in parallel with both Kar9 and Dyn1 pathways in the spindle orientation process.

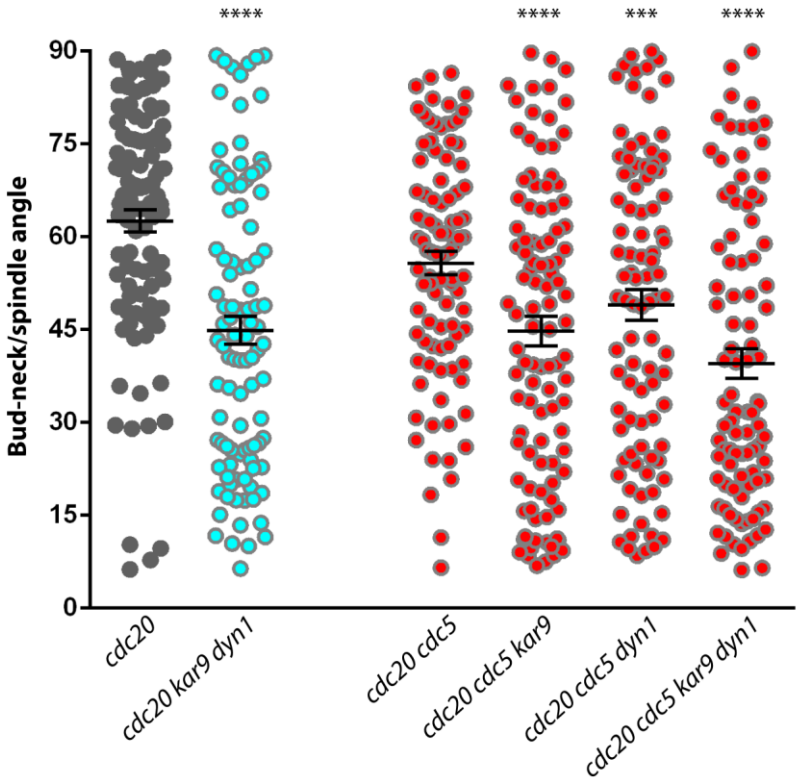

Figure 3.21. Cdc5 works in parallel to both the Kar9 and the Dyn1 pathways to guide spindle orientation. Bud-neck/spindle angles were determined in *cdc20-AID* (Ry4853), *cdc20-AID kar9*Δ *dyn1-AID* (Ry7545), *cdc20-AID cdc5-as1* (Ry4936), *cdc20-AID cdc5-as1 kar9*Δ (Ry7702), *cdc20-AID cdc5-as1 dyn1-AID* (Ry7749), and *cdc20-AID cdc5-as1 kar9*Δ *dyn1-AID* (Ry7746) cells arrested at their terminal phenotype (160 minutes after the release)**.** (n=100; mean +/- SEM is shown; ***=p<0.001 - ****=p<0.0001 – cells were compared to *cdc20* cells as control)

To further tackle how Cdc5 affects aMT functions, we moved our analysis to anaphase arrested cells. In this cell cycle phase, spindle positioning can be easily evaluated by looking at the different segregation of the two SPBs in the two daughter cells (**figure 3.22a**). We analyzed both *cdc15* and *cdc5* single mutant cells, which arrest in anaphase due to an impairment in mitotic exit, in combination with Kar9 and/or Dyn1 impairment. Similar to *cdc20* arrested cells, single inactivation of Kar9 or Dyn1 results in a very mild positioning defect in *cdc15* cells, while their concomitant impairment drastically affects spindle positioning (**figure 3.22b**; on average, only 0.35% of *cdc15* cells carry mispositioned spindles, compared with 41% of *cdc15 kar9 dyn1* cells). On the contrary, the sole inactivation of Dyn1 generates a spindle positioning defect in *cdc5* cells that is

comparable with that of *cdc15 kar9 dyn1* mutant cells (**figure 3.22b**; on average, 7% of *cdc5* cells carry mispositioned spindles, compared with 47% of *cdc5 dyn1* cells). Furthermore, in *cdc5 kar9 dyn1* triple mutant cells, the percentage of cells with mispositioned spindles is almost doubled when compared with *cdc15 kar9 dyn1* mutant cells (**figure 3.22b**; on average, 77% of *cdc5 kar9 dyn1* cells carry mispositioned spindles). Altogether, these results indicate that Cdc5 works in parallel with both Kar9 and Dyn1 pathways in both spindle orientation and positioning processes, although the single contribution of the pathways differs depending on the given process. Indeed, while Kar9, Dyn1 and Cdc5 contribute to spindle orientation to a similar extent and the sole activity of one of these pathways is not sufficient to drive the orientation process, Dyn1 is the major driver of the spindle positioning process and its sole activity is sufficient to correctly drive the process.

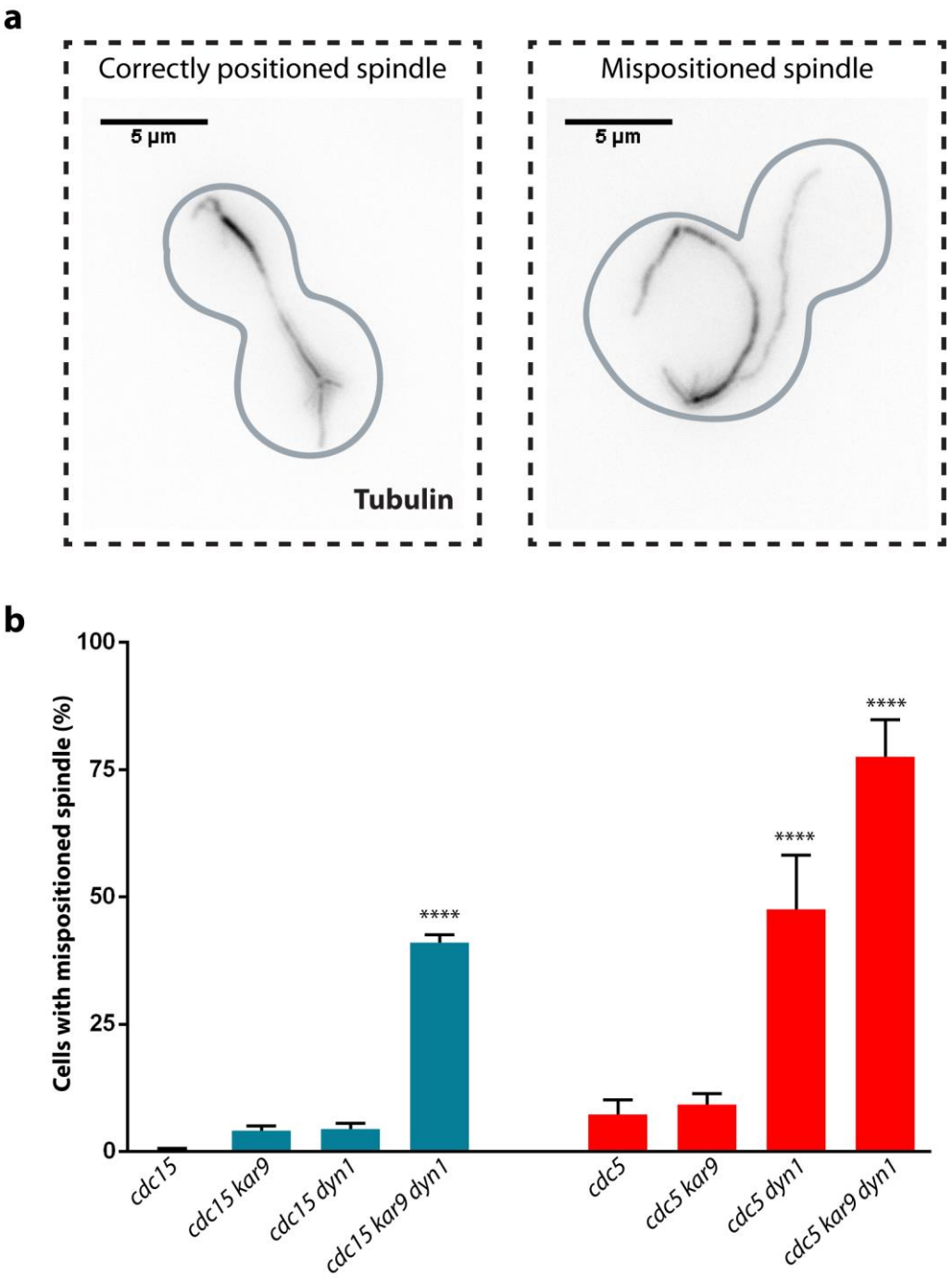

Figure 3.22. Cdc5 guides anaphase spindle positioning. (**a**) Examples of anaphase cells with correctly positioned or mispositioned spindles are shown. Correctly positioned anaphase spindles extend along both mother and daughter cells. Mispositioned anaphase spindles remain in one single cell. (**b**) Spindle position was assessed in *cdc15-as1* (Ry1112), *cdc15-as1 kar9*Δ (Ry7626), *cdc15-as1 dyn1-AID* (Ry7623), *cdc15-as1 kar9*Δ *dyn1-AID* (Ry7620), *cdc5-as1* (Ry2446), *cdc5-as1 kar9*Δ (Ry7589), *cdc5-as1 dyn1-AID* (Ry7697), *cdc5-as1 kar9*Δ *dyn1*-AID (Ry7694) cells at their terminal phenotype (180 minutes after the release). (n=100; mean +/- SEM is shown; ****=p<0.0001 – cells were compared to *cdc15* as control)

4. DISCUSSION

Cells progress through the mitotic cell cycle with the ultimate goal of generating two daughter cells that are genetically identical to the mother cell. When something goes wrong and the newly generated cells end up retaining different DNA contents, dramatic effects occur that alter the proper physiology of the cells[2]. Luckily, this situation rarely arises, probably because the processes that drive cell cycle progression are under the control of strict surveillance mechanisms, which prevents a "no-return" event to take place before cells are set up correctly. One of these highly regulated processes is chromosome segregation, which occurs during mitosis and is under the control of the Spindle Assembly Checkpoint (SAC). The SAC prevents chromosome segregation, until every sister chromatid pair is correctly bound to the mitotic spindle machinery. It does it by preventing the activation of the ubiquitin ligase Anaphase Promoting Complex or Cyclosome (APC/C) through the sequestration of its activator subunit Cdc20[163]. Once active, the APC/C^{Cdc20} targets for degradation different proteins, with the ultimate goal of triggering sister chromatid separation and segregation - via the dissolution of the cohesin complex and the distancing of the two chromosome sets, respectively. Chromosome segregation requires the modulation of spindle microtubules, which serve the purpose of pulling the sister chromatids towards different poles first, and next move them away by spindle elongation. In respect to their function, spindle microtubules are conventionally classified into three different categories: kMTs, which link the spindle to the chromosomes, iMTs, which form a bundle that allows spindle elongation in anaphase, and aMTs, which guide the segregation of the two chromosome sets toward the two newly generated cells. Although changes in both kMT and iMT dynamics are known to occur during chromosome segregation, whether and how the dynamics of aMTs also change at anaphase onset remains unclear. The finding that, in budding yeast, the activity of at least one between the CDK-counteracting phosphatase Cdc14 and the polo-like kinase Cdc5 is

required to trigger spindle elongation[63] prompted us to investigate whether these two proteins were involved in the overall regulation of microtubules, including the astral ones. Our finding that *cdc14 cdc5* double mutant cells carry highly stable aMTs provided us with the right framework to shed light on the regulation of this overlooked class of microtubules. Here we show that central to their regulation is the activation of the APC/C^{Cdc20} toward a yet to be identified substrate and we propose a model connecting the microtubule cycle with specific molecular cell cycle events.

4.1. APC/C^{Cdc20}: the "mastermind" behind spindle microtubule regulation during chromosome segregation

The APC/C^{Cdc20} gets activated at the metaphase to anaphase transition and it has the fundamental role of targeting for degradation many substrates, some of which are known to inhibit anaphase progression. While in mammalian cells, the degradation of two APC/C^{Cdc20} substrates – namely securin and the M-phase cyclin B – is essential for cells to progress into anaphase[17], in budding yeast, only the degradation of Pds1 – the yeast homologue of securin – seems to be required[151,152]. Pds1 degradation leads to the activation of the protease Esp1 – the yeast homologue of separase – that in turn drives the chromosome segregation process as it cleaves the cohesin subunit Scc1 – hence releases sister chromatid cohesion[30] –, and it promotes the transient activation of Cdc14[31], which in turn triggers spindle elongation[63]. Both these events influence spindle microtubule dynamics. On the one hand, Scc1 cleavage promotes the pulling of the two chromosome sets toward opposite poles via kMT shortening[89]. On the other hand, FEAR-mediated Cdc14 activation promotes spindle elongation through the stabilization of iMTs[93] and the assembly of the "spindle midzone"[47], a structure made of iMTs, motor proteins and MAPs[46]. Our finding that the essential requirement for aMT stabilization is the activity of the APC/C^{Cdc20} further consolidate the role of this ubiquitin ligase in the overall control of microtubule dynamics. However, the mechanisms by which the APC/C^{Cdc20} controls

the three classes of microtubules differ. Indeed, whilst the regulation of kMTs and iMTs relies on Pds1 degradation, hence Esp1 activation and ultimately cohesin cleavage, the modulation of aMTs seems to go via a different circuit at least in respect to Esp1 activation and cohesin cleavage. Indeed, cells that proficiently activate the APC/C^{Cdc20}, but that are impaired in either Esp1 activity or Scc1 cleavage, show aMTs as stable as the ones in *cdc14 cdc5* double mutants. This set of data, however, does not formally exclude the requirement for Pds1 degradation. If, it is true that depleting Pds1 in metaphase arrested cells is not sufficient to stabilize aMT, it is also true that to rule out the requirement of Securin degradation we should assess the phenotype of aMT in *cdc14 cdc5* cells expressing a non-degradable version of Pds1 (*pGAL-PDS1-*Δ*destructionbox*[151]). Unfortunately the mechanism by which the APC/C^{Cdc20} influences aMT dynamics remains elusive and its elucidation will require the identification of the APC/C^{Cdc20} critical substrate(s). So far, we managed to show that none of the known substrates is *per se* the culprit. Driven by the knowledge that the degradation of M-phase cyclins is essential to trigger anaphase progression in mammalian cells[17], we, first, considered this class of proteins. In budding yeast, the APC/C^{Cdc20} promotes the degradation of the S-phase cyclin Clb5 and the partial depletion of the M-phase cyclin Clb2. As Clb2 levels remain high in double mutant cells[63], we excluded this cyclin and assessed the consequences of depleting Clb5. Similarly to Pds1, also in this case, we found that depletion of Clb5 was not sufficient to stabilize aMTs in cells lacking APC/C^{Cdc20} activity. Having excluded cyclins, we moved to test additional putative APC/C^{Cdc20} substrates including: the motor protein Kip1[60], the haspin-like kinase Alk2[153], the APC/C^{Cdh1} inhibitor Acm1[154], and the DNA replication-promoting kinase Dbf4[155] but again none of the tested proteins turned out to be the critical APC/C^{Cdc20} substrate whose removal determines aMT stabilization. The question remains as to how the APC/C^{Cdc20} regulates aMT dynamics. We envision two

different scenarios: (i) a yet to be identified/tested substrate is involved in the process or (ii) aMT stabilization requires the removal of two or more APC/C^{Cdc20} substrates.

To answer this question, on the one hand we interrogated the proteome of metaphase and anaphase cells, searching for proteins whose expression profile typifies the one of APC/C^{Cdc20} targets, on the other we are prompt to evaluate, on aMT dynamics, the consequences of depleting APC/C^{Cdc20} substrates in various combinations. Our proteomic analysis identified four additional proteins: the 3-phosphoglycerate dehydrogenase Ser3, the high-affinity glucose transporter Hxt4, the ammonium transmembrane transporter Mep2, and a protein of unknown function named Tma10. Although none of them shows any obvious connection with aMT regulation, their individual contribution will eventually be considered. Regardless of whatever the molecular mechanism turns out to be our data directly link the removal of an APC/C^{Cdc20} substrate with the control of aMTs.

4.2. Phosphatase Cdc14 and Polo-like kinase Cdc5: at the crossroad between interpolar and astral microtubules

Although our data suggest that the regulation of iMTs and aMTs follows a similar trend, as both classes of microtubules are stabilized upon anaphase entry, the mechanism controlling the two differs in respect to the role played by Cdc14 and Cdc5. Indeed, when we compared cells arrested in "mini-anaphase" – by means of Cdc14 and Cdc5 inactivation –, which carry unstable iMTs[63,93], with those of cells arrested in anaphase, which show stable iMTs hence elongated spindles, we found that aMTs of cells in "mini-anaphase" resulted more stable than their anaphase counterpart, suggesting that Cdc14 and Cdc5 regulate iMT and aMT dynamics in opposite directions. Since we knew that iMT stabilization requires Cdc14 and Cdc5 activities[63,93], which modulate the kinesin-5 motor protein Cin8[149] and the spindle "midzone" protein Ase1[47], we envisioned a similar mechanism also for aMT dynamics. Instead, our finding revealed that Cdc14 and Cdc5

promote iMTs stabilization, but aMTs destabilization. Three possible scenarios can explain this finding (**figure 4.1**): (i) Cdc14 and Cdc5 negatively affect aMT stabilization by promoting iMT stabilization and spindle elongation – suggesting that a direct cross talk between iMTs and aMTs exists; (ii) Cdc14 and Cdc5 act on one or more proteins that simultaneously control both iMT and aMT dynamics, but with opposite effects; (iii) Cdc14 and Cdc5 modulate proteins that independently regulate a specific class of microtubules. Of course the three scenarios are not mutually exclusive. In fact, data in support and against every single one exist. Data in favor of a cross talk between iMTs and aMTs would predict the existence of limiting factors in microtubule dynamics, which preferentially promote iMT rather than aMT stabilization. The microtubule polymerase Stu2 (XMAP215 in mammalian cells) and tubulin fit this prediction, with the first being limiting because of changes in its subcellular localization, the second because of a strict control on its levels. Indeed, Stu2 is a protein that shuttles between the nucleus and the cytoplasm, but that in mitosis is retained preferentially in the nucleus where it promotes nuclear microtubule polymerization at the expenses of aMTs[52]. Tubulin is a protein whose intracellular concentration is highly regulated because when in excess it is toxic for the cells. Furthermore, when tubulin levels decreases, aMTs are the first type of microtubule that is negatively affected[91]. Against the microtubule cross talk model is our finding that spindle elongation "*per se*" does not prevent aMT stabilization. As indicated by the observation that the simultaneous inactivation of the Kar9 and Dyn1 pathways – which promote aMT stabilization – in a *cdc15* background resulted in stable aMTs albeit the *cdc15 kar9 dyn1* mutant was perfectly capable of elongating its spindle. A caveat with this analysis is that spindle elongation in these cells occurred entirely in the mother cell compartment, a situation rarely observed in *cdc15* cells. As such, if we can exclude an inhibitory effect on aMT by spindle elongation "*per se*" we cannot rule out that spindle elongation negatively affects aMT dynamics indirectly by promoting spindle entry into

the bud. Indeed multiple proteins specifically localize in the bud, and they trigger aMT destabilization specifically in this cellular compartment[33,138]. In agreement with the existence of different regulatory circuits in the mother and the bud cellular compartments is the "two zone model" proposed by Amon and colleagues that is at the bases of mitotic exit regulation[38,164]. On the other hand, supporting the hypothesis that Cdc14 and Cdc5 regulate iMTs and aMTs via the same proteins but with opposite effects is the knowledge that metaphase arrested cells lacking Cin8 or Ase1 – two proteins that promote iMT stabilization[149] – show an increased number of aMTs[59] and that ectopic expression of Cin8 slightly decreases aMT length by directly destabilizing their plus-ends[58]. Although to envision a role for Cin8 and Ase1 in aMT regulation is somehow difficult, as they both localize exclusively in the nuclear compartment[47,165], one could argue that their activity might affect something in the nucleus – for instance the SPB structure and/or separation, as previously proposed[59] – that in turn alters aMT dynamics in the cytoplasm. Finally, a third scenario envisioned that Cdc14 and Cdc5 modulate iMTs and aMTs through different proteins. If this was the case, one could expect it possible to interfere with iMT dynamics without affecting aMTs and vice versa. So far, at the best of our knowledge, an experimental set up by which it will be possible to interfere with one class of spindle microtubules only does not exist thereby making the testing of this model somehow difficult. For instance, one possible way of stabilizing the iMTs of *cdc14 cdc5* cells exists and it is based upon the over-expression of Cin8[149]. However, Cin8 over-expression is a non-physiological condition that alters the protein intracellular localization, as it can be found also in the cytoplasmic compartment where it directly affects aMT dynamics[58]. In conclusion, although we did not manage to clarify the fine mechanism by which Cdc14 and Cdc5 regulate iMT and aMT dynamics, the finding that they influence the two classes of microtubules in opposite fashion further contribute to link the spindle cycle with molecular cell cycle events.

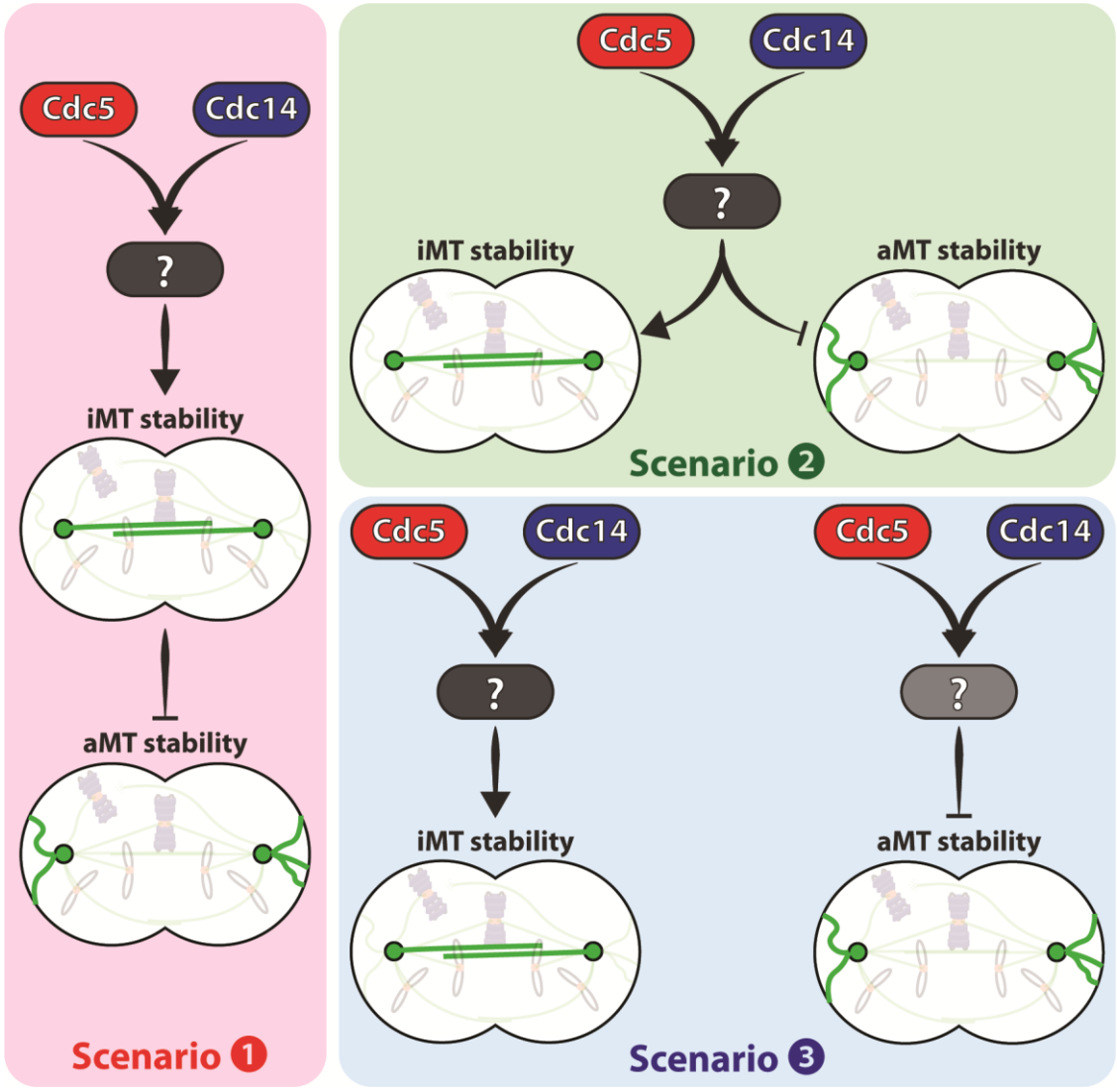

Figure 4.1. Three possible scenarios could explain the Cdc14 and Cdc5 concomitant regulation of iMT and aMT dynamics.

4.3. Wrapping our heads around astral microtubule stabilization

Microtubule regulations are often mediated by changes in the phosphorylation status of specific residues within motor and MAPs[47,63,103,107,149]. Since this is also the case for aMTs[44,58,59,66,73,96,109,138,146,166], to pinpoint a specific class of proteins and gain insights into the mechanism underlying their regulation we probed several specific microtubule dynamic parameters and performed a phospho-proteome analysis. So far, our data identified: (i) a slight change in almost all the parameters measured – pointing towards the modulation of multiple microtubule-regulating proteins; (ii) several proteins connected to the regulation of aMT dynamics, including the MAPs Ase1[59], Stu2[146], Bim1

and Bik1[44], and the motor proteins Kip2[73] and Cin8[59], with at least one residue whose phosphorylation status changes from metaphase to anaphase onset; and (iii) an altered kinetic of interaction between the aMTs and the cellular cortex – with, aMTs of *cdc14 cdc5* cells remaining associated for longer time than their counterpart in metaphase arrested cells. Whether the latter is a cause or a consequence of aMT stabilization remains to be established. aMT shrinking events are connected to the activity of the two spindle positioning pathways: the Kar9 pathway directs aMTs toward the bud-neck, where aMTs depolymerize through a septin ring-dependent mechanism[135], and the Dyn1 pathway induces aMT shortening both directly through Dyn1 depolymerizing activity and indirectly via a Kip3-dependent mechanism[72,96,138]. Our finding, that impairing these two pathways in metaphase results in an aMT phenotype that mimics the one of aMTs in *cdc14 cdc5* mutants, suggests that the aMT stabilization observed in the double mutant may be due to a defect in the interaction of the aMTs with the cortex, possibly through the modulation of both the Kar9 and Dyn1 pathways. If this was the case, then either common factors or individual components of the two pathways maybe affected in these cells. Given that our results indicate that neither the actin cytoskeleton nor the septin ring – two common factors of the spindle positioning pathways – account for the aMT phenotype of *cdc14 cdc5* cells, we speculate that it may rather be due to the concomitant modulation of specific components. In agreement with this hypothesis, the phospho-proteomic analysis of metaphase and anaphase cells identified single residues of both the Kar9 actin motor protein Myo2 and the Dyn1 cortical receptor Num1 with different phosphorylated status between the two conditions. Altogether, our findings point towards the modulation of multiple factors rather than a single protein in the generation of the highly stable aMT phenotype proper of "mini-anaphase" cells. To identify these proteins, we will monitor the aMT morphology in double mutant cells upon depletion and/or over-expression of the candidates found in the phospho-proteomic screen, individually or in

combination, and next we will evaluate the consequences of expressing phospho-mutants or phospho-mimicking alleles of the proteins of interest on aMT dynamics.

4.4. The complex mechanisms of spindle orientation and positioning

While the aim of kMTs and iMTs is to separate and distance sister chromatids, the main goal of aMTs is to direct chromosomes towards the two newly generated cells. Indeed, cells lacking aMTs proficiently separate the two DNA masses and elongate their spindle, but they do so within the mother cell compartment[91]. aMTs achieve their goal via the spindle positioning process, which guides spindle orientation towards the polarity axis and generates the pulling force required to attract one SPB into the bud cell compartment. Spindle orientation normally occurs in metaphase, when spindles are short and nuclei are in close proximity with the bud-neck, with the aim of facilitating the immediate entry of chromosomes into the bud upon the triggering of spindle elongation. Vice-versa the pulling of the bud-directed SPB within the bud normally occurs in anaphase, often concomitantly to spindle elongation, although eventually after the completion of the elongation process. Although driven by the same two pathways – namely the Kar9 and Dyn1 pathway – the mechanisms involved in these two tasks somehow differ. While spindle orientation is thought to be achieved mainly through the Kar9 pathway, the pulling force required to position the spindle is mainly generated by the Dyn1 pathway. In line with that, Dyn1 activity is normally kept low in metaphase upon She1-mediated inhibition, and increases only at anaphase onset[75]. Our work further clarifies the mechanisms controlling the spindle positioning process. First, we found that the aMT instability typical of metaphase cells positively affects the spindle orientation process – as indicated by the rescue of the spindle orientation defect observed in double mutant cells when preventing aMT stabilization. This result is in line with both the pivoting behavior of aMTs – a property that requires high dynamicity and that positively influences spindle orientation[166] – and with the spindle orientation defects seen in cells with

stabilized aMTs[20,96]. Second, we unveiled a novel role of Cdc5 in both the orientation and the positioning processes. As it has been proposed that the Mitotic Exit Network (MEN) – of which Cdc5 is an upstream component – controls Kar9 asymmetric localization on the two SPBs[110], Cdc5 may be involved in spindle orientation and positioning through the modulation of MEN activity. However, our finding that the inactivation of the MEN kinase Cdc15 does not affect the spindle positioning machinery strongly suggests that this is not case. This is in agreement with a recent study that argues against MEN activity prior to anaphase onset – even partially –, at least in our background strain[167]. So how does Cdc5 control spindle orientation and positioning? We addressed this question by attempting to position Cdc5 within one of the pathways by epistasis analyses. To this aim, we combined the individual and concomitant inactivation of Kar9 and Dyn1 with the impairment of the polo-like kinase in metaphase arrested cells. To our surprise, our data are consistent with Cdc5 working in parallel to both the Kar9 and Dyn1 pathway – at least in respect to spindle orientation – as indicated by the orientation defect of both *cdc20 cdc5 kar9* and *cdc20 cdc5 dyn1* cells. This result suggests the existence of a third "*bona-fide*" spindle positioning pathway, whose nature is unclear but to witch Cdc5 belongs. However, the formal identification of a third pathway would require the observation of an additive effect on the positioning defect of *kar9 dyn1* cells upon Cdc5 inactivation. This additive effect cannot be assessed monitoring spindle orientation, due to an intrinsic caveat of the analysis that does not allow to evaluate a worsening of spindle orientation upon reaching the randomization of bud-neck/spindle angles – which is already achieved by the concomitant inactivation of the Kar9 or the Dyn1 pathways. As such, we cannot exclude that the effect seen upon Cdc5 inactivation is due to a partial requirement of its activity to sustain the proper functionality of both pathways (for example affecting actin or microtubule dynamics). We tried to solve this problem by performing our epistasis analyses in anaphase arrested cells – where defects in the spindle positioning can be

evaluated measuring the percentage of cells that elongate their spindle in a single cell compartment. In this case, the concomitant impairment of Kar9 and Dyn1 results in around 40% of cells with mispositioned spindles, while the combined inactivation of Cdc5, Kar9 and Dyn1 extend the defect to about 80% of cells. This result would be in agreement with the existence of a third Cdc5-dependent spindle positioning pathway. However a caveat with this experiment exists and it is that the *dyn1-AID* allele used in the epistasis analysis is not completely efficient in Dyn1 degradation[38]. As such the additive effect observed could be explained by the activity of a residual Dyn1 pool that resists Auxin-mediated removal and that requires Cdc5 activity. The use of this allele is necessary to analyze cells lacking both Kar9 and Dyn1, given that the concomitant deletion of their genes is lethal. To test whether the additive effect of Cdc5 inactivation on the positioning defects of *kar9 dyn1* cells is due to a residual Dyn1 activity, we compared spindle position of *cdc5* cells - whose Dyn1 activity is impaired through its Auxin-mediated degradation - with that of *cdc5* cells that do not express Dyn1 at all – thought *DYN1* deletion. Our finding that the combination of Cdc5 inactivation with *DYN1* deletion resulted in approximately 80% of cells with mispositioned spindles – indicates that this might be the case (*data not shown*). We will further investigate the role of the kinase analyzing the results of the phospho-proteomic screens, in a three step manner: first, we will search for phospho-residues that are less abundant in *cdc14 cdc5* cells; second, we will select only those that are located within the Cdc5 putative recognition motif; third, we will assess whether these residues belong to proteins of the Kar9 and Dyn1 pathways, or else can be somehow connected to spindle positioning.

4.5. Current model of microtubule regulation in mitosis

Over the years, budding yeast has proven to be an amazing model system to identify complex cellular mechanisms, whose concepts – and eventually proteins – often proved to be conserved in higher eukaryotes. The work presented in this thesis sheds light on the

regulation of spindle microtubules, a process that turned out to be intimately linked with the individual steps of the metaphase to anaphase transition. Indeed if the metaphase to anaphase transition is conventionally defined by cohesin cleavage, it can be further dissected into three clearly identifiable molecular events: (i) APC/C^{Cdc20} activation, following the correct bipolar attachment of each sister chromatid pair to the mitotic spindle; (ii) Separase/Esp1 activation, consequently to APC/C^{Cdc20}-mediated degradation of Securin/Pds1; and (iii) Esp1-mediated cleavage of the cohesin subunit Scc1. Our work managed to associate each individual step of the transition with the regulation of a specific class of spindle microtubules – namely, kMTs that guide chromosomes to the spindle poles, iMTs that drive spindle elongation, and aMTs that direct the segregation towards the two daughter cells –, suggesting that this might sets the time and order of events at the core of the chromosome segregation process (see the proposed model in **figure 4.2**). In metaphase, all microtubules are unstable, hence helping the "search and capture" mechanism[42], keeping the spindle short, promoting a stable position of the spindle next to the bud-neck[20] and correctly orienting the spindle along the polarity axis. When every chromosome has been correctly captured by kMTs, the activation of the APC/C^{Cdc20} targets for degradation several substrates, including Pds1, mitotic cyclins and a yet to be identified substrate that directly stabilize aMT dynamics. This stabilization is connected to the increased interaction between aMTs and the cellular cortex, which may help to establish the contact between the bud cortex and the aMTs emanating from the bud-directed SPB and the generation of the Dyn1-mediated pulling force[96] – with the ultimate goal of directing the spindle that is going to elongate toward the bud compartment. Secondly, Pds1 degradation releases Esp1 activity that in turn cleaves the cohesin complex. Cohesin cleavage affects kMT dynamics, as the mechanism that promoted their stabilization while sister chromatids were bound together senses the tension drop at the kinetochores and drives kMT destabilization[89]. Finally, Esp1 promotes Cdc14 activation

that in turn regulates motors and MAPs – of which Cin8 is key – to stabilize iMTs [46,63,93], thereby promoting spindle elongation and hence segregating farther away the two chromosome sets. This regulation is brilliant as it reflects the proper sequence of events necessary to guarantee a faithful mitosis. Interestingly Cdc14, in combination with Cdc5, counteracts aMT stabilization coordinating spindle elongation with aMT shortening. This makes sense, since once the segregation of the two chromosome sets has been correctly achieved, aMTs are not supposed to extend toward distant locations, as they might displace the spindle from its correct position. In line with this, a Bud6-dependent mechanism is known to trigger their destabilization when they eventually reach the bud-neck during anaphase[95].

It will be interesting to see whether this ordered regulation of spindle microtubules at the transition from metaphase to anaphase is conserved in vertebrates. It has been recently proposed that in human cells Cdk1-CyclinB activity destabilizes aMTs to ensure proper spindle orientation[168]. Strikingly, Cdk1-CyclinB activity is high in metaphase, and decreases at anaphase onset due to APC/C^{Cdc20}-mediated degradation of the cyclin B subunit[17]. As such, it is likely that the aMT regulatory function of the APC/C^{Cdc20} may be conserved in human cells. Importantly, aMT stabilization increases the Dyn1-generated pulling forces[96], hence APC/C^{Cdc20} modulation of aMT dynamics may contribute to generation of the Dyn1 activity trend seen in mammalian cells – that is low in metaphase and high in anaphase[169–171]. Furthermore, aMTs are often reported as shrinking during human cell anaphase – meaning that a counteraction of aMT stability connected to spindle elongation, similar to what we observed in budding yeast, may exist even in higher eukaryotes. Finally, we identified Cdc5 as a novel regulator of spindle positioning in budding yeast. In line with this, the human homologue of Cdc5 Plk1, has been intensively linked to spindle positioning regulation[162]. Indeed, Plk1-dependent phosphorylation of several components of the cortex platform that binds to aMTs is required to correctly

orient and position the spindle in line with the cleavage plane[14]. Investigating how Cdc5 influences these processes may further clarify the role of the kinase in higher eukaryotes and possibly indicate how it coordinates spindle position with other late mitotic events that are highly modulated by the polo kinases, including sister chromatid separation and mitotic exit.

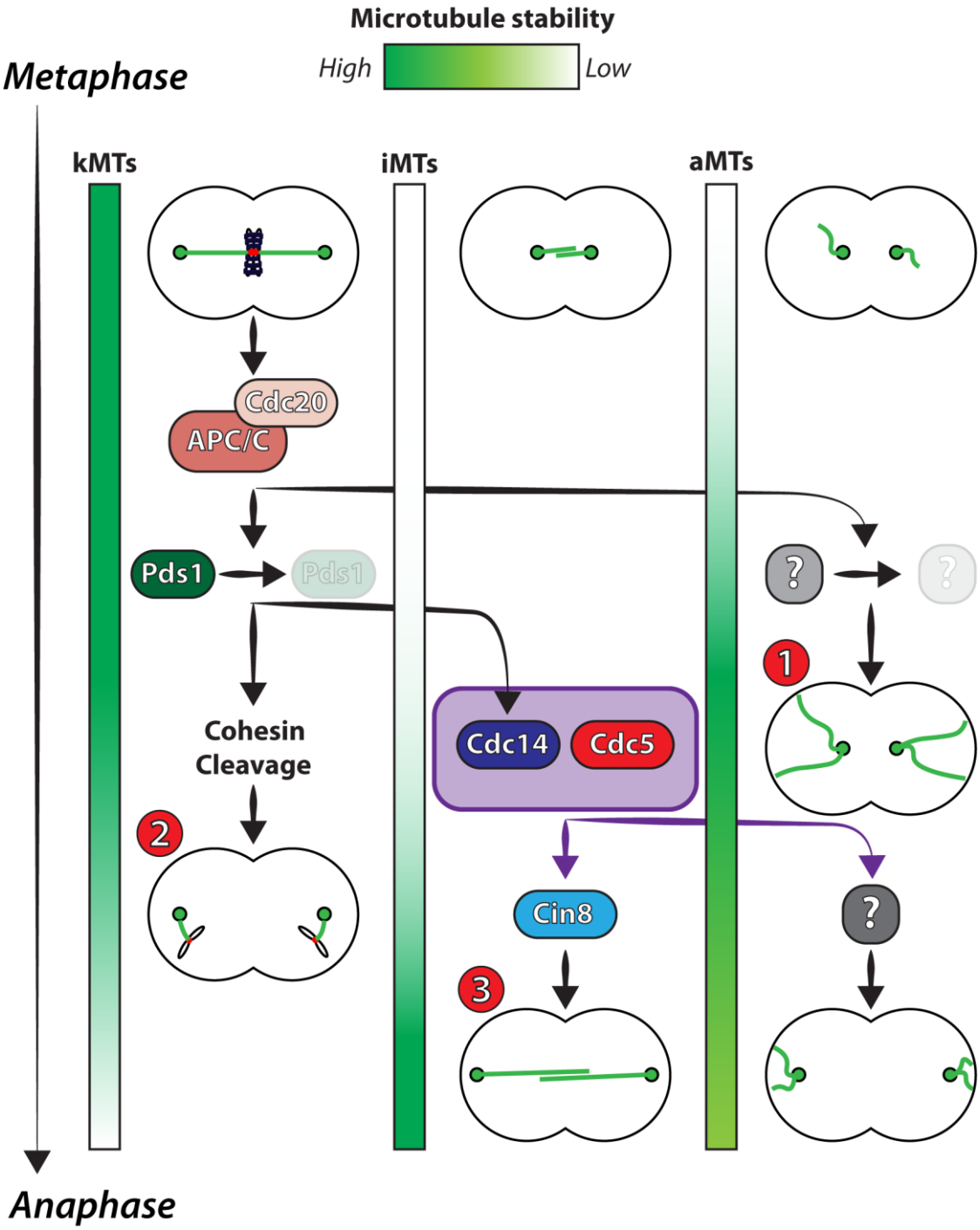

Figure 4.2. Proposed model of spindle microtubule regulation during chromosome segregation.

REFERENCES

1. Mcintosh, J. R. & Hays, T. A Brief History of Research on Mitotic Mechanisms. *Biology (Basel).* 1–38 (2016). doi:10.3390/biology5040055

2. Santaguida, S. & Amon, A. Short- and long-term effects of chromosome mis-segregation and aneuploidy. *Nat. Rev. Mol. Cell Biol.* **16**, 473–485 (2015).

3. Stegmeier, F. & Amon, A. Closing Mitosis: The Functions of the Cdc14 Phosphatase and Its Regulation. *Annu. Rev. Genet.* **38**, 203–232 (2004).

4. Nakatogawa, H., Suzuki, K., Kamada, Y. & Ohsumi, Y. Dynamics and diversity in autophagy mechanisms : lessons from yeast. *Nat. Rev. Mol. Cell Biol.* **10**, (2009).

5. Finger, F. P. & Novick, P. Spatial Regulation of Exocytosis: Lessons from Yeast. *J. Cell Biol.* **142**, 609–612 (1998).

6. Plaschka, C., Newman, A. J. & Nagai, K. Structural Basis of Nuclear pre-mRNA Splicing : Lessons from Yeast. *Cold Spring Harb. Perspect. Biol.* (2019). doi:10.1101/cshperspect.a032391

7. Cavanaugh, A. M. & Jaspersen, S. L. Big Lessons from Little Yeast : Budding and Fission Yeast Centrosome Structure , Duplication , and Function. *Annu. Rev. Genet.* (2017).

8. Peterson, J. B. & Ris, H. ELECTRON-MICROSCOPIC STUDY OF THE SPINDLE AND CHROMOSOME MOVEMENT IN THE YEAST SACCHAROMYCES CEREVISIAE. *J. Cell Sci.* **242**, 219–242 (1976).

9. Winey, M. Three-Dimensional Ultrastructural Analysis of the Saccharomyces cerevisiae Mitotic Spindle. **129**, 1601–1615 (1995).

10. Roostalu, J., Schiebel, E. & Khmelinskii, A. Cell cycle control of spindle elongation. *Cell Cycle* **9**, 1084–1090 (2010).

11. Pearson, C. G. & Bloom, K. Dynamic microtubules lead the way for spindle positioning. *Nat. Rev. Mol. Cell Biol.* **5**, 481–92 (2004).

12. Knoblich, J. A. Asymmetric cell division: recent developments and their implications for tumour biology. *Nat. Rev. Mol. Cell Biol.* **11**, 849–860 (2010).

13. Gómez-López, S., Lerner, R. G. & Petritsch, C. Asymmetric cell division of stem and progenitor cells during homeostasis and cancer. *Cell. Mol. Life Sci.* **71**, 575–597 (2014).

14. Bergstralh, D. T., Dawney, N. S. & Johnston, D. S. Spindle orientation : a question of complex positioning. *Development* **5**, 1137–1145 (2017).

15. Blagosklonny, M. V, Pardee, A. B. & Pardee, A. B. The Restriction Point of the Cell Cycle. *Cell Cycle* **4101**, (2002).

16. Malumbres, M. & Barbacid, M. Cell cycle, CDKs and cancer: a changing paradigm. *Nat. Rev. Cancer* **9**, (2009).

17. Sullivan, M. & Morgan, D. O. Finishing mitosis , one step at a time. *Nat. Rev. Mol. Cell Biol.* **8**, (2007).

18. Juanes, M. A. & Piatti, S. The final cut : cell polarity meets cytokinesis at the bud neck in S . cerevisiae. *Cell. Mol. Life Sci.* **73**, 3115–3136 (2016).

19. Chao, J. T. *et al.* Polarization of the endoplasmic reticulum by ER-septin tethering. *Cell* **158**, 620–632 (2014).

20. Yeh, E. *et al.* Dynamic positioning of mitotic spindles in yeast: role of microtubule motors and cortical determinants. *Mol. Biol. Cell* **11**, 3949–3961 (2000).

21. Morgan, D. O. Principles of CDK regulation. *Nature* (1995).

22. Visintin, R. *et al.* The Phosphatase Cdc14 Triggers Mitotic Exit by Reversal of Cdk-Dependent Phosphorylation. *Mol. Cell* **2**, 709–718 (1998).

23. Jin, F., Richmond, D. & Wang, Y. The multilayer regulation of the metaphase-to-anaphase transition. *Cell Cycle* **8**, 700–704 (2009).

24. Rock, J. M. & Amon, A. The FEAR network. *Curr. Biol.* 1063–1068 (2009).

25. Visintin, R., Hwang, E. S. & Amon, a. Cfi1 prevents premature exit from mitosis by anchoring Cdc14 phosphatase in the nucleolus. *Nature* **398**, 818–823 (1999).

26. Manzoni, R. *et al.* Oscillations in Cdc14 release and sequestration reveal a circuit underlying mitotic exit. *J. Cell Biol.* **190**, 209–222 (2010).

27. Touati, S. A., Kataria, M., Jones, A. W., Snijders, A. P. & Uhlmann, F. Phosphoproteome dynamics during mitotic exit in budding yeast. *EMBO J.* 1–15 (2018). doi:10.15252/embj.201798745

28. Visintin, R., Prinz, S. & Amon, A. CDC20 and CDH1: a family of substrate-specific activators of APC-dependent proteolysis. *Science (80-.).* **278**, 460–3 (1997).

29. Uhlmann, F., Wernic, D., Poupart, M. a, Koonin, E. V & Nasmyth, K. Cleavage of cohesin by the CD clan protease separin triggers anaphase in yeast. *Cell* **103**, 375–386 (2000).

30. Uhlmann, F., Lottspelch, F. & Nasmyth, K. Sister-chromatid separation at anaphase onset is promoted by cleavage of the cohesin subunit Scc1. *Nature* **400**, 37–42 (1999).

31. Stegmeier, F., Visintin, R. & Amon, A. Separase, polo kinase, the kinetochore protein Slk19, and Spo12 function in a network that controls Cdc14 localization during early anaphase. *Cell* **108**, 207–220 (2002).

32. Campbell, I. W., Zhou, X. & Amon, A. The Mitotic Exit Network integrates temporal and spatial signals by distributing regulation across multiple components. *Elife* **2**, 1–23 (2019).

33. Bardin, A. J., Visintin, R. & Amon, A. A Mechanism for Coupling Exit from Mitosis to Partitioning of the Nucleus. *Cell* **102**, 21–31 (2000).

34. Hu, F. *et al.* Regulation of the Bub2 / Bfa1 GAP Complex by Cdc5 and Cell Cycle Checkpoints. *Cell* **107**, 655–665 (2001).

35. Pereira, G., Manson, C., Grindlay, J. & Schiebel, E. Regulation of the Bfa1p – Bub2p complex at spindle pole bodies by the cell cycle phosphatase Cdc14p. *J. Cell Biol.* 367–379 (2001). doi:10.1083/jcb.200112085

36. Visintin, C. *et al.* APC/C-Cdh1-mediated degradation of the Polo kinase Cdc5 promotes the return of Cdc14 into the nucleolus. *Genes Dev.* **22**, 79–90 (2008).

37. Lara-gonzalez, P. & Westhorpe, F. G. The Spindle Assembly Checkpoint. *Curr. Biol.* **22**, R966–R980 (2012).

38. Falk, J. *et al.* Spatial signals link exit from mitosis to spindle position. *Elife* **5**, 1–23 (2016).

39. Pereira, G. & Schiebel, E. Kin4 kinase delays mitotic exit in response to spindle alignment defects. *Mol. Cell* **19**, 209–221 (2005).

40. D'Aquino, K. E. *et al.* The protein kinase Kin4 inhibits exit from mitosis in response to spindle position defects. *Mol. Cell* **19**, 223–234 (2005).

41. Brouhard, G. J. & Rice, L. M. Microtubule dynamics: an interplay of biochemistry and mechanics. *Nat. Rev. Mol. Cell Biol.* **19**, 1–13 (2018).

42. Prosser, S. L. & Pelletier, L. Mitotic spindle assembly in animal cells : a fine balancing act. *Nat. Rev. Mol. Cell Biol.* doi:10.1038/nrm.2016.162

43. Dumont, S. & Mitchison, T. J. Force and Length in the Mitotic Spindle. *Curr. Biol.* **19**, R749–R761 (2009).

44. Blake-hodek, K. A., Cassimeris, L. & Huffaker, T. C. Regulation of Microtubule Dynamics by Bim1 and Bik1 , the Budding Yeast Members of the EB1 and CLIP-170 Families of Plus-End Tracking Proteins. *Mol. Biol. Cell* **21**, 2013–2023 (2010).

45. Winey, M. & Bloom, K. Mitotic spindle form and function. *Genetics* **190**, 1197–1224 (2012).

46. Khmelinskii, A. & Schiebel, E. Assembling the spindle midzone in the right place at the right time Assembling the spindle midzone in the right place at the right time. *Cell Cycle* **4101**, (2008).

47. Khmelinskii, A., Lawrence, C., Roostalu, J. & Schiebel, E. Cdc14-regulated midzone assembly controls anaphase B. *J. Cell Biol.* **177**, 981–993 (2007).

48. Jensen, S., Segal, M., Clarke, D. J. & Reed, S. I. A novel role of the budding yeast separin Esp1 in anaphase spindle elongation: Evidence that proper spindle association of Esp1 is regulated by Pds1. *J. Cell Biol.* **152**, 27–40 (2001).

49. Ruchaud, S., Carmena, M. & Earnshaw, W. C. Chromosomal passengers : conducting cell division. *Nat. Rev. Mol. Cell Biol.* **8**, (2007).

50. Pereira, G. & Schiebel, E. INCENP – Aurora B Anaphase Spindle Function Through Cdc14. *Science (80-.).* **302**, 2120–2125 (2003).

51. Gunzelmann, J. *et al.* The microtubule polymerase Stu2 promotes oligomerization of the g -TuSC for cytoplasmic microtubule nucleation. *Elife* 1–27 (2018).

52. Vaart, B. Van Der *et al.* TORC1 signaling exerts spatial control over microtubule dynamics by promoting nuclear export of Stu2. *J. Cell Biol.* **216**, 3471–3484 (2017).

53. Hildebrandt, E. R. & Hoyt, M. A. Mitotic motors in Saccharomyces cerevisiae. *Biochim. Biophys. Acta - Mol. Cell Res.* **1496**, 99–116 (2000).

54. Thiede, C. *et al.* Directionality of Individual Kinesin-5 Cin8 Motors is Modulated by Loop 8, Ionic Strength and Microtubule Geometry. *EMBO J.* (2011). doi:10.1038/emboj.2011.403

55. Hoyt, M. A., He, L., Loo, K. K. & Saunders, W. S. Kinesin-related Gene Products Required for Mitotic Spindle Assembly. *J. Cell Biol.* **118**, 109–120 (1992).

56. Gerson-Gurwitz, A. *et al.* Mid-anaphase arrest in S. cerevisiae cells eliminated for the function of Cin8 and dynein. *Cell. Mol. Life Sci.* **66**, 301–313 (2009).

57. Scholey, J. M., Civelekoglu-scholey, G. & Brust-mascher, I. Anaphase B. *Biology (Basel).* 1–30 (2016). doi:10.3390/biology5040051

58. Gardner, M. K. *et al.* Chromosome Congression by Kinesin-5 Motor-Mediated Disassembly of Longer Kinetochore Microtubules. *Cell* **135**, 894–906 (2008).

59. Gramont, A. De, Barbour, L., Ross, K. E. & Cohen-fix, O. The Spindle Midzone Microtubule-Associated Proteins Ase1p and Cin8p Affect the Number and Orientation of Astral Microtubules in Saccharomyces cerevisiae. *Cell Cycle* **4101**, (2007).

60. Gordon, D. M. & Roof, D. M. Degradation of the kinesin Kip1p at anaphase onset is mediated by the anaphase-promoting complex and Cdc20p. *Proc Natl Acad Sci* **98**, (2001).

61. Hildebrandt, E. R. & Hoyt, M. A. Cell cycle-dependent degradation of the Saccharomyces cerevisiae spindle motor Cin8p requires APC(Cdh1) and a bipartite destruction sequence. *Mol. Biol. Cell* **12**, 3402–16 (2001).

62. Chee, M. K. & Haase, S. B. B-Cyclin / CDKs Regulate Mitotic Spindle Assembly by Phosphorylating Kinesins-5 in Budding Yeast. *PLoS Genet.* **6**, (2010).

63. Roccuzzo, M., Visintin, C., Tili, F. & Visintin, R. FEAR-mediated activation of Cdc14 is the limiting step for spindle elongation and anaphase progression. *Nat. Cell Biol.* **17**, (2015).

64. Saunders, W., Lengyel, V. & Hoytl, M. A. Mitotic Spindle Function in Saccharomyces cerevisiae Requires a Balance between Different Types of Kinesin-related Motors. *Mol. Biol. Cell* **8**, 1025–1033 (1997).

65. Manning, B. D., Barrett, J. G., Wallace, J. A., Granok, H. & Snyder, M. Differential Regulation of the Kar3p Kinesin-related Protein by Two Associated Proteins, Cik1p and Vik1p. *J. Cell Biol.* **144**, 1219–1233 (1999).

66. Maddox, P. S., Stemple, J. K., Satterwhite, L., Salmon, E. D. & Bloom, K. The Minus End-Directed Motor Kar3 Is Required for Coupling Dynamic Microtubule Plus Ends to the Cortical Shmoo Tip in Budding Yeast. *Curr. Biol.* **13**, 1423–1428 (2003).

67. Chen, C. J., Rayment, I. & Gilbert, S. P. Kinesin Kar3Cik1 ATPase Pathway for Microtubule Cross-linking. *J. Biol. Chem.* **286**, 29261–29272 (2011).

68. Dave, S. *et al.* Discrete regions of the kinesin-8 Kip3 tail differentially mediate astral microtubule stability and spindle disassembly. *Mol. Biol. Cell* (2018). doi:10.1091/mbc.E18-03-0199

69. Gupta, M. L., Carvalho, P., Roof, D. M. & Pellman, D. Plus end-specific depolymerase activity of Kip3 , a kinesin-8 protein , explains its role in positioning the yeast mitotic spindle. *Nat. Cell Biol.* **8**, (2006).

70. Dezwaan, T. M., Ellingson, E., Pellman, D. & Roof, D. M. Kinesin-related KIP3 of Saccharomyces cerevisiae Is Required for a Distinct Step in Nuclear Migration Todd. *J. Cell Biol.* **138**, 1023–1040 (1997).

71. Shaw, S. L., Yeh, E., Maddox, P., Salmon, E. D. & Bloom, K. Astral Microtubule Dynamics in Yeast: A Microtubule-based Searching Mechanism for Spindle Orientation and Nuclear Migration into the Bud. *J. Cell Biol.* **139**, 985–994 (1997).

72. Hoopen, R. *et al.* Mechanism for Astral Microtubule Capture by Cortical Bud6p Priming Spindle Polarity in S . cerevisiae. *Curr. Biol.* 1075–1083 (2012). doi:10.1016/j.cub.2012.04.059

73. Chen, X. *et al.* Remote control of microtubule plus-end dynamics and function from the minus- end. *Elife* 1–32 (2019).

74. Lammers, L. G. & Markus, S. M. The dynein cortical anchor Num1 activates dynein motility by relieving Pac1/LIS1-mediated inhibition. *J. Cell Biol.* **211**, 309–322 (2015).

75. Jeffrey B. Woodruff, David G. Drubin, and G. B. Dynein-Driven Mitotic Spindle Positioning Restricted to Anaphase by She1p Inhibition of Dynactin Recruitment. *Mol. Biol. Cell* **20**, 3003–3011 (2009).

76. Burns, S. *et al.* Structured illumination with particle averaging reveals novel roles for yeast centrosome components during duplication. *Elife* 1–27 (2015). doi:10.7554/eLife.08586

77. Winey, M., Goetsch, L., Baum, P. & Byers, B. MPSI and MPS2 : Novel Yeast Genes Defining Distinct Steps of Spindle Pole Body Duplication. *J. Cell Biol.* **114**, 745–754 (1981).

78. Geymonat, M. *et al.* Orderly assembly underpinning built-in asymmetry in the yeast centrosome duplication cycle requires cyclin-dependent kinase. *Elife* (2020).

79. Crasta, K., Huang, P., Morgan, G., Winey, M. & Surana, U. Cdk1 regulates centrosome separation by restraining proteolysis of microtubule-associated proteins. *EMBO J.* **25**, 2551–2563 (2006).

80. Rüthnick, D. & Schiebel, E. Duplication of the Yeast Spindle Pole Body Once per Cell Cycle. *Mol. Cell. Biol.* **36**, 1324–1331 (2016).

81. Elserafy, M. *et al.* Molecular Mechanisms that Restrict Yeast Centrosome Duplication to One Event per Cell Cycle. *Curr. Biol.* 1456–1466 (2014). doi:10.1016/j.cub.2014.05.032

82. Avena, J. S. *et al.* Licensing of Yeast Centrosome Duplication Requires Phosphoregulation of Sfi1. *PLoS Genet.* **10**, (2014).

83. Lengefeld, J. & Barral, Y. Asymmetric Segregation of Aged Spindle Pole Bodies During Cell Division : Mechanisms and Relevance Beyond Budding Yeast ? *BioEssays* **1800038**, 1–9 (2018).

84. Rees, D., Ades, S., Singer, S. & Hynes, R. Regulation of microtubule dynamics by cdc2 protein kinase in cell-free extracts of Xenopus eggs. *Nature* **374**, 685–689 (1990).

85. Belmont, L. D., Hyman, A. A., Sawin, K. E. & Mitchison, T. J. Real-time visualization of cell cycle-dependent change in microtubule dynamics in cytoplasmic extracts. *Cell* **62**, 579–589 (1990).

86. Bouck, D. C., Joglekar, A. P. & Bloom, K. S. Design Features of a Mitotic Spindle: Balancing Tension and Compression at a Single Microtubule Kinetochore Interface in Budding Yeast. *Annu. Rev. Genet.* 335–359 (2010). doi:10.1146/annurev.genet.42.110807.091620.Design

87. Wollman, R. *et al.* Efficient Chromosome Capture Requires a Bias in the ' Search-and-Capture ' Process during Mitotic-Spindle Assembly. *Curr. Biol.* **15**, 828–832 (2005).

88. Tanaka, T. U. Kinetochore – microtubule interactions : steps towards bi-orientation. *EMBO J.* **29**, 4070–4082 (2010).

89. Asbury, C. L. Anaphase A : Disassembling Microtubules Move Chromosomes toward Spindle Poles. *Biology (Basel).* (2017). doi:10.3390/biology6010015

90. Pearson, C. G., Maddox, P. S., Salmon, E. D. & Bloom, K. Budding Yeast Chromosome Structure and Dynamics during Mitosis. *J. Cell Biol.* **152**, 1255–1266 (2001).

91. Sullivan, D. S. & Huffaker, T. C. Astral Microtubules are not required for anaphase b in Saccharomyces Cerevisiae. *J. Cell Biol.* **119**, 379–388 (1992).

92. Yeh, E., Skibbens, R. V, Cheng, J. W., Salmon, E. D. & Bloom, K. Spindle Dynamics and Cell Cycle Regulation of Dynein in the Budding Yeast, Saccharomyces cerevisiae. *J. Cell Biol.* **130**, (1995).

93. Higuchi, T. & Uhlmann, F. Stabilization of microtubule dynamics at anaphase onset promotes chromosome segregation. *Nature* **433**, 171–176 (2005).

94. Maddox, P. S., Bloom, K. S. & Salmon, E. D. The polarity and dynamics of microtubule assembly in the budding yeast Saccharomyces cerevisiae. *Nat Cell Biol.* **2**, 36–41 (2000).

95. Segal, M., Bloom, K. & Reed, S. I. Kar9p-independent Microtubule Capture at Bud6p Cortical Sites Primes Spindle Polarity before Bud Emergence in Saccharomyces cerevisiae. *Mol. Biol. Cell* **13**, 4141–4155 (2002).

96. Estrem, C., Fees, C. P. & Moore, J. K. Dynein is regulated by the stability of its microtubule track. *J. Cell Biol.* **216**, (2016).

97. Vogel, J. *et al.* Phosphorylation of gamma-Tubulin Regulates Microtubule Organization in Budding Yeast. *Dev. Cell* **1**, 621–631 (2001).

98. Liakopoulos, D., Kusch, J., Grava, S., Vogel, J. & Barral, Y. Asymmetric Loading of Kar9 onto Spindle Poles and Microtubules Ensures Proper Spindle Alignment. *Cell* **112**, 561–574 (2003).

99. Juanes, M. A. *et al.* Spindle Pole Body History Intrinsically Links Pole Identity with Asymmetric Fate in Budding Yeast. *Curr. Biol.* **23**, 1310–1319 (2013).

100. Lengefeld, J. *et al.* Spatial cues and not spindle pole maturation drive the asymmetry of astral microtubules between new and preexisting spindle poles. *Elife* (2018). doi:10.1091/mbc.E16-10-0725

101. Pereira, G., Tanaka, T. U., Nasmyth, K. & Schiebel, E. Modes of spindle pole body inheritance and segregation of the Bfa1p ± Bub2p checkpoint protein complex. *EMBO J.* **20**, 6359–6370 (2001).

102. Maekawa, H., Usui, T., Knop, M. & Schiebel, E. Yeast Cdk1 translocates to the plus end of cytoplasmic microtubules to regulate bud cortex interactions. *EMBO J.* **22**, (2003).

103. Maekawa, H. & Schiebel, E. Cdk1 – Clb4 controls the interaction of astral microtubule plus ends with subdomains of the daughter cell cortex. 1709–1724 (2004). doi:10.1101/gad.298704.2001

104. Keck, J. M. *et al.* A Cell Cycle Phosphoproteome of the Yeast Centrosome. *Science (80-.).* **332**, 1557–1562 (2011).

105. Lin, T. *et al.* Phosphorylation of the Yeast c -Tubulin Tub4 Regulates Microtubule Function. *PLoS One* **6**, (2011).

106. Shulist, K. *et al.* Interrogation of γ -tubulin alleles using high-resolution fitness measurements reveals a distinct cytoplasmic function in spindle alignment. *Sci. Rep.* 1–14 (2017). doi:10.1038/s41598-017-11789-7

107. Drechsler, H., Tan, A. N. & Liakopoulos, D. Yeast GSK-3 kinase regulates astral microtubule function through phosphorylation of the microtubule-stabilizing kinesin Kip2. *J. Cell Sci.* **128**, 3910–21 (2015).

108. Hibbel, A., Bogdanova, A., Mahamdeh, M., Liakopoulos, D. & Howard, J. Kinesin Kip2 enhances microtubule growth in vitro through length-dependent feedback on polymerization and catastrophe. *Elife* **2**, 1–11 (2015).

109. Beach, D. L., Thibodeaux, J., Maddox, P., Yeh, E. & Bloom, K. The role of the proteins Kar9 and Myo2 in orienting the mitotic spindle of budding yeast. *Curr. Biol.* 1497–1506 (2000).

110. Hotz, M. *et al.* Spindle pole bodies exploit the mitotic exit network in metaphase to drive their age-dependent segregation. *Cell* **148**, 958–972 (2012).

111. Lengefeld, J., Hotz, M., Rollins, M., Baetz, K. & Barral, Y. Budding yeast Wee1 distinguishes spindle pole bodies to guide their pattern of age-dependent segregation. *Nat. Cell Biol.* **19**, (2017).

112. Scarfone, I. *et al.* Asymmetry of the budding yeast Tem1 GTPase at spindle poles is required for spindle positioning but not for mitotic exit. *PLoS Genet.* **11**, e1004938 (2015).

113. Pereira, G., Höfken, T., Grindlay, J., Manson, C. & Schiebel, E. The Bub2p spindle checkpoint links nuclear migration with mitotic exit. *Mol. Cell* **6**, 1–10 (2000).

114. Cepeda-garcı, C. *et al.* Actin-mediated Delivery of Astral Microtubules Instructs Kar9p Asymmetric Actin-mediated Delivery of Astral Microtubules Instructs Kar9p Asymmetric Loading to the Bud-Ward Spindle Pole. (2010). doi:10.1091/mbc.E10

115. Moore, J. K. & Miller, R. K. The Cyclin-dependent Kinase Cdc28p Regulates Multiple Aspects of Kar9p Function in Yeast. *Mol. Biol. Cell* **18**, 1187–1202 (2007).

116. Hotz, M., Lengefeld, J. & Barral, Y. The MEN mediates the effects of the spindle assembly checkpoint on Kar9-dependent spindle pole body inheritance in budding yeast. *Cell Cycle* 3109–3116 (2012).

117. Maekawa, H. & Schiebel, E. Cdk1 – Clb4 controls the interaction of astral microtubule plus ends with subdomains of the daughter cell cortex. *Genes Dev.* 1709–1724 (2004). doi:10.1101/gad.298704.2001

118. Gareau, J. R. & Lima, C. D. The SUMO pathway: emerging mechanisms that shape specificity, conjugation and recognition. *Nat. Rev. Mol. Cell Biol.* **11**, 861–871 (2011).

119. Meednu, N. *et al.* The Spindle Positioning Protein Kar9p Interacts With the Sumoylation Machinery in Saccharomyces cerevisiae. *Genetics* **2055**, 2033–2055 (2008).

120. Leisner, C. *et al.* Regulation of Mitotic Spindle Asymmetry by SUMO and the Spindle-Assembly Checkpoint in Yeast. *Curr. Biol.* 1249–1255 (2008). doi:10.1016/j.cub.2008.07.091

121. Stevermann, L., Panigada, D., Kammerer, D. & Liakopoulos, D. Regulation of a Spindle Positioning Factor at Article Regulation of a Spindle Positioning Factor at Kinetochores by SUMO-Targeted Ubiquitin Ligases. *Dev. Cell* 415–427 (2016). doi:10.1016/j.devcel.2016.01.011

122. Segal, M. *et al.* Coordinated Spindle Assembly and Orientation Requires Clb5p-dependent Kinase in Budding Yeast. *J. Cell Biol.* **148**, 441–451 (2000).

123. Grava, S., Schaerer, F., Faty, M., Philippsen, P. & Barral, Y. Asymmetric Recruitment of Dynein to Spindle Poles and Microtubules Promotes Proper Spindle Orientation in Yeast. *Dev. Cell* 425–439 (2006).

124. Moore, J. K., Stuchell-brereton, M. D. & Cooper, J. A. Function of Dynein in Budding Yeast : Mitotic Spindle Positioning in a Polarized Cell. *Cell Motil. Cytoskelet.* **555**, 546–555 (2009).

125. Moore, J. K., Silva, S. D. & Miller, R. K. The CLIP-170 Homologue Bik1p Promotes the Phosphorylation and Asymmetric Localization of Kar9p. *Mol. Biol. Cell* **17**, 178–191 (2006).

126. Balasubramanian, M. K., Bi, E. & Glotzer, M. Comparative Analysis of Cytokinesis in Budding Yeast , Fission Yeast and Animal Cells. *Curr. Biol.* **14**, 806–818 (2004).

127. Segal, M., Bloom, K. & Reed, S. I. Bud6 Directs Sequential Microtubule Interactions with the Bud Tip and Bud Neck during Spindle Morphogenesis in Saccharomyces cerevisiae. *Mol. Biol. Cell* **11**, 3689–3702 (2000).

128. Farkasovsky, M. & Kiintzel, H. Yeast Num1p Associates with the Mother Cell Cortex during S/G2 Phase and Affects Microtubular Functions. *J. Cell Biol.* **131**, 1003–1014 (1995).

129. Zahner, J. E., Harkins, H. A. & Pringle, J. R. Genetic Analysis of the Bipolar Pattern of Bud Site Selection in the Yeast Saccharomyces cerevisiae. *Mol. Cell. Biol.* **16**, 1857–1870 (1996).

130. Hoopen, R. & Cepeda-garcı, C. Article Mechanism for Astral Microtubule Capture by Cortical Bud6p Priming Spindle Polarity in S . cerevisiae. 1075–1083 (2012). doi:10.1016/j.cub.2012.04.059

131. Graziano, B. R. *et al.* Mechanism and cellular function of Bud6 as an actin nucleation – promoting factor. *Mol. Biol. cellu* (2011). doi:10.1091/mbc.E11-05-0404

132. Yin, H., Pruyne, D., Huffaker, T. C. & Bretscher, A. Myosin V orientates the mitotic spindle in yeast. *Nature* **1**, 1013–1015 (2000).

133. Hwang, E., Kusch, J., Barral, Y. & Huffaker, T. C. Spindle orientation in Saccharomyces cerevisiae depends on the transport of microtubule ends along polarized actin cables. *J. Cell Biol.* **9**, 483–488 (2000).

134. Miller, R. K. *et al.* Function Differently in Nuclear Migration in Yeast. *Mol. Biol. Cell* **9**, 2051–2068 (1998).

135. Kusch, J., Meyer, A., Snyder, M. P. & Barral, Y. Microtubule capture by the cleavage apparatus is required for proper spindle positioning in yeast. *Genes Dev.* 1627–1639 (2002). doi:10.1101/gad.222602.been

136. Tang, X., Germain, B. S. & Lee, W. A novel patch assembly domain in Num1 mediates dynein anchoring at the cortex during spindle positioning. *J. Cell Biol.* **196**, 743–756 (2012).

137. Kraft, L. M. & Lackner, L. L. Mitochondria-driven assembly of a cortical anchor for mitochondria and dynein. *J. Cell Biol.* **216**, 3061–3071 (2017).

138. Omer, S., Greenberg, S. R. & Lee, W. Cortical dynein pulling mechanism is regulated by differentially targeted attachment molecule Num1. *Elife* 1–30 (2018).

139. Laan, L. *et al.* Cortical Dynein Controls Microtubule Dynamics to Generate Pulling Forces that Position Microtubule Asters. *Cell* (2012). doi:10.1016/j.cell.2012.01.007

140. West, R. W., Chen, S., Putz, H., Butler, G. & Banerjee, M. GAL1-GAL1O divergent promoter region of Saccharomyces cerevisiae contains negative control elements in addition to functionally separate and possibly overlapping upstream activating sequences. *Genes Dev.* 1118–1131 (1987).

141. Care, R. S., Trevethick, J., Binley, K. M. & Sudbery, P. E. The MET3 promoter : a new tool for Candida albicans molecular genetics. *Mol. Microbiol.* **34**, 792–798 (1999).

142. Shetty, A., Reim, N. I. & Winston, F. Auxin-Inducible Degron System for Depletion of Proteins in Saccharomyces cerevisiae. *Curr. Protoc. Mol. Biol.* (2019). doi:10.1002/cpmb.104

143. Snead, J. L. *et al.* A Coupled Chemical-Genetic and Bioinformatic Approach to Polo-like Kinase Pathway Exploration. *Chem. Biol.* **14**, 1261–1272 (2007).

144. Paulo, J. A. & Gygi, S. P. A comprehensive proteomic and phosphoproteomic analysis of yeast deletion mutants of 14-3-3 orthologs and associated effects of rapamycin. *Proteomics* **15**, 474–486 (2015).

145. Fees, C. P., Estrem, C. & Moore, J. K. High-resolution Imaging and Analysis of Individual Astral Microtubule Dynamics in Budding Yeast. *J. Vis. Exp.* 1–7 (2017). doi:10.3791/55610

146. Kosco, K. A. *et al.* Control of Microtubule Dynamics by Stu2p Is Essential for Spindle Orientation and Metaphase Chromosome Alignment in Yeast. *Mol. Biol. cellog* **12**, 2870–2880 (2001).

147. Toso, R. J., Jordan, M. A., Farrel, K. W., Matsumoto, B. & J, L. W. Kinetic Stabilization of Microtubule Dynamic Instability in Vitro by Vinblastine. *biochemestry* 1285–1293 (1993).

148. Morgan, D. O. Regulation of the APC and the exit from mitosis. *Nat. Cell Biol.* **1**, (1999).

149. Claudi, C., S. Matuglia, F., Roccuzzo, M., Visintin, C. & Visintin, R. Polo-like kinase Cdc5 contributes to mitotic spindle elongation via the kinesin-5 motor protein Cin8 - Manuscript in preparation.

150. Martinez, J. S., Hall, H., Bartolowits, M. D. & Hall, M. C. Acm1 contributes to nuclear positioning by inhibiting Cdh1-substrate interactions. *Cell cycle* **11**, 384–394 (2012).

151. Cohen-fix, O., Peters, J., Kirschner, M. W. & Koshland, D. Anaphase initiation in Saccharomyces cerevisiae is controlled by the APC-dependent degradation of the anaphase inhibitor Pds1p. *Genes Dev.* 3081–3093 (1996).

152. Yamamoto, A., Guacci, V. & Koshland, D. Pds1p , an Inhibitor of Anaphase in Budding Yeast , Plays a Critical Role in the APC and Checkpoint Pathway (s). *J. Cell Biol.* **133**, 99–110 (1996).

153. Nespoli, A., Vercillo, R., Nola, L., Plevani, P. & Muzi-falconi, M. Alk1 and Alk2 are Two New Cell Cycle-Regulated Haspin-Like Proteins. *Cell Cycle* 1464–1471 (2006).

154. Enquist-newman, M., Sullivan, M. & Morgan, D. O. Modulation of the mitotic regulatory network by APC-dependent destruction of the Cdh1 inhibitor Acm1. *Mol. Cell* **30**, 437–446 (2008).

155. Ferreira, M. G., Santocanale, C., Drury, L. S. & Diffley, J. F. X. Dbf4p , an Essential S Phase-Promoting Factor , Is Targeted for Degradation by the Anaphase-Promoting Complex. *Mol. Cell. Biol.* **20**, 242–248 (2000).

156. Panigada, D. *et al.* Yeast Haspin Kinase Regulates Polarity Cues Necessary for Mitotic Spindle Positioning and Is Required to Tolerate Mitotic Arrest. *Dev. Cell* **26**, 483–495 (2013).

157. Chernyakov, I., Santiago-Tirado, F. & Bretscher, A. Active segregation of yeast mitochondria by Myo2 is essential and mediated by Mmr1 and Ypt11. *Curr. Biol.* **23**, 1818–1824 (2013).

158. Macgilvray, M. E. *et al.* The phosphoproteome response to dithiothreitol reveals unique versus shared features of Saccharomyces cerevisiae stress responses. *J. Proteome Res.* (2020). doi:10.1021/acs.jproteome.0c00253

159. Albuquerque, C. P. *et al.* A Multidimensional Chromatography Technology for In-depth Phosphoproteome Analysis. *Mol. Cell. proteomics* 1389–1396 (2008). doi:10.1074/mcp.M700468-MCP200

160. Holt, L. J. Global Analysis of Cdk1 Substrate Phosphorylation Sites Provides Insights into Evolution. *Science (80-.).* **1682**, (2009).

161. Swaney, D. L. *et al.* Global analysis of phosphorylation and ubiquitylation cross-talk in protein degradation. *Nat. Methods* **10**, (2013).

162. di Pietro, F., Echard, A. & Morin, X. Regulation of mitotic spindle orientation: an integrated view. *EMBO Rep.* **17**, 1106–1130 (2016).

163. Musacchio, A. The Molecular Biology of Spindle Assembly Checkpoint Signaling Dynamics. *Curr. Biol.* **25**, R1002–R1018 (2015).

164. Chan, L. Y. & Amon, A. Spindle position is coordinated with cell-cycle progression through establishment of mitotic exit-activating and -inhibitory zones. *Mol. Cell* **39**, 444–454 (2010).

165. Duselder, A. *et al.* Deletion of the Tail Domain of the Kinesin-5 Cin8 Affects Its. *J. Biol. Chem.* (2015). doi:10.1074/jbc.M114.620799

166. Baumgärtner, S. & Tolić, I. M. Astral microtubule pivoting promotes their search for cortical anchor sites during mitosis in budding yeast. *PLoS One* **9**, (2014).

167. Wu, M., Wu, X. & De Camilli, P. Calcium oscillations-coupled conversion of actin travelling waves to standing oscillations. *Proc Natl Acad Sci U S A* **110**, 1339–1344 (2013).

168. Singh, D., Schmidt, N., Müller, F., Bange, T. & Bird, A. W. Cdk1-dependent destabilization of long astral microtubules is required for spindle orientation. *bioRxiv Prepr.* (2020).

169. Kotak, S., Busso, C. & Gonczy, P. NuMA phosphorylation by CDK1 couples mitotic progression with cortical dynein function. *EMBO J.* **32**, 2517–2529 (2013).

170. Kiyomitsu, T. & Cheeseman, I. M. Cortical Dynein and Asymmetric Membrane Elongation Coordinately Position the Spindle in Anaphase. *Cell* **154**, 391–402 (2013).

171. Kiyomitsu, T. & Cheeseman, I. M. Chromosome- and spindle-pole-derived signals generate an intrinsic code for spindle position and orientation. *Nat. Cell Biol.* **14**, 311–317 (2012).